

Nonlinear Attitude Control of the Micro-Satellite ESEO

*A thesis submitted in fulfillment of the requirements
for the degree of Master of Science*

by

Morten Pedersen Topland



Department of Engineering Cybernetics
Norwegian University of Science and Technology
N-7491 TRONDHEIM, Norway



MASTEROPPGAVE

Kandidatens navn: Morten Topland

Fag: Teknisk Kybernetikk

Oppgavens tittel (norsk): *Regulering av orientering for mikrosatellitten ESEO*

Oppgavens tittel (engelsk): Nonlinear attitude control of the micro-satellite ESEO

Oppgavens tekst:

This project is part of ESAs Space Exploration & Technology Initiative (SSETI). The focus of this thesis is design, stability analysis and simulation of Attitude and Orbit Control System (AOCS), specifically:

- Study the field of control of attitude for spacecraft. Present AOCS for SSETI/ESMO.
- Derive a mathematical model for the attitude of ESMO. Include also models of the actuators, a reaction wheel and cold gas thrusters. The model is to be implemented in Simulink. This implementation should be as modular as possible. This part of the work is to be done in cooperation with MSc-student Øyvind Hergrenæs.
- It has been proposed to control the thrusters by way of a PD-controller. Study how this control system is planned to be implemented and perform a stability analysis of the system. The analysis should be supported by simulations.
- Propose at least one other control law that can be used in connection with large deviations from desired attitude. Analyze stability and perform simulations. Compare the results with the proposed PD-controller.

Oppgaven gitt: 12. januar 2004

Besvarelsen leveres: 2. juli 2004

Besvarelsen levert: 2. juli 2004

Utført ved Institutt for teknisk kybernetikk

Trondheim, den 12. januar 2004

Jan Tommy Gravdahl
Faglærer

Preface

The purpose of this Master thesis is to develop and simulate linear and nonlinear attitude control strategies for the micro-satellite European Student Earth Orbiter (ESEO). ESEO is part of the Student Space Exploration and Technology Initiative (SSETI), which is a project supported by the Education Office of the European Space Agency (ESA). Work on ESEO started in the year 2000, and launch is scheduled to 2005. SSETI is also planning a satellite which will orbit the moon, the European Student Moon Orbiter (ESMO). Work on this satellite is about to begin, and the first student team to be recruited was the ESMO Attitude Determination and Control System (ADCS) team. This Norwegian team is based at the Norwegian University of Science and Technology (NTNU) in Trondheim and Narvik University College (HiN) in Narvik. The first task of the ESMO ADCS team was to do a case study of ESEO. The work presented in this thesis is part of this study.

The development of the mathematical model used in this study, is done in cooperation with Øyvind Hegrenæs, and I would like to thank him for helpful discussions along the way. I would also like to acknowledge the support from my tutor, Jan Tommy Gravdahl, and I wish to thank the rest of the ESMO ADCS team in Narvik, especially Jøran Antonsen and Frank Robert Blindheim, for interesting discussions and support regarding interaction with SSETI. Lastly, I acknowledge the support of SSETI, and I would like to thank them for letting this thesis be based on a real space mission.

Trondheim, July 1, 2004

Morten P. Topland

Contents

Abstract	vi
1 Introduction	1
1.1 Purpose of report	1
1.2 Background	1
1.3 Outline of report	1
2 Background information	3
2.1 Previous work	3
2.2 SSETI	3
2.2.1 History and organisation structure	3
2.2.2 Planned missions	4
2.3 Technical data for ESEO	5
2.3.1 Orbital data	5
2.3.2 Inertial data	6
2.3.3 Sensors	6
2.3.4 Actuators	6
2.3.5 Attitude Estimation	7
2.3.6 Attitude Control	7
3 Mathematical background	10
3.1 Keplerian Orbits	10
3.2 Reference frames	11
3.2.1 Earth Centered Inertial frame	11
3.2.2 Earth Centered Earth Fixed frame	11
3.2.3 North East Down frame	11
3.2.4 Orbit frame	12
3.2.5 Body frame	12
3.3 Rigid body dynamics	12
3.3.1 Vectors	13
3.3.2 Rotation	13
3.3.3 Euler angles	14
3.3.4 Euler parameters	15
3.3.5 Kinematic differential equations	17

3.3.6	Attitude error	17
3.3.7	Angular velocity error	18
3.3.8	Momentum, angular momentum and the inertia matrix	18
3.4	Gyrostat model	19
3.4.1	Equations of motion	19
3.4.2	Kinetic energy	20
3.5	Disturbance torques	21
3.5.1	Gravity gradient torque	21
3.5.2	Potential energy	22
3.6	Stability analysis	22
3.6.1	Linear systems	22
3.6.2	Nonlinear systems	22
3.7	Linear control algorithms	23
3.7.1	Controllability	23
3.7.2	Basic linear controllers	23
3.7.3	Quaternion feedback control	24
3.8	Nonlinear control algorithms	25
3.8.1	Control laws from Lyapunov analysis	25
3.8.2	Feedback linearization	25
3.8.3	Sliding mode control	26
3.9	Thruster control	29
3.9.1	Bang-bang controller	29
3.9.2	Schmitt trigger	29
3.9.3	Pulse-Width Pulse-Frequency modulator	30
4	Theoretical analysis	32
4.1	Mathematical modelling	32
4.1.1	Kinematical model	32
4.1.2	Dynamical model	32
4.1.3	Model assumptions	34
4.1.4	Linearized model	35
4.2	Linear control	35
4.2.1	Local stabilization	36
4.2.2	Global stabilization	38
4.3	Nonlinear control	41
4.3.1	Lyapunov controller 1	42
4.3.2	Lyapunov controller 2	42
4.3.3	Lyapunov controller 3	44
4.3.4	Sliding mode controller	45
5	Simulation	47
5.1	SIMULINK model of ESEO	47
5.1.1	Mathematical model	47
5.1.2	Simulation parameters	47
5.2	Linear control	49
5.2.1	Local controller	49
5.3	Nonlinear control	49
5.3.1	Lyapunov controller 1	50

5.3.2	Lyapunov controller 3	50
5.3.3	Sliding mode controller	51
6	Discussion and conclusion	53
6.1	Discussion	53
6.1.1	Theoretical analysis	53
6.1.2	Simulation	54
6.1.3	Implementation issues	56
6.2	Conclusion	56
6.3	Recommendations	57
	Bibliography	60
A	Mathematical appendix	61
A.1	Calculus	61
A.1.1	Definitions	61
A.1.2	Vector and matrix norm properties	62
A.1.3	Matrix inversion	62
A.1.4	Inequalities	63
A.2	Theoretical analysis	63
A.2.1	Positive definiteness of V_r	63
A.2.2	Positive definiteness of V_g	64
A.2.3	Time derivative of V_a	64
A.2.4	Calculation of $\mathbf{J}\tilde{\omega}$	65
A.2.5	Gain selection for linear controller	66
A.2.6	Solution to $\mathbf{c}_3 = \begin{bmatrix} 0, \sqrt{1/2}, \sqrt{1/2} \end{bmatrix}^T$, $c_{22}c_{32} = 0$	68
A.2.7	Convergence of sliding manifold	69
A.2.8	Parameter error terms	70
A.2.9	Stability of local PD controller	70
B	Simulation plots	76
C	Maple and MATLAB/SIMULINK input	86
D	Conference and Workshop Documents	98

Abstract

In this Master thesis, attitude control of a spacecraft using thrusters and reaction wheels as actuators is studied. A nonlinear mathematical model of the spacecraft is developed, based on the assumption that the satellite is a rigid body. Linearization and Lyapunov theory is used to derive two linear and four nonlinear controllers. Three of the nonlinear controllers rely on cancellation of system nonlinearities, while the fourth is a sliding mode controller. By restricting the spacecraft inertia, simpler controllers can be found. Except for the controller based on linearization, all controllers can be used to control any spacecraft using thrusters and an arbitrary number of reaction wheels. Implementation issues regarding the controllers are also discussed.

Several controllers are compared in simulations in MATLAB/SIMULINK. The simulations use data from the micro-satellite European Student Earth orbiter (ESEO), which has one reaction wheel. A bang-bang controller with dead-zone is used for thruster control. The simulations show that all controllers obtain a desired accuracy of $\pm 1^\circ$ in Euler angles. Some of the controllers do not use the reaction wheel actively to control the satellite's attitude, but they perform just as well as the others. Whether or not the reaction wheel is used actively, the Euler angle which is affected by the reaction wheel converges faster than the other Euler angles, and it is closer to its desired value. This is due to the presence of the reaction wheel, and it is suggested that it adds a damping effect to the system. Note that the controllers which use the reaction wheel actively are nonlinear.

ESEO is a mission of the Student Space Exploration and Technology Initiative (SSETI), which is supported by the Education Office of the European Space Agency (ESA). Another planned SSETI mission is the European Student Moon Orbiter (ESMO). The Norwegian SSETI team, the ESMO Attitude Determination and Control System (ADCS) team, will use ESEO as a case study to prepare for work on ESMO. This work is part of that study. The ESMO ADCS team is based in the Norwegian University of Science and Technology (NTNU) in Trondheim and Narvik University College (HiN) in Narvik.

Chapter 1

Introduction

1.1 Purpose of report

The purpose of this report is to apply nonlinear control methods to control the attitude of a satellite, and compare their performance with a linear controller. A nonlinear mathematical model of the satellite is developed, and data for the European Student Earth Orbiter (ESEO) is used in simulations in MATLAB/SIMULINK. The actuators of this micro-satellite are thrusters and a reaction wheel. Both of these types of actuators provide challenges for an attitude control system, which are addressed. Furthermore, implementation issues and reusability of these control strategies for other satellites are discussed.

1.2 Background

This report is written in cooperation between the Department of Engineering Cybernetics at the Norwegian University of Science and Technology (NTNU) and the European Space Agency's (ESA) educational programme Student Space Exploration and Technology Initiative (SSETI). The author is a member of the SSETI ESMO ADCS team, together with Øyvind Hegrenæs and a group of students from Narvik University College (HiN). ESMO ADCS stands for European Student Moon Orbiter Attitude Determination and Control System. This team will start to work on ESMO this fall. This spring, the team has performed a case study of ESEO, which this report is part of, to prepare for work on ESMO. Communication between SSETI and NTNU has been maintained by weekly chat sessions over the internet, and two workshops which the author has attended in December 2003 and May 2004 as a team coordinator. In addition, the team has been present at the Space Technology Education Conference (STEC) in April 2004. This report is a Master thesis, which means that it contains the work equivalent to one semester of studies (30 credits). An article based on its contents has been accepted at the 55th International Astronautical Conference (IAC) in Vancouver in October 2004.

1.3 Outline of report

The two first chapters of this report contain background information. Chapter 2 provides a brief overview of previous work regarding attitude control of satellites. In addition, there is more information on SSETI and on technical data for ESEO. The mathematical background for this report can be found in chapter 3 and in appendix A.1. Chapter 4 and appendix A.2 contain the

theoretical analysis of this report. Information regarding the simulator and simulation results are found in chapter 5 and the appendices B and C. A discussion of the results and conclusions take place in chapter 6.

Chapter 2

Background information

2.1 Previous work

Hughes (1986) and Wie (1998) are standard references on spacecraft dynamics. Concerning attitude control of spacecraft, Wie, Weiss and Arapostathis (1989) show that a PD controller stabilizes a spacecraft. They use the classical spacecraft model with no moving parts. Hall (2000) has studied spacecraft attitude control using several reaction wheels as actuators. Additionally, Hall (1997) has investigated use of such reaction wheels to store energy. Hall, Tsiotras and Shen (2001) suggest an attitude control system with thrusters and reaction wheels which in addition store energy. Hall, Tsiotras and Shen (2002) describe nonlinear attitude control for a spacecraft with thrusters and an arbitrary number of reaction wheels, where the modified Rodrigues parameters are used to describe the attitude of the spacecraft. The use of Euler parameters or unit quaternions in attitude control problems, is treated by Fjellstad and Fossen (1994), but the results are applied to underwater vehicles. A nonlinear sliding mode controller is proposed by Lee, Park and Park (1993). Show, Juang and Jan (2003) present a nonlinear attitude controller based on a linear matrix inequality method. Song and Agrawal (2001) studies vibration suppression during attitude control for flexible spacecraft, and present various methods of transforming a continuous input torque to thruster torque pulses. These methods are compared with emphasis on vibrations in the spacecraft structure.

At the Norwegian University of Science and Technology (NTNU), Soglo (1994), Kristiansen (2000), Fauske (2002) and others have studied attitude control of satellites with magnetic coils and reaction wheels as actuators. Their results are part of the foundation of the NCUBE projects, where pico-satellites are launched into Earth orbit. For more information on NCUBE, see Gravdahl, Eide, Skavhaug, Svartveit, Fauske and Indergaard (2003) and Riise, Samuelsen, Sokolova, Cederblad, Fasselund, Nordin, Otterstad, Fauske, Eriksen, Indergaard, Svartveit, Furebotten, Sæther, and Eide (2003).

2.2 SSETI

2.2.1 History and organisation structure

The Student Space Exploration and Technology Initiative (SSETI) is a project supported by the Education Office of the European Space Agency (ESA). It started in the year 2000, and its objective is stated as follows (SSETI PR team, 2004):

To create a network of students, educational institutions and organisations (via the internet) to perform the distributed design, construction and launch of (micro) satellites and other spacecraft. This objective is reached when a spacecraft is designed, built and launched by a significant number of European students in a highly distributed way. The completion of this project objective is independent of a mission success or failure.

Students from ten different European countries participate in SSETI. ESA's Education Office manages the project, and coordinates the efforts from all the European universities involved. ESA facilitates testing and launch of satellites. Experts from ESA are involved in review sessions where they meet the students to check the quality of their work. Communication between the SSETI participants is done via weekly internet chat sessions, use of internet newsgroups and annual workshops at ESTEC in Noordwijk in the Netherlands. For more information on SSETI, see SSETI PR team (2004).

2.2.2 Planned missions

The SSETI missions (figure 2.1) are part of a layered structure where the aim is to finally land on the moon. The layers are represented by three missions. The first is an earth orbiter, the second a moon orbiter and the third a moon lander.

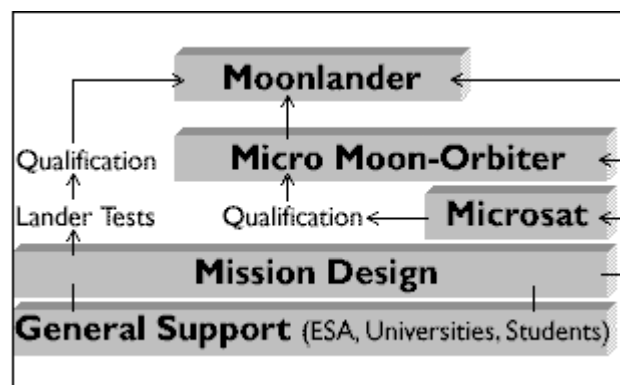


Figure 2.1: SSETI missions (SSETI PR team, 2004)

Development phases

Each mission has to pass several phases in order to be launched. These phases are listed here (SSETI PR team, 2004):

Phase 0 Pre-assessment study

Phase A Feasibility study

Phase B Detailed definition

Phase C Development

Phase D Manufacture, Integration, Test

Phase E Launch

Phase F Mission Operation

ESEO

The first SSETI mission is the European Student Earth Orbiter (ESEO), and work on this mission started when SSETI was founded in the year 2000. It is a micro-satellite which will enter geo-stationary transfer orbit (GTO) in 2005. This orbit is elliptical, and it is an intermediate stage between a low Earth orbit (LEO) and a geostationary orbit (GSO). Satellites in GSO are always at the same point in the sky when observed from the same point on the Earth. ESEO will be launched as an auxiliary structure for Ariane 5, the so called piggyback launch. A piggyback launch is a launch where several small satellites are launched together with a big one. In other words, ESEO and several other micro satellites will be launched together with a bigger satellite. The most important objectives of the ESEO mission are (SSETI PR team, 2004):

- Test and qualify the propulsion system for orbit manoeuvres and for the future moon missions.
- Test a small, low power plasma thruster.
- Test and qualify a star-tracker developed from a commercial device.
- Take pictures of the earth for the public with the help of installed cameras.
- Stay in orbit for at least 28 days.

SSETI Express

Work on SSETI Express started in December 2003, and this satellite will orbit the Earth. SSETI Express is much smaller than ESEO, and is scheduled to be launched first among the SSETI missions. It will serve as a precursor to ESEO.

ESMO

The European Student Moon Orbiter (ESMO) is the third SSETI mission. The objective is to reach moon orbit with a small satellite. Recruitment for this mission has just started. The ESMO ADCS team was the first recruited team, and they started their work in January 2004. A case study of ESEO was their first task, and this thesis is part of that team's contribution.

Moon Rover

The fourth mission involves a moon landing with a vehicle, a Moon Rover. Work on this mission has not yet begun.

2.3 Technical data for ESEO

2.3.1 Orbital data

According to the SSETI ESEO Mission Analysis (MIAS) team (SSETI ESEO MIAS team, 2003), the most likely orbit of insertion for ESEO is AR5 ECA Standard GTO. Some orbital parameters for this insertion are listed in table 2.1.

Apogee altitude	35950 km
Perigee altitude	250 km

Table 2.1: Orbital parameters for ESEO

2.3.2 Inertial data

The maximum weight of ESEO is 120 kg including payload, and the maximum dimensions are 600 mm x 600 mm x 800 mm. Power will be supplied by solar panels. A prototype has not been built yet, hence accurate inertial data is not available. When modeling and simulating a satellite, it is important to know the inertia matrix (definition 3.6). Although it may change, in this thesis we will use the most recent inertia matrix (SSETI ESEO AOCS team, 2004a):

$$\mathbf{I} = \begin{bmatrix} 4.3500 & 0 & 0 \\ 0 & 4.3370 & 0 \\ 0 & 0 & 3.6640 \end{bmatrix} \quad (2.1)$$

2.3.3 Sensors

ESEO will have sun sensors, a horizon sensor, a star tracker and a magnetometer (Trottemant et al., 2001). The magnetometer uses the International Geomagnetic Reference Field (IGRF) in modeling the magnetic field.

2.3.4 Actuators

Thrusters

ESEO's primary actuators are thrusters. The SSETI Propulsion (PROP) team is responsible for the development of the thruster systems. The thrusters are either on or off, i.e. they create a certain torque or no torque at all. It is important to note that thrusters have limited fuel capacity, which means that they will eventually run out of fuel. The thrusters are divided into three thruster systems. The Orbit Control System (OCS) uses one powerful thruster to give enough thrust in order to change ESEO's orbit. The Reaction Control System (RCS) shall stabilize ESEO's attitude while performing a change of orbit with the OCS. The third thruster system is the Attitude Control System (ACS), which is used to control ESEO's attitude in orbit.

The focus of this thesis is the ACS thrusters. These thrusters create torques about ESEO's body reference frame. For more details on reference frames, see section 3.2. The nominal ACS torques are given in table 2.2.

<i>x</i> axis	0.0484 Nm
<i>y</i> axis	0.0484 Nm
<i>z</i> axis	0.0398 Nm

Table 2.2: ACS nominal torques (SSETI PROP team, 2003)

Reaction wheel

A reaction wheel will be included, spinning about the y axis of ESEO's body (SSETI AOCS team, 2004b). The SSETI Attitude and Orbit Control System (AOCS) team is developing it. According to them, the reaction wheel's purpose is to prolong the life of ESEO in orbit by saving thruster fuel. The wheel will help the thrusters to control the spacecraft. Note that reaction wheels can go into saturation, i.e. they reach maximum speeds, and can therefore no longer provide torques. When this happens, it is possible to unload the wheel, i.e. slow it down, by for instance firing appropriate thrusters. Relevant properties of the reaction wheel are presented in table 2.3.

Moment of inertia:	$i_s = 4 \cdot 10^{-5} \text{ kgm}^2$
Maximum angular velocity:	$(\omega_s)_{max} = 5035 \text{ rpm} = 527.2640 \text{ rad/s}$

Table 2.3: Properties of the reaction wheel (SSETI AOCS team, 2004b)

2.3.5 Attitude Estimation

The SSETI ESEO AOCS team is responsible for developing the attitude estimation system. ESEO will use two different methods to estimate ESEO's attitude. The first method is the Extended Kalman Filter (EKF). This will be the primary method of estimation, since it is robust. However, it is computationally intensive, and has an initialization problem. Singular Value Decomposition (SVD) is the other method of choice. It is simple to implement, and does not need initial conditions to work, as opposed to the EKF. On the other hand, the SVD method requires at least two independent sets of sensor data in order to produce good estimates. This is an important disadvantage, and the explanation for preferring the EKF. The initialization problem of the EKF can be solved by using the SVD to provide initial values. If computer resources are running low, using the SVD instead of the EKF may prove useful, provided that enough sensor data are available. For details on these two estimation methods, see SSETI ESEO AOCS team (2004c).

2.3.6 Attitude Control

The attitude control system will be developed by the SSETI ESEO AOCS team. The most important general requirements for the attitude control system are listed below. Requirements for stability during orbital transfer is omitted, as this is not relevant to this thesis.

- Initial angular rates should be damped within 2 hours after separation from launcher.
- A pointing mode which points to the Earth centre should be provided. The attitude should be controlled and maintained within a specified accuracy.

ESEO will have several control modes. These are shown in figure 2.2. Some requirements for the attitude control system will vary according to the active control mode. The SSETI ESEO AOCS team will develop two controllers for ESEO, a nominal controller and an experimental controller. Information regarding the experimental controller is not yet available, but analysis of the nominal controller has begun. It is based on linearization of the physical system of the spacecraft. The controller is called a modified PD controller, and its block diagram is

shown in figure 2.3. For more information on linear controllers, see section 4.2. The modified PD controller has two control loops. The inner loop controls the angular velocity of ESEO, while the outer loop controls its attitude. The SSETI ESEO AOCS team (2004c) has more information on ESEO's attitude control system.

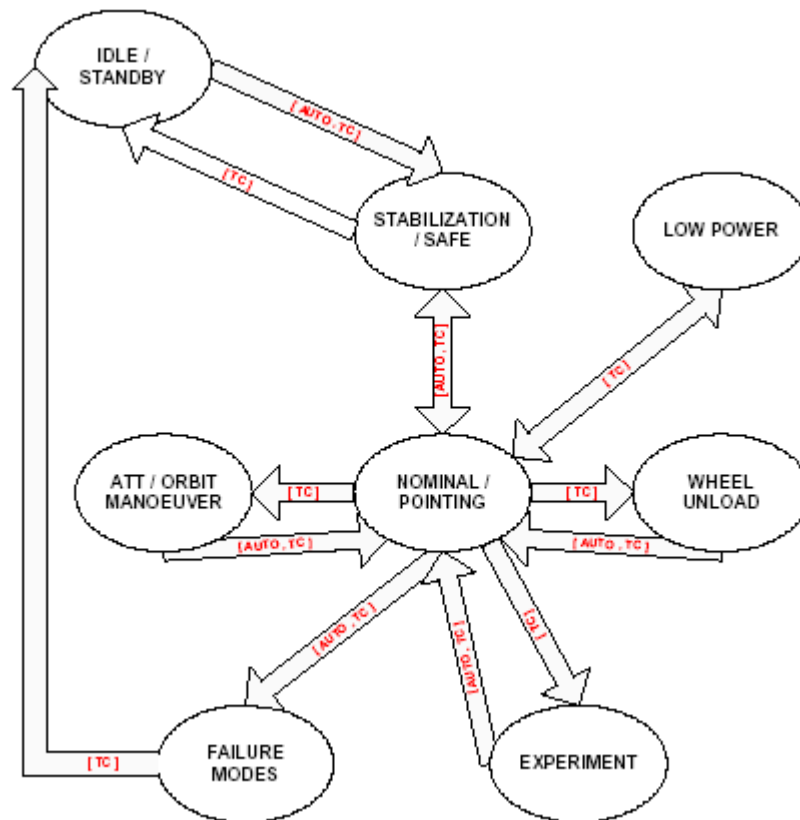


Figure 2.2: Control modes (SSETI ESEO AOCS team, 2004c)

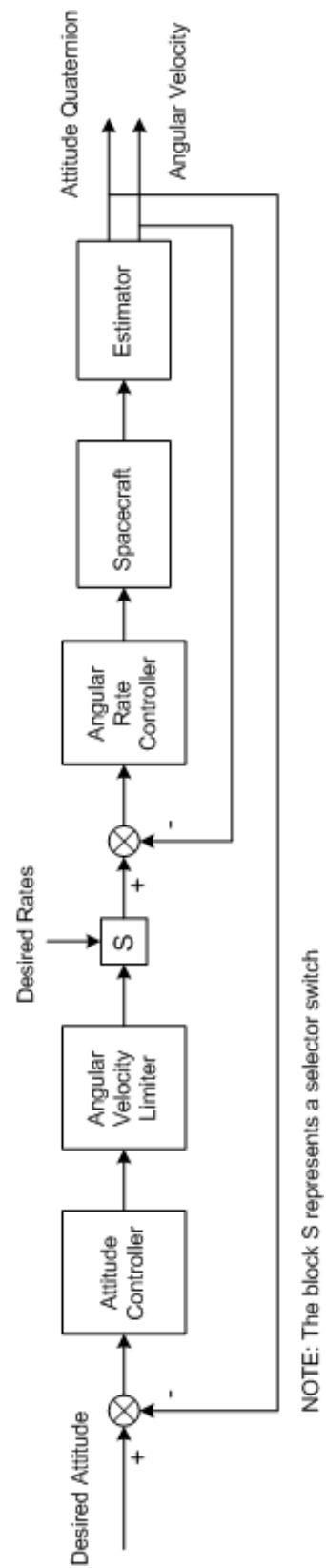


Figure 2.3: Modified PD controller (SSETI ESEO AOCs team, 2004c)

Chapter 3

Mathematical background

3.1 Keplerian Orbits

The motion of celestial bodies has been studied by Johannes Kepler, and he formulated the following laws based on his research (Wertz and Larson, 1999):

First Law: The orbit of each planet is an ellipse, with the Sun at one focus.

Second Law: The line joining the planet to the Sun sweeps out equal areas in equal times.

Third Law: The square of the period of a planet is proportional to the cube of its mean distance from the Sun.

These laws also apply to satellite motion in Earth orbit, i.e. replace the Sun with the Earth and planet with satellite in the above laws. Figure 3.1 shows a satellite in elliptic Earth orbit. An explanation to this figure is presented in table 3.1. For further information on Keplerian orbits, see Wertz et al. (1999).

\mathbf{r}	position vector of the satellite relative to Earth's center
\mathbf{V}	velocity vector of the satellite relative to Earth's center
ϕ	<i>flight-path-angle</i> , the angle between the velocity vector and a line perpendicular to the position vector
a	semimajor axis of the ellipse
b	semiminor axis of the ellipse
c	the distance from the center of the orbit to one of the foci
v	the <i>polar angle</i> of the ellipse, also called the <i>true anomaly</i> , measured in the direction of motion from the direction of perigee to the position vector
r_A	<i>radius of apogee</i> , the distance from Earth's center to the farthest point on the ellipse
r_P	<i>radius of perigee</i> , the distance from Earth's center to the point of closest approach to the Earth

Table 3.1: Explanation to figure 3.1

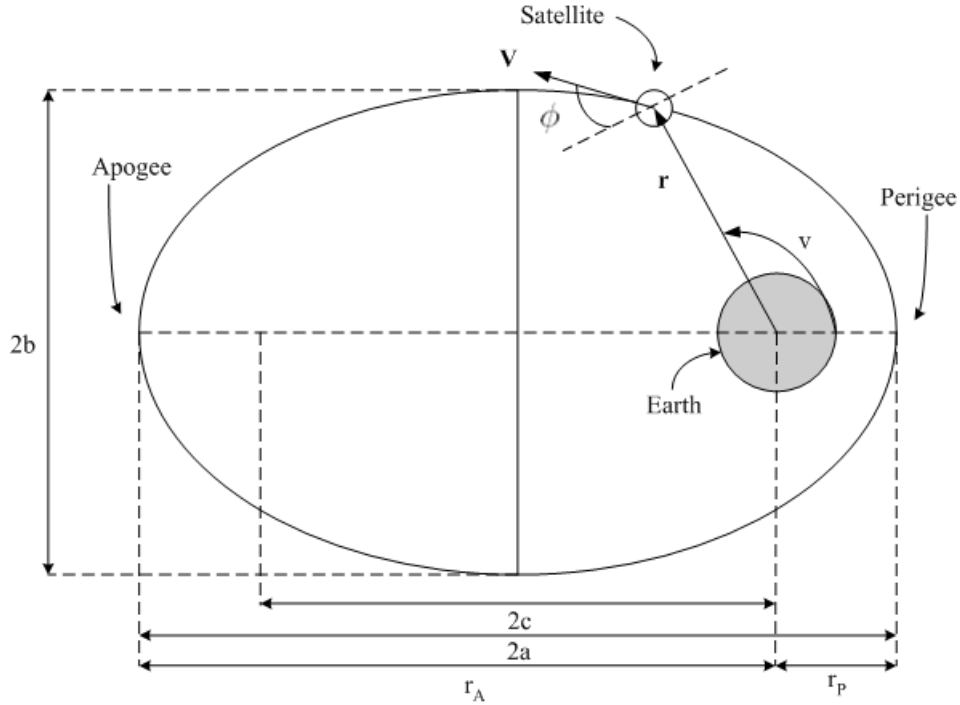


Figure 3.1: Elliptic orbit (Wertz et al., 1999)

3.2 Reference frames

To analyze the motion of a satellite, it is necessary to define reference frames which this motion is relative to. These frames are shown in figure 3.2, and are the same as those used by Fossen (2002) and Kristiansen (2000).

3.2.1 Earth Centered Inertial frame

The Earth Centered Inertial (ECI) frame, from now on denoted \mathcal{F}_i , has its origin at the center of the earth. Its unit vectors are x_i, y_i, z_i , where z_i is directed along the Earth's rotation axis. This frame is non-accelerated, i.e. inertial, which means that the laws of Newton apply.

3.2.2 Earth Centered Earth Fixed frame

The Earth Centered Earth Fixed (ECEF) frame, denoted \mathcal{F}_e , has the same origin as \mathcal{F}_i . However \mathcal{F}_e rotates relative to \mathcal{F}_i with a constant angular velocity $\omega_e = 7.2921 \cdot 10^{-5}$ rad/s. This is the same as the angular velocity of the Earth about its rotation axis. The unit vectors of \mathcal{F}_e are x_e, y_e, z_e , where z_e is directed along the Earth's rotation axis.

3.2.3 North East Down frame

The North East Down (NED) frame, denoted \mathcal{F}_n , is defined as the tangent plane on the surface of the earth, moving with the spacecraft. Its unit vectors are x_n, y_n and z_n , where x_n points

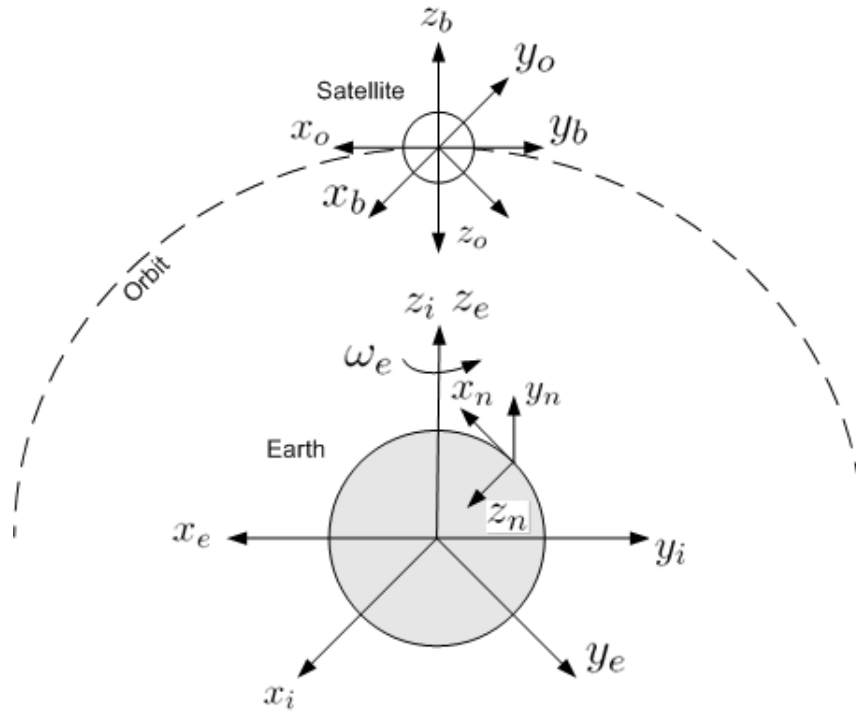


Figure 3.2: Reference frames

towards true north, y_n points to the east and z_n points towards the center of the Earth. The location of \mathcal{F}_n relative to \mathcal{F}_e is determined by using two angles l (longitude) and μ (latitude).

3.2.4 Orbit frame

The Orbit (O) frame, denoted \mathcal{F}_o , is located at the center of mass of the satellite, with the unit vectors x_o, y_o and z_o . z_o points towards the center of the Earth, while x_o points in the travelling direction of the satellite, tangent to the orbit. y_o is found using the right hand rule.

3.2.5 Body frame

The Body (B) frame, denoted \mathcal{F}_b , has its origin at the center of mass of the satellite. This frame is fixed to the satellite body. Its unit vectors x_b, y_b and z_b are usually chosen to coincide with the spacecraft's principal axes of inertia. This simplifies the spacecraft's equations of motion. Rotations about x_b, y_b and z_b are called *roll*, *pitch* and *yaw* respectively.

3.3 Rigid body dynamics

The contents of this section is largely based on the corresponding chapter in Egeland and Gravdahl (2001), hence definitions and equations found there are not referenced.

3.3.1 Vectors

Notation

A vector \vec{v} can be uniquely described in an orthogonal coordinate frame \mathcal{F}_a . The coordinates are collected in a column vector, and in \mathcal{F}_a it is denoted \mathbf{v}^a .

$$\mathbf{v}^a = \begin{bmatrix} v_{a1} \\ v_{a2} \\ v_{a3} \end{bmatrix} \quad (3.1)$$

Skew-symmetric form

The *skew-symmetric form* of a vector $\mathbf{v} = [v_1, v_2, v_3]^T$ is defined as:

$$\mathbf{v}^\times = \begin{bmatrix} 0 & -v_3 & v_2 \\ v_3 & 0 & -v_1 \\ -v_2 & v_1 & 0 \end{bmatrix} \quad (3.2)$$

The skew-symmetric form of a vector is a *skew-symmetric matrix*, defined in appendix A.4, which can be used to define the vector cross product in \mathcal{F}_a :

$$\vec{w} = \vec{u} \times \vec{v} \Leftrightarrow \mathbf{w} = (\mathbf{u}^a)^\times \mathbf{v}^a = -(\mathbf{v}^a)^\times \mathbf{u}^a \quad (3.3)$$

3.3.2 Rotation

Rotation matrix

A *rotation matrix* is a matrix $\mathbf{R} \in SO(3)$, defined by

$$SO(3) = \{ \mathbf{R} \mid \mathbf{R} \in \mathbb{R}^{3 \times 3}, \mathbf{R}^T \mathbf{R} = \mathbf{1}, \det \mathbf{R} = 1 \}, \quad (3.4)$$

where $\mathbf{1}$ is the identity matrix and $SO(3)$ is the special orthogonal group of order three. The rotation matrix transforms a coordinate vector from one reference frame to another, for instance the matrix \mathbf{R}_o^b transforms \mathbf{v}^o into \mathbf{v}^b :

$$\mathbf{v}^b = \mathbf{R}_o^b \mathbf{v}^o \quad (3.5)$$

The rotation matrix can be parameterized as

$$\mathbf{R}_{k,\theta} = \cos \theta \mathbf{1} + \mathbf{k}^\times \sin \theta + \mathbf{k} \mathbf{k}^T (1 - \cos \theta), \quad (3.6)$$

where \mathbf{k} is an arbitrary unit vector in an arbitrary reference frame, and the angle θ represents the rotation about \mathbf{k} . The parameters \mathbf{k} and θ are known as *angle-axis parameters*. Such a rotation is called a *simple rotation*. In a rotation matrix \mathbf{R} , each element c_{ij} is a directional cosine, and these can be arranged into column vectors:

$$\mathbf{R} = \begin{bmatrix} c_{11} & c_{12} & c_{13} \\ c_{21} & c_{22} & c_{23} \\ c_{31} & c_{32} & c_{33} \end{bmatrix} \quad (3.7)$$

$$\mathbf{c}_1 = \begin{bmatrix} c_{11} \\ c_{21} \\ c_{31} \end{bmatrix}, \mathbf{c}_2 = \begin{bmatrix} c_{12} \\ c_{22} \\ c_{32} \end{bmatrix}, \mathbf{c}_3 = \begin{bmatrix} c_{13} \\ c_{23} \\ c_{33} \end{bmatrix} \quad (3.8)$$

It follows that:

$$\mathbf{R} = [\mathbf{c}_1 \quad \mathbf{c}_2 \quad \mathbf{c}_3] \quad (3.9)$$

In fact, these vectors are unit vectors, hence:

$$\mathbf{c}_i^T \mathbf{c}_i = 1 \quad (3.10)$$

A composite rotation is represented by the product of two rotation matrices. The rotation from \mathcal{F}_i to \mathcal{F}_b can be expressed as follows:

$$\mathbf{R}_i^b = \mathbf{R}_o^b \mathbf{R}_i^o \quad (3.11)$$

Angular velocity

Definition 3.1. The angular velocity vector of \mathcal{F}_o relative to \mathcal{F}_b , written in \mathcal{F}_b is defined by the corresponding rotation matrix, and its time derivative:

$$(\omega_{bo}^b)^\times = \dot{\mathbf{R}}_o^b (\mathbf{R}_o^b)^T \quad (3.12a)$$

$$\omega_{bo}^b = -\omega_{ob}^b \quad (3.12b)$$

It can be shown that a similar relation exists for the directional cosines (Kristiansen, 2000):

$$\dot{\mathbf{c}}_i = (\mathbf{c}_i)^\times \omega_{ob}^b \quad (3.13)$$

3.3.3 Euler angles

Simple rotation matrices

The rotation matrices corresponding to simple rotations about the x , y and z -axis are respectively given by $\mathbf{R}_{x,\phi}$, $\mathbf{R}_{y,\theta}$ and $\mathbf{R}_{z,\psi}$. The angles ϕ , θ and ψ represent the rotations about the x , y and z -axis respectively in a rotation from one frame to another. These angles are called the Euler angles:

$$\Theta = [\phi, \theta, \psi]^T \quad (3.14)$$

The rotation matrices are given as follows:

$$\mathbf{R}_{x,\phi} = \begin{bmatrix} 1 & 0 & 0 \\ 0 & \cos \phi & -\sin \phi \\ 0 & \sin \phi & \cos \phi \end{bmatrix} \quad (3.15a)$$

$$\mathbf{R}_{y,\theta} = \begin{bmatrix} \cos \theta & 0 & \sin \theta \\ 0 & 1 & 0 \\ -\sin \theta & 0 & \cos \theta \end{bmatrix} \quad (3.15b)$$

$$\mathbf{R}_{z,\psi} = \begin{bmatrix} \cos \psi & -\sin \psi & 0 \\ \sin \psi & \cos \psi & 0 \\ 0 & 0 & 1 \end{bmatrix} \quad (3.15c)$$

Roll-pitch-yaw

The Euler angles *roll*, *pitch* and *yaw* are commonly used to describe the motion of rigid bodies like aircraft, spacecraft, ships and underwater vehicles. The rotation from \mathcal{F}_o to \mathcal{F}_b is described by a rotation ψ (yaw) about the z_o -axis, then a rotation θ about the current (rotated) y -axis (pitch) and finally a rotation ϕ about the current x -axis (roll). Using the notation $c(\cdot) = \cos(\cdot)$ and $s(\cdot) = \sin(\cdot)$, the rotation matrix becomes:

$$\mathbf{R}_o^b = \mathbf{R}_{z,\psi} \mathbf{R}_{y,\theta} \mathbf{R}_{x,\phi} = \begin{bmatrix} c\psi c\theta & -s\psi c\theta + c\psi s\theta s\phi & s\psi s\phi + c\psi c\phi s\theta \\ s\psi c\theta & c\psi c\phi + s\phi s\theta s\psi & -c\psi s\phi + s\theta s\psi c\phi \\ -s\theta & c\theta s\phi & c\theta c\phi \end{bmatrix} \quad (3.16)$$

It must be noted that \mathbf{R}_o^b is singular for $\theta = \pm\pi/2$, which means that this representation will introduce singularities into the mathematical model of a dynamic system. These singularities can be avoided when the rigid body has limits to its orientation. A satellite however can have all possible orientations, which means that this parametrization is not ideal.

3.3.4 Euler parameters

Definition of Euler parameters

The Euler parameters, also called unit quaternions, give a representation of the rotation matrix without singularities. This is done by using four parameters instead of three.

Definition 3.2. The Euler parameters are defined in terms of the angle-axis parameters, and are given by the scalar η and the vector ϵ . In coordinate form this is written

$$\eta = \cos \frac{\theta}{2} \quad (3.17)$$

$$\epsilon = [\epsilon_1, \epsilon_2, \epsilon_3]^T = \mathbf{k} \sin \frac{\theta}{2} \quad (3.18)$$

where \mathbf{k} is a unit vector. The Euler parameters satisfy the following property:

$$\eta^2 + \epsilon^T \epsilon = 1 \quad (3.19)$$

Rotation matrix in Euler parameters

The rotation matrix $\mathbf{R}_{k,\theta}$ from (3.6) can be expressed in Euler parameters as:

$$\mathbf{R}_{k,\theta} = \mathbf{R}_{\eta,\epsilon} = \mathbf{1} + 2\eta\epsilon^\times + 2(\epsilon^\times)^2 \quad (3.20)$$

A rotation matrix $\mathbf{R}_{k,\theta}$ corresponds to two sets of Euler parameters:

$$\mathbf{R}_{\eta,\epsilon} = \mathbf{R}_{-\eta,-\epsilon} \quad (3.21)$$

The inverse of $\mathbf{R}_{\eta,\epsilon}$ is given by:

$$\mathbf{R}_{\eta,\epsilon}^T = \mathbf{R}_{\eta,-\epsilon} \quad (3.22)$$

Using (3.20), the rotation matrix \mathbf{R}_o^b can be written as:

$$\mathbf{R}_o^b = \begin{bmatrix} 1 - 2(\epsilon_2^2 + \epsilon_3^2) & 2(\epsilon_1\epsilon_2 - \epsilon_3\eta) & 2(\epsilon_1\epsilon_3 + \epsilon_2\eta) \\ 2(\epsilon_1\epsilon_2 + \epsilon_3\eta) & 1 - 2(\epsilon_1^2 + \epsilon_3^2) & 2(\epsilon_2\epsilon_3 - \epsilon_1\eta) \\ 2(\epsilon_1\epsilon_3 - \epsilon_2\eta) & 2(\epsilon_2\epsilon_3 + \epsilon_1\eta) & 1 - 2(\epsilon_1^2 + \epsilon_2^2) \end{bmatrix} \quad (3.23)$$

The column vectors of (3.8) can now be expressed as:

$$\mathbf{c}_1 = \begin{bmatrix} 1 - 2(\epsilon_2^2 + \epsilon_3^2) \\ 2(\epsilon_1\epsilon_2 + \epsilon_3\eta) \\ 2(\epsilon_1\epsilon_3 - \epsilon_2\eta) \end{bmatrix}, \quad \mathbf{c}_2 = \begin{bmatrix} 2(\epsilon_1\epsilon_2 - \epsilon_3\eta) \\ 1 - 2(\epsilon_1^2 + \epsilon_3^2) \\ 2(\epsilon_2\epsilon_3 + \epsilon_1\eta) \end{bmatrix}, \quad \mathbf{c}_3 = \begin{bmatrix} 2(\epsilon_1\epsilon_3 + \epsilon_2\eta) \\ 2(\epsilon_2\epsilon_3 - \epsilon_1\eta) \\ 1 - 2(\epsilon_1^2 + \epsilon_2^2) \end{bmatrix} \quad (3.24)$$

Unit quaternions

Definition 3.3. The set Q of unit quaternions is defined as

$$Q = \left\{ \mathbf{q} \mid \mathbf{q}^T \mathbf{q} = 1, \mathbf{q} = [\eta, \epsilon^T]^T, \epsilon \in \mathbb{R}^3, \eta \in \mathbb{R} \right\}, \quad (3.25)$$

where \mathbf{q} is the unit quaternion corresponding to $\mathbf{R}_{\eta,\epsilon}$. The unit quaternion corresponding to $\mathbf{R}_{\eta,-\epsilon}$ is the *inverse unit quaternion* $\bar{\mathbf{q}}$, and the unit quaternion corresponding to the identity matrix $\mathbf{R}_{1,0} = \mathbf{1}$ is the identity quaternion \mathbf{q}_{id} . These quaternions are defined by:

$$\bar{\mathbf{q}} = \begin{bmatrix} \eta \\ -\epsilon \end{bmatrix} \quad (3.26)$$

$$\mathbf{q}_{id} = \begin{bmatrix} 1 \\ 0 \end{bmatrix} \quad (3.27)$$

Note that the inverse rotation matrix now can be written as follows (Fjellstad et al., 1994):

$$\mathbf{R}^{-1}(\mathbf{q}) = \mathbf{R}^T(\mathbf{q}) = \mathbf{R}(\bar{\mathbf{q}}) \quad (3.28)$$

Quaternion product

Definition 3.4. The quaternion product between two vectors $\mathbf{q}_1 = [\eta_1, \epsilon_1^T]^T$ and $\mathbf{q}_2 = [\eta_2, \epsilon_2^T]^T$ is defined by (Fjellstad et al., 1994):

$$\mathbf{q}_1 \mathbf{q}_2 = \begin{bmatrix} \eta_1 & -\epsilon_1^T \\ \epsilon_1 & \eta_1 \mathbf{1} + \epsilon_1^\times \end{bmatrix} \begin{bmatrix} \eta_2 \\ \epsilon_2 \end{bmatrix}, \quad (3.29)$$

where $\eta_1, \eta_2 \in \mathbb{R}$ and $\epsilon_1, \epsilon_2 \in \mathbb{R}^3$. It should be noted that the vectors do not need to be unit quaternions.

A rotation can be described by the quaternion product. The transformation $\mathbf{R}_{\eta, \epsilon} \mathbf{v}$, where \mathbf{v} is a vector, can be calculated with the following quaternion product:

$$\begin{bmatrix} 0 \\ \mathbf{R}_{\eta, \epsilon} \end{bmatrix} = \begin{bmatrix} \eta \\ \epsilon \end{bmatrix} \begin{bmatrix} 0 \\ \mathbf{v} \end{bmatrix} \begin{bmatrix} \eta \\ -\epsilon \end{bmatrix} \quad (3.30)$$

As stated in section 3.3.3, successive rotations involves multiplication of rotation matrices. It can be shown that (Fjellstad et al., 1994):

$$\mathbf{R}(\mathbf{q}_1) \mathbf{R}(\mathbf{q}_2) = \mathbf{R}(\mathbf{q}_1 \mathbf{q}_2) \quad (3.31)$$

3.3.5 Kinematic differential equations

The kinematic differential equations in reference to \mathcal{F}_a and \mathcal{F}_b in Euler parameters are given as:

$$\dot{\eta} = -\frac{1}{2} \epsilon^T \omega_{ab} \quad (3.32a)$$

$$\dot{\epsilon} = \frac{1}{2} [\eta \mathbf{1} + \epsilon^\times] \omega_{ab} \quad (3.32b)$$

3.3.6 Attitude error

The actual attitude of a spacecraft is given by the rotation matrix $\mathbf{R} = \mathbf{R}_i^b$. Let \mathcal{F}_o be a desired orientation, represented by $\mathbf{R}_d = \mathbf{R}_i^o$. This means that we want \mathcal{F}_b to coincide with \mathcal{F}_o , i.e. $\mathbf{R} = \mathbf{R}_d$. Fjellstad et al. (1994) defines the attitude error $\tilde{\mathbf{R}}$ as:

$$\tilde{\mathbf{R}} = \mathbf{R}_d^{-1} \mathbf{R} = \mathbf{R}_d^T \mathbf{R} \quad (3.33)$$

When the attitude error is zero, then $\tilde{\mathbf{R}} = \mathbf{1}$. When using unit quaternions, the error quaternion $\tilde{\mathbf{q}}$ can be written as (Fjellstad et al., 1994)

$$\tilde{\mathbf{q}} = \tilde{\mathbf{q}}_d \mathbf{q} = \begin{bmatrix} \eta_d & \epsilon_d^T \\ -\epsilon_d & \eta_d \mathbf{1} - \epsilon_d^\times \end{bmatrix} \begin{bmatrix} \eta \\ \epsilon \end{bmatrix}, \quad (3.34)$$

where \mathbf{q}_d is the desired quaternion. This expression is found by combining (3.28), (3.29) and (3.31). This can be written on component form as:

$$\begin{bmatrix} \tilde{q}_1 \\ \tilde{q}_2 \\ \tilde{q}_3 \\ \tilde{q}_4 \end{bmatrix} = \begin{bmatrix} q_{1d} & q_{2d} & q_{3d} & q_{4d} \\ -q_{2d} & q_{1d} & q_{4d} & -q_{3d} \\ -q_{3d} & -q_{4d} & q_{1d} & q_{2d} \\ -q_{4d} & q_{3d} & -q_{2d} & q_{1d} \end{bmatrix} \begin{bmatrix} q_1 \\ q_2 \\ q_3 \\ q_4 \end{bmatrix} \quad (3.35)$$

For zero attitude error, the error quaternion has two possible values (Fjellstad et al., 1994):

$$\mathbf{q} = \mathbf{q}_d \Leftrightarrow \tilde{\mathbf{q}} = \begin{bmatrix} \pm 1 \\ 0 \end{bmatrix} \quad (3.36)$$

The attitude error differential equations becomes (Fjellstad et al., 1994)

$$\dot{\tilde{\eta}} = -\frac{1}{2} \tilde{\epsilon}^T \tilde{\omega} \quad (3.37a)$$

$$\dot{\tilde{\epsilon}} = -\frac{1}{2} [\tilde{\eta} \mathbf{1} + \tilde{\epsilon}^\times] \tilde{\omega} \quad (3.37b)$$

where $\tilde{\omega}$ is the error in angular velocity. Note that (3.37) has the same form as (3.32).

3.3.7 Angular velocity error

The error in angular velocity $\tilde{\omega}$ is given in reference to a desired reference frame \mathcal{F}_d . The error is zero when \mathcal{F}_b and \mathcal{F}_d have the same angular velocity. An expression for the angular velocity error can be obtained from the following:

$$\omega_{ib}^b = \omega_{db}^b + \omega_{id}^b = \omega_{db}^b + \mathbf{R}_d^b \omega_{id}^d \quad (3.38)$$

We can see from this expression that ω_{db}^b is a representation of the error in angular velocity. When this is zero, \mathcal{F}_b rotates with the same angular velocity as \mathcal{F}_d . Thus, the angular velocity error is:

$$\tilde{\omega} = \omega_{db}^b = \omega_{ib}^b - \mathbf{R}_d^b \omega_{id}^d \quad (3.39)$$

This definition is used in Hall et al. (2002) and Kristiansen (2000).

3.3.8 Momentum, angular momentum and the inertia matrix

Definition 3.5. The *momentum* \mathbf{p}^b of a rigid body with mass m , written in \mathcal{F}_b , is

$$\mathbf{p}^b = m \mathbf{v}^b \quad (3.40)$$

where \mathbf{v}^b is the body's linear velocity.

The *angular momentum* or spin \mathbf{h}^b of a rigid body in \mathcal{F}_b about its center of mass is given by

$$\mathbf{h}^b = \int_b (\mathbf{r}^b)^\times (\omega_{ib}^b)^\times \mathbf{r}^b dm \quad (3.41)$$

$$= \int_b \left[(\mathbf{r}^b)^2 \mathbf{1} - \mathbf{r}^b (\mathbf{r}^b)^T \right] dm \omega_{ib}^b \quad (3.42)$$

where \mathbf{r}^b is the distance from the center of mass to the mass element dm . This leads to the definition of the inertia matrix.

Definition 3.6. The inertia matrix about the center of mass of a rigid body is defined as:

$$\mathbf{I} = \int_b \left[(\mathbf{r}^b)^2 \mathbf{1} - \mathbf{r}^b (\mathbf{r}^b)^T \right] dm \quad (3.43)$$

Definition 3.7. The angular momentum of a rigid body about its center of mass is given by:

$$\mathbf{h}^b = \mathbf{I} \omega_{ib}^b \quad (3.44)$$

3.4 Gyrostat model

3.4.1 Equations of motion

A gyrostat is a rigid body, fixed to one or more spinning wheels (rotors). The wheel can be inside or outside the rigid body. The equations of motion of a one wheel gyrostat in \mathcal{F}_b in reference to \mathcal{F}_i is given in Hughes (1986) as

$$\mathbf{p}^b = m \mathbf{v}^b - (\mathbf{c}^b)^\times \omega_{ib}^b \quad (3.45a)$$

$$\mathbf{h}^b = (\mathbf{c}^b)^\times \mathbf{v}^b + \mathbf{I} \omega_{ib}^b + \mathbf{a}^b i_s \omega_s \quad (3.45b)$$

$$h_a = i_s \mathbf{a}^T \omega_{ib}^b + i_s \omega_s \quad (3.45c)$$

where \mathbf{p}^b is the momentum of the gyrostat, m is its total mass, \mathbf{v}^b is its linear velocity, \mathbf{c}^b is a constant vector, ω_{ib}^b is the body's angular velocity, \mathbf{h}^b is the angular momentum of the gyrostat, \mathbf{I} is the inertia matrix of the entire system, \mathbf{a}^b is a unit vector giving the axis of rotation of the rotor, i_s is the moment of inertia of the rotor, ω_s is the rotor's angular velocity and h_a is the angular momentum of the rotor. The time derivatives of these equations are given by

$$\dot{\mathbf{p}}^b = -(\omega_{ib}^b)^\times \mathbf{p}^b + \mathbf{f}^b \quad (3.46a)$$

$$\dot{\mathbf{h}}^b = -(\omega_{ib}^b)^\times \mathbf{h}^b - (\mathbf{v}^b)^\times \mathbf{p}^b + \boldsymbol{\tau}_e \quad (3.46b)$$

$$\dot{h}_a = \tau_a \quad (3.46c)$$

where \mathbf{f}^b is the external force acting on the gyrostat, $\boldsymbol{\tau}_e$ is the resulting external torque and τ_a is the net torque applied to the rotor.

This model can be simplified, by placing the origin of \mathcal{F}_b in the center of mass of the gyrostat (Hughes, 1986). In that case, \mathbf{c}^b becomes zero, and the translational motion and the rotational motion become decoupled. This has been done by Hall, Tsiotras and Shen (2002), who have developed a similar model for an N -wheel gyrostat. By neglecting the translational motion, the rotational equations of motion for a rigid body, with internal momentum wheels, can be expressed as

$$\dot{\mathbf{h}}^b = (\mathbf{h}^b)^\times \mathbf{J}^{-1}(\mathbf{h}^b - \mathbf{A}\mathbf{h}_a^b) + \tau_e \quad (3.47a)$$

$$\dot{\mathbf{h}}_a^b = \tau_a \quad (3.47b)$$

where \mathbf{h}^b is the system angular momentum, which in \mathcal{F}_b is given by

$$\mathbf{h}^b = \mathbf{I}\omega_{ib}^b + \mathbf{A}\mathbf{I}_s\omega_s, \quad (3.48)$$

and \mathbf{h}_a^b is the N dimensional vector of axial angular momenta of the rotors:

$$\mathbf{h}_a^b = \mathbf{I}_s\mathbf{A}^T\omega_{ib}^b + \mathbf{I}_s\omega_s \quad (3.49)$$

The vector ω_s is N dimensional, representing the axial angular velocities of the rotors relative to the body, while τ_e is the 3 dimensional vector of external torques (e.g. thrusters and gravitation), τ_a is the N dimensional vector of internal axial torques applied by the rigid body to the rotors, \mathbf{A} is the $3 \times N$ matrix containing the axial vectors of the N rotors, and \mathbf{I} is the angular momentum, or inertia matrix, of the system, including the rotors. The matrix $\mathbf{I}_s = \text{diag}\{i_{s1}, \dots, i_s\}$ is an $N \times N$ diagonal matrix containing the axial moments of inertia of the rotors. The matrix \mathbf{J} is an inertia-like matrix defined as

$$\mathbf{J} = \mathbf{I} - \mathbf{A}\mathbf{I}_s\mathbf{A}^T \quad (3.50)$$

and can be interpreted as the inertia matrix of an equivalent system where all the rotors have zero axial moment of inertia. The angular velocity ω_{ib}^b of the body frame in reference to an inertial frame, can be written as

$$\omega_{ib}^b = \mathbf{J}^{-1}(\mathbf{h}^b - \mathbf{A}\mathbf{h}_a^b) \quad (3.51)$$

3.4.2 Kinetic energy

According to Hughes (1986), the kinetic energy E_k and its time derivative of a one wheel gyrostat can be expressed as:

$$E_k = \frac{1}{2}m(\mathbf{v}^b)^T\mathbf{v}^b + \frac{1}{2}(\omega_{ib}^b)^T\mathbf{I}\omega_{ib}^b + \frac{1}{2}i_s\omega_s^2 - \mathbf{v}^T\mathbf{c}^\times\omega_{ib}^b + i_s\omega_s\mathbf{a}^T\omega_{ib}^b \quad (3.52a)$$

$$\dot{E}_k = \mathbf{f}^T\mathbf{v}^b + \tau_e^T\omega_{ib}^b + \tau_a\omega_s \quad (3.52b)$$

3.5 Disturbance torques

There are several external disturbance torques affecting a spacecraft. Hughes (1986) include the gravitational torque, the aerodynamic torque, radiation torques and the magnetic torque. The aerodynamic torque is only applicable at low altitudes. In this thesis, we will suppose that all disturbance torques can be neglected, except for the gravitational torque.

3.5.1 Gravity gradient torque

The expression describing the gravity gradient torque is greatly simplified by making the following assumptions (Hughes, 1986):

1. Only one celestial primary is considered (e.g. Earth).
2. The celestial primary possesses a spherically symmetrical mass distribution.
3. The spacecraft is small compared to its distance from the mass center of the celestial primary.
4. The spacecraft consists of a single body.

Hughes (1986) has shown that by making these assumptions, the expression for the gravity gradient is

$$\vec{\tau}_g = 3 \left(\frac{\mu}{r_c^3} \right) \vec{z}_o \times \mathbf{I} \vec{z}_o \quad (3.53)$$

where r_c is the distance from the center of mass of the celestial primary to the mass center of the spacecraft. The constant $\mu = Gm_p$, where G is the universal gravitational constant and m_p is the mass of the celestial primary. If the Earth is considered as the celestial primary, G , m_p and μ have the following numerical values:

$$G = 6.67 \cdot 10^{-11} \text{ Nm}^2/\text{kg}^2 \quad (3.54)$$

$$m_p = 5.97 \cdot 10^{24} \text{ kg} \quad (3.55)$$

$$\mu = 3.986 \cdot 10^{14} \text{ Nm}^2/\text{kg} \quad (3.56)$$

We will now introduce the following notation:

$$\omega_c^2 = \frac{\mu}{r_c^3} \quad (3.57)$$

According to Hughes (1986), " $\omega_c r_c$ is the speed of the spacecraft in a circular orbit of radius r_c ". This means that ω_c represents the angular velocity of the orbit frame \mathcal{F}_o about its y_o axis. Note that ω_c is constant if the orbit is circular, since r_c will be constant. The gravity gradient written in the body frame \mathcal{F}_b is

$$\tau_g = 3\omega_c^2 \mathbf{c}_3 \times \mathbf{I} \mathbf{c}_3 = 3\omega_c^2 (\mathbf{c}_3)^\times \mathbf{I} \mathbf{c}_3 \quad (3.58)$$

where \mathbf{c}_3 is defined in (3.8). The vector \mathbf{c}_3 transforms the z_b axis to the z_o axis. Since $\vec{z}_b = [0, 0, 1]^T$ in \mathcal{F}_b , the unit vector in \mathcal{F}_b corresponding to \vec{z}_o is \mathbf{c}_3 .

3.5.2 Potential energy

The potential energy of a spacecraft due to gravity is given by (Hughes, 1986):

$$E_p = -\frac{\mu m}{r_c} - \frac{1}{2}\omega_c^2 (i_x + i_y + i_z) + \frac{3}{2}\mathbf{c}_3^T \mathbf{I} \mathbf{c}_3 \quad (3.59)$$

Note that the two first terms are constants if the spacecraft orbit is circular.

3.6 Stability analysis

3.6.1 Linear systems

Stability analysis for linear systems is quite straightforward. The theorem below is sufficient, and can be found in Khalil (2000) as Theorem 4.6. A linear time-invariant system can be written as:

$$\dot{\mathbf{x}} = \mathbf{A} \mathbf{x} \quad (3.60)$$

Theorem 3.1. *The equilibrium point $\mathbf{x} = 0$ of (3.60) is stable if and only if all eigenvalues λ_i of \mathbf{A} satisfy $\text{Re}\lambda_i \leq 0$ and for every eigenvalue with $\text{Re}\lambda_i = 0$ and algebraic multiplicity $q_i \geq 2$, $\text{rank}(\mathbf{A} - \lambda_i \mathbf{1}) = n - q_i$, where n is the dimension of \mathbf{x} . The equilibrium point $\mathbf{x} = 0$ is (globally) asymptotically stable if and only if all eigenvalues of \mathbf{A} satisfy $\text{Re}\lambda_i < 0$. If this is the case, \mathbf{A} is called a Hurwitz matrix.*

3.6.2 Nonlinear systems

Lyapunov analysis is widely used to prove stability of equilibrium points in nonlinear dynamical systems. The following theorem is also known as Lyapunov's direct method, and can be found in Khalil (2000) as Theorem 4.1.

Theorem 3.2. *Let $\mathbf{x} = 0$ be an equilibrium point for the system $\dot{\mathbf{x}} = f(\mathbf{x})$ and $D \subset \mathbb{R}^n$ be a domain containing $\mathbf{x} = 0$. Let $V : D \rightarrow \mathbb{R}$ be a continuously differentiable function such that:*

$$V(0) = 0 \text{ and } V(\mathbf{x}) > 0 \text{ in } D - \{0\} \quad (3.61)$$

$$\dot{V}(\mathbf{x}) \leq 0 \text{ in } D \quad (3.62)$$

Then, $\mathbf{x} = 0$ is stable. $\mathbf{x} = 0$ is asymptotically stable if:

$$\dot{V}(\mathbf{x}) < 0 \text{ in } D - \{0\} \quad (3.63)$$

The next theorem is known as LaSalle's theorem. The following two corollaries are useful consequences of this theorem. They are taken from Khalil (2000), where they are known as Theorem 4.4, Corollary 4.1 and Corollary 4.2.

Theorem 3.3. *(LaSalle) Let $\Omega \subset D$ be a compact set that is positively invariant with respect to $\dot{\mathbf{x}} = f(\mathbf{x})$. Let $V : D \rightarrow \mathbb{R}$ be a continuously differentiable function such that $\dot{V}(\mathbf{x}) \leq 0$ in Ω . Let E be the set of all points in Ω where $\dot{V}(\mathbf{x}) = 0$. Let M be the largest invariant set in E . Then every solution starting in Ω approaches M as $t \rightarrow \infty$.*

Corollary 3.1. Let $\mathbf{x} = 0$ be an equilibrium point for $\dot{\mathbf{x}} = f(\mathbf{x})$. Let $V : D \rightarrow \mathbb{R}$ be a continuously differentiable positive definite function on a domain D containing the origin $\mathbf{x} = 0$, such that $\dot{V}(\mathbf{x}) \leq 0$ in D . Let $S = \{\mathbf{x} \in D \mid \dot{V}(\mathbf{x}) = 0\}$ and suppose that no solution can stay identically in S , other than the trivial solution $\mathbf{x}(t) \equiv 0$. Then, the origin is asymptotically stable.

Corollary 3.2. Let $x = 0$ be an equilibrium point for $\dot{\mathbf{x}} = f(\mathbf{x})$. Let $V : \mathbb{R}^n \rightarrow \mathbb{R}$ be a continuously differentiable, radially unbounded, positive definite function such that $\dot{V}(\mathbf{x}) \leq 0$ for all $\mathbf{x} \in \mathbb{R}^n$. Let $S = \{\mathbf{x} \in \mathbb{R}^n \mid \dot{V}(\mathbf{x}) = 0\}$ and suppose that no solution can stay identically in S , other than the trivial solution $\mathbf{x}(t) \equiv 0$. Then the origin is globally asymptotically stable.

3.7 Linear control algorithms

3.7.1 Controllability

The linear control problem can be stated as follows (Khalil, 2000):

$$\dot{\mathbf{x}} = \mathbf{A}\mathbf{x} + \mathbf{B}\mathbf{u} \quad (3.64)$$

To be able to control a linear system, it must be *controllable*. This property can be verified by applying the following definition (Balchen, Andresen and Foss, 2001).

Definition 3.8. The system (3.64) is controllable if and only if the rank of $\mathbf{Q}_c = n$, where n is the dimension of \mathbf{x} , and \mathbf{Q}_c is given by:

$$\mathbf{Q}_c = [\mathbf{B}, \mathbf{A}\mathbf{B}, \mathbf{A}^2\mathbf{B}, \dots, \mathbf{A}^{n-1}\mathbf{B}] \quad (3.65)$$

3.7.2 Basic linear controllers

Consider the system (3.64). Choosing the control input $\mathbf{u} = -\mathbf{K}_p\mathbf{x}$ where $\mathbf{K}_p > 0$ yields:

$$\dot{\mathbf{x}} = (\mathbf{A} - \mathbf{B}\mathbf{K}_p)\mathbf{x} \quad (3.66)$$

This system is globally asymptotically stable if $(\mathbf{A} - \mathbf{B}\mathbf{K}_p)$ is Hurwitz (theorem 3.1). This can be done if (3.64) is controllable (Khalil, 2000). The control law is $\mathbf{u} = -\mathbf{K}_p\mathbf{x}$ is called a P controller. Linear controllers have the following form:

$$\mathbf{u} = -\mathbf{K}_p\mathbf{x} - \mathbf{K}_d\dot{\mathbf{x}} - \mathbf{K}_i \int \mathbf{x} dt \quad (3.67a)$$

$$\mathbf{K}_p > 0, \mathbf{K}_d \geq 0, \mathbf{K}_i \geq 0 \quad (3.67b)$$

If all terms are greater than zero, the controller is called a PID controller. The second term is the D term. It makes the controller work faster at high frequencies (Balchen et al., 2001). The third (I) term corresponds to integral control. It is used to eliminate steady-state errors (Balchen et al., 2001).

3.7.3 Quaternion feedback control

The classical model of a spacecraft as a rigid body is presented below (Wie, 1998):

$$\mathbf{I}\dot{\omega}_{ib}^b = (\omega_{ib}^b)^\times \mathbf{I}\omega_{ib}^b + \tau \quad (3.68)$$

Wie (1998) suggests the following controller using quaternion feedback to control the attitude of the rigid spacecraft (3.68)

$$\tau = -\mathbf{K}_\epsilon \tilde{\epsilon} - \mathbf{K}_\omega \omega_{ib}^b \quad (3.69a)$$

$$\mathbf{K}_\epsilon = [\alpha \mathbf{I} + \beta \mathbf{1}]^{-1} \quad (3.69b)$$

$$\mathbf{K}_\epsilon^{-1} \mathbf{K}_\omega > 0 \quad (3.69c)$$

where τ is the applied torque, $\tilde{\mathbf{q}} = [\tilde{\eta}, \tilde{\epsilon}^T]^T$ is the attitude error quaternion vector, and \mathbf{K}_q and \mathbf{K}_ω are constant controller gain matrices. This is essentially a PD controller, since $\tilde{\mathbf{q}}$ represents the attitude while ω_{ib}^b is the angular velocity. Note that $\dot{\tilde{\mathbf{q}}} \neq \omega_{ib}^b$. The attitude error quaternion is calculated as in (3.34). We will assume that the desired attitude quaternion equals the origin, i.e. $\tilde{\mathbf{q}} = [1, 0, 0, 0]^T$. There is no loss of generality in this assumption, since all desired quaternions can be translated to the origin. Note that the quaternion $[-1, 0, 0, 0]^T$ is an equivalent definition of the origin, since this quaternion corresponds to the same orientation as \mathbf{q}_d (Wie, 1998). In the following example, we will prove that (3.69) indeed stabilizes (3.68) using Lyapunov analysis. This proof can be found in Wie, Weiss and Arapostathis (1989).

Example 3.1. The mathematical model of a rigid spacecraft is given by (3.68) and (3.37)

$$\mathbf{I}\dot{\omega}_{ib}^b = (\omega_{ib}^b)^\times \mathbf{I}\omega_{ib}^b + \tau \quad (3.70a)$$

$$\dot{\tilde{\eta}} = -\frac{1}{2} \tilde{\epsilon}^T \tilde{\omega} \quad (3.70b)$$

$$\dot{\tilde{\epsilon}} = -\frac{1}{2} [\tilde{\eta} \mathbf{1} + \tilde{\epsilon}^\times] \tilde{\omega} \quad (3.70c)$$

where τ is given by (3.69a). The desired angular velocity is $\omega_{ib}^b = 0$, which means that $\tilde{\omega} = \omega_{ib}^b$. To use theorem 3.2, a Lyapunov function candidate (LFC) must be chosen. We will use the following function where the state vector $\mathbf{x} = [(\omega_{ib}^b)^T, \tilde{\mathbf{q}}^T]^T$:

$$V = \frac{1}{2} (\omega_{ib}^b)^T \mathbf{K}_\epsilon^{-1} \mathbf{I} \omega_{ib}^b + \tilde{\epsilon}^T \tilde{\epsilon} + (\tilde{\eta} - 1)^2 \quad (3.71)$$

Note that $V > 0$ when $\mathbf{x} \neq 0$ and for the equilibrium point $\mathbf{x}^* = [0, 0, 0, 1, 0, 0, 0]^T$, $V = 0$. An important remark is that $V = 0$ only if $\tilde{\eta} = 1$, not -1 , even though $\tilde{\eta} = \pm 1$ represents the same orientation. Applying (3.19), V can be rewritten as:

$$V = \frac{1}{2} (\omega_{ib}^b)^T \mathbf{K}_\epsilon^{-1} \mathbf{I} \omega_{ib}^b + 2(1 - \tilde{\eta}) \quad (3.72)$$

Assuming that $\mathbf{K}_\epsilon \mathbf{I} = (\mathbf{K}_\epsilon^{-1} \mathbf{I})^T$, we get the following expression for \dot{V} :

$$\dot{V} = (\omega_{ib}^b)^T \mathbf{K}_\epsilon^{-1} \mathbf{I} \dot{\omega}_{ib}^b - 2\dot{\tilde{\eta}} \quad (3.73)$$

$$= (\omega_{ib}^b)^T \mathbf{K}_\epsilon^{-1} \left[(\omega_{ib}^b)^\times \mathbf{I} \omega_{ib}^b - \mathbf{K}_\epsilon \tilde{\epsilon} - \mathbf{K}_\omega \omega_{ib}^b \right] + (\omega_{ib}^b)^T \tilde{\epsilon} \quad (3.74)$$

$$= (\omega_{ib}^b)^T \mathbf{K}_\epsilon^{-1} (\omega_{ib}^b)^\times \mathbf{I} \omega_{ib}^b - (\omega_{ib}^b)^T \mathbf{K}_\epsilon^{-1} \mathbf{K}_\omega \omega_{ib}^b \quad (3.75)$$

For stability we require $\dot{V} \leq 0$. The second term in the final expression for \dot{V} is quadratic, and it is negative if $\mathbf{K}_\epsilon^{-1} \mathbf{K}_\omega > 0$. We now choose $\mathbf{K}_\epsilon^{-1} = \alpha \mathbf{I} + \beta \mathbf{1}$, where $\alpha \geq 0$, $\beta \geq 0$ and $\mathbf{K}_\epsilon^{-1} \neq 0$. The first term becomes:

$$(\omega_{ib}^b)^T \mathbf{K}_\epsilon^{-1} (\omega_{ib}^b)^\times \mathbf{I} \omega_{ib}^b = (\omega_{ib}^b)^T [\alpha \mathbf{I} + \beta \mathbf{1}] (\omega_{ib}^b)^\times \mathbf{I} \omega_{ib}^b \quad (3.76)$$

$$= \alpha (\mathbf{I} \omega_{ib}^b)^T (\omega_{ib}^b)^\times (\mathbf{I} \omega_{ib}^b) + \beta (\omega_{ib}^b)^T (\omega_{ib}^b)^\times \mathbf{I} \omega_{ib}^b \quad (3.77)$$

The first term is equal to zero because of the skew-symmetric form (see definition A.4). The second term involves a vector cross product of the same vector, and is hence zero. The final expression for \dot{V} is:

$$\dot{V} = -(\omega_{ib}^b)^T \mathbf{K}_\epsilon^{-1} \mathbf{K}_\omega \omega_{ib}^b \leq 0 \quad (3.78)$$

Choosing $\mathbf{K}_\omega = k_\omega \mathbf{1}$ or $\mathbf{K}_\omega = k_\omega \mathbf{J}$ ensures that $\mathbf{K}_\epsilon^{-1} \mathbf{K}_\omega > 0$. It is now possible to apply corollary 3.2 to prove global asymptotic stability for \mathbf{x}^* . It follows from (3.78) that $\omega_{ib}^b \rightarrow 0$. This implies that $\dot{\omega}_{ib}^b \rightarrow 0$, which means that $\tau \rightarrow 0 \Rightarrow \tilde{\epsilon} \rightarrow 0 \Rightarrow \tilde{\eta} \rightarrow 1 \Rightarrow \mathbf{x} \rightarrow \mathbf{x}^*$. Hence \mathbf{x}^* is globally asymptotically stable. Note that the orientation $\tilde{\mathbf{q}} = [-1, 0, 0, 0]^T$ is unstable although representing the same orientation as $\tilde{\mathbf{q}}^* = [1, 0, 0, 0]^T$.

3.8 Nonlinear control algorithms

3.8.1 Control laws from Lyapunov analysis

A common way of designing control laws for dynamical systems, is to perform Lyapunov analysis, and choose an appropriate control law which yields a stable system by assuring that theorem 3.2 holds. This is done with a gyrostat in Hall et al. (2002).

3.8.2 Feedback linearization

The following example will illustrate the idea of feedback linearization. The concept is to cancel nonlinearities to obtain a linear control problem.

Example 3.2. The pendulum equation with a control input u can be written as (Khalil, 2000)

$$\dot{x}_1 = x_2 \quad (3.79a)$$

$$\dot{x}_2 = -\frac{g}{l} \sin x_1 - \frac{k}{m} x_2 + b u \quad (3.79b)$$

where g is the gravity constant, l is the length of the rigid rod with zero mass, m is the mass of the bob, k is a coefficient of friction and c is a constant. These parameters are all positive. If

we choose the following control law, we will cancel the nonlinear term and introduce a virtual control input v :

$$u = \frac{1}{b} \left(\frac{g}{l} \sin x_1 + v \right) \quad (3.80)$$

Inserting this control law, our system equations become:

$$\dot{x}_1 = x_2 \quad (3.81a)$$

$$\dot{x}_2 = -\frac{k}{m} x_2 + v \quad (3.81b)$$

This system is linear, and it is therefore possible to substitute v with a linear controller to stabilize the system. Note that canceling nonlinearities to stabilize a system is not always possible, nor advisable in practice. In practice canceling nonlinearities may lead to unnecessary large control inputs. To be able to use nonlinearity cancellation, the nonlinear state equation must have the structure

$$\dot{\mathbf{x}} = \mathbf{A}\mathbf{x} + \mathbf{B}\mathbf{G}(\mathbf{x}) [\mathbf{u} - \mathbf{H}(\mathbf{x})] \quad (3.82)$$

where $\mathbf{G}(\mathbf{x})$ is nonsingular. For more details see Khalil (2000).

3.8.3 Sliding mode control

The idea of sliding mode control is to bring the system states to a manifold or surface where the states stay for all future time. The manifold is designed in such a way that once the system states are on the manifold, they will converge to the desired states. One of the great advantages of sliding mode control, is that it is robust to parameter uncertainties. This technique is explained in the following example, which is the motivating example in Khalil (2000).

Example 3.3. Consider the following system

$$\dot{x}_1 = x_2 \quad (3.83a)$$

$$\dot{x}_2 = h(\mathbf{x}) + g(\mathbf{x}) u \quad (3.83b)$$

where $\mathbf{x} = [x_1, x_2]^T$, h and g are unknown nonlinear functions, and $g(\mathbf{x}) \geq g_0 > 0$ for all \mathbf{x} . To stabilize the origin, we will design a control law that constrains the motion of the system to a manifold or surface. We will choose this manifold s :

$$s = a_1 x_1 + x_2 = 0 \quad (3.84)$$

On the above manifold, the motion is governed by $\dot{x}_1 = -a_1 x_1$. Choosing $a_1 > 0$ guarantees that \mathbf{x} reaches zero. The rate of convergence is controlled by the choice of a_1 . We will now find a way to bring the system states to the manifold $s = 0$. \dot{s} is given by:

$$\dot{s} = a_1 \dot{x}_1 + \dot{x}_2 = a_1 x_2 + h(\mathbf{x}) + g(\mathbf{x}) u \quad (3.85)$$

Suppose that h and g satisfy the following inequality

$$\left| \frac{a_1 x_2 + h(\mathbf{x})}{g(\mathbf{x})} \right| \leq \delta(\mathbf{x}), \quad \forall x \in \mathbb{R}^2 \quad (3.86)$$

where $\delta(\mathbf{x})$ represents the uncertainty due to the unknown functions h and g . We now choose the LFC

$$V = \frac{1}{2}s^2, \quad (3.87)$$

and find its time derivative:

$$\dot{V} = s\dot{s} = s[a_1 x_2 + h(\mathbf{x})] + g(\mathbf{x})su \quad (3.88)$$

$$\leq g(\mathbf{x})|s|\delta(\mathbf{x}) + g(\mathbf{x})su \quad (3.89)$$

The control input is chosen as:

$$u = -\beta(\mathbf{x}) \operatorname{sgn}(s) \quad (3.90a)$$

$$\beta(\mathbf{x}) \geq \sigma(\mathbf{x}) + \beta_0, \quad \beta_0 > 0 \quad (3.90b)$$

$$\operatorname{sgn}(s) = \begin{cases} 1, & s > 0 \\ 0, & s = 0 \\ -1, & s < 0 \end{cases} \quad (3.90c)$$

This yields:

$$\dot{V} \leq g(\mathbf{x})|s|\delta(\mathbf{x}) - g(\mathbf{x})[\delta(\mathbf{x}) + \beta_0]s \operatorname{sgn}(s) = -g(\mathbf{x})\beta_0|s| \quad (3.91)$$

$$\leq -g_0\beta_0|s| \quad (3.92)$$

For $s \neq 0$, $\dot{V} < 0 \Rightarrow s \rightarrow 0$. This means that the system states reaches the manifold $s = 0$ in finite time, which is known as the *reaching phase*. When the manifold is reached, $\mathbf{x} \rightarrow 0$ in the so called *sliding phase*. The manifold $s = 0$ is called a *sliding manifold* or a *sliding surface*. The control input $u = -\beta(\mathbf{x}) \operatorname{sgn}(s)$ is called *sliding mode control*. The great advantage of sliding mode control is that we only need to know the upper bound $\delta(\mathbf{x})$, as opposed to requiring accurate models of h and g .

A weakness of sliding mode control is the presence of *chattering*. Chattering occurs because of imperfections in switching, which is caused by the function $\operatorname{sgn}(s)$. When implementing a sliding mode controller, there will always be a delay between the time the sign of s changes and the time the control switches. This means that the system states never actually reach the sliding manifold. Instead they oscillate, as shown in figure 3.3. This results in low accuracy and strain on mechanical parts. To remedy this, the sign function can be replaced by a saturation function, i.e. the control law becomes

$$u = -\beta(\mathbf{x}) \operatorname{sat}(s/\gamma) \quad (3.93a)$$

$$\operatorname{sat}(s/\gamma) = \begin{cases} s/\gamma, & |s/\gamma| \leq 1 \\ \operatorname{sgn}(s/\gamma), & |s/\gamma| > 1 \end{cases} \quad (3.93b)$$

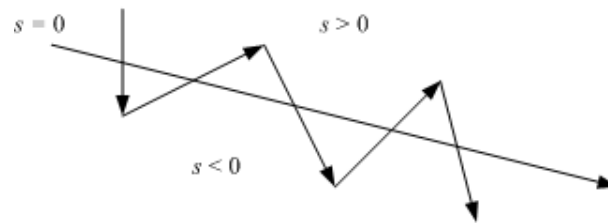


Figure 3.3: Chattering

where γ is a positive constant. To get a good approximation of the sign function, γ should be chosen small. Another function which can replace the sign function is the hyperbolic tangent, as in Fossen (2002), i.e. the control law is chosen as:

$$u = -\beta(\mathbf{x}) \tanh(s/\gamma) \tag{3.94}$$

Note that this function is smooth, as opposed to the sign function and the saturation function. The sign function and its approximations are shown in figure 3.4. Both substitutions can eliminate chattering. The cost is decreased accuracy. The system states never converge to the sliding manifold, but remains within a boundary layer which depends on the parameter γ , as shown in figure 3.5.

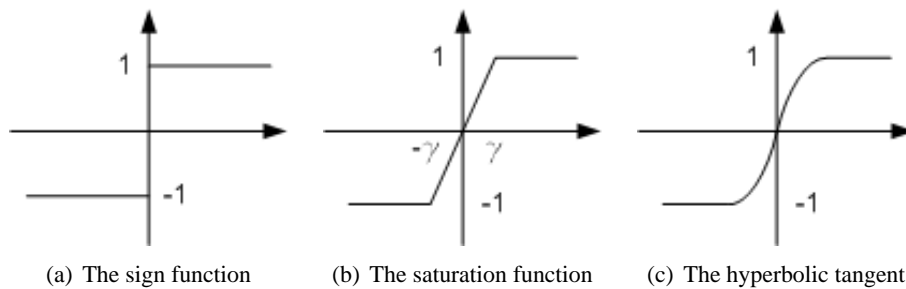


Figure 3.4: The sign function with approximations

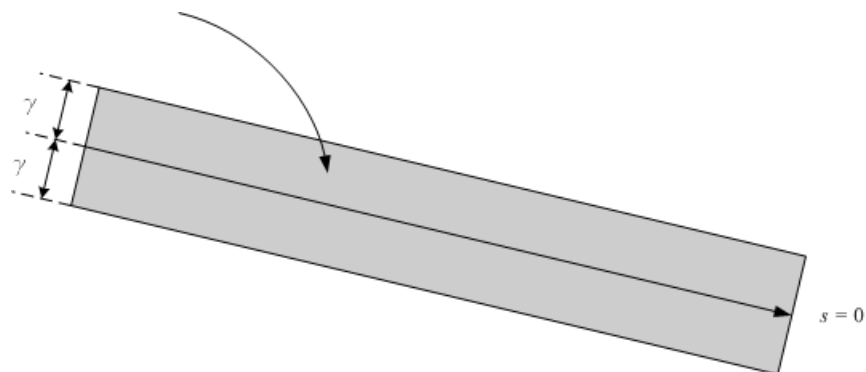


Figure 3.5: Boundary layer when using the saturation function

3.9 Thruster control

ESEO will use thrusters for attitude control. These thrusters are on or off by nature. A reaction wheel on the other hand can give a continuous torque. This means that a continuous signal of commanded torques must be translated to pulses which decide whether a thruster should be on or off. There are several ways to do this, and some of them are presented below.

3.9.1 Bang-bang controller

A bang-bang controller is a simple control scheme where the thrusters are fired if the commanded torque is greater than zero (Song et al., 2001), as illustrated in figure 3.6. A problem with this approach is that the thrusters might fire all the time, thereby consuming a lot of fuel. A solution to this problem is to introduce a dead-zone, as in figure 3.7. Tuning the size of the dead-zone, it is possible to emphasize fuel consumption by choosing it large, or place emphasis on accuracy by having a small dead-zone.

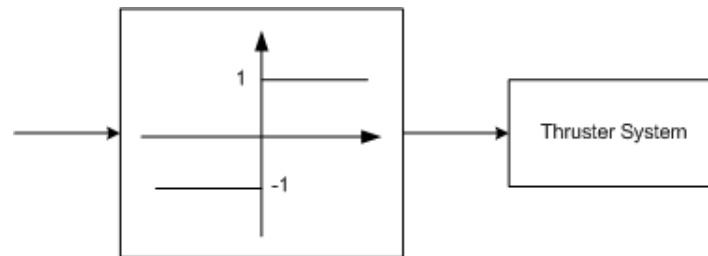


Figure 3.6: Bang-bang controller

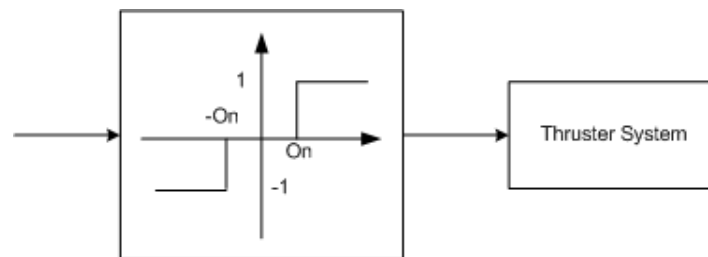


Figure 3.7: Bang-bang controller with dead-zone

3.9.2 Schmitt trigger

The Schmitt trigger can be used in the same way as a bang-bang controller. It can be defined as a relay with a dead-zone and hysteresis (Wie, 1998) as shown in figure 3.8. It can be thought of as a bang-bang controller with a dead-zone and a feedback loop (figure 3.9). Compared to the bang-bang controller scheme, the Schmitt trigger has one more tunable parameter, and it is more complex because of the feedback loop.

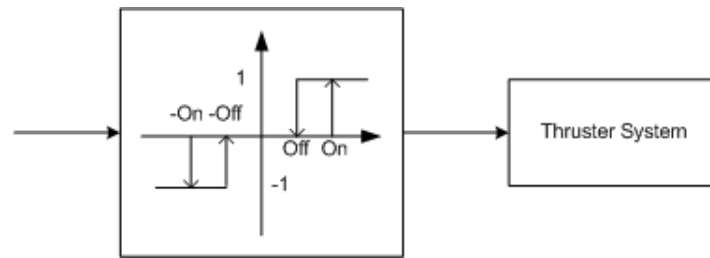


Figure 3.8: Schmitt trigger

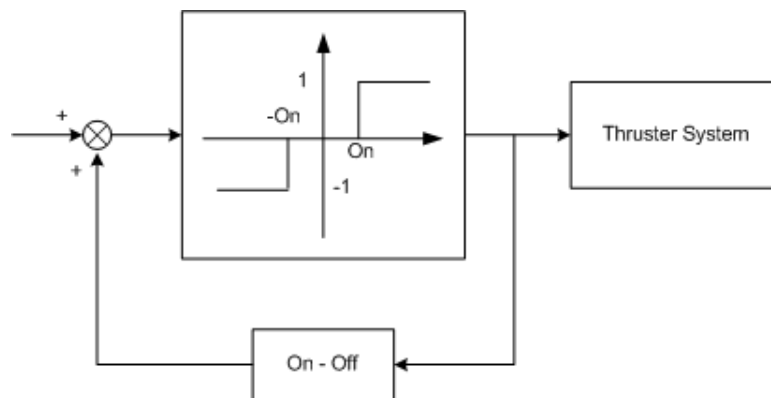


Figure 3.9: Alternative representation of the Schmitt trigger

3.9.3 Pulse-Width Pulse-Frequency modulator

The pulse-width pulse-frequency (PWPF) modulator is presented in Wie (1998) and Song et al. (2001). It produces a pulse sequence to the thrusters by adjusting the pulse width and pulse frequency. In its linear range, the average torque output of the PWPF modulator equals the average commanded torque input. The PWPF modulator consists of a first order lag filter, a Schmitt trigger and a feedback loop, as illustrated in figure 3.10. Compared to the former methods of thruster control, the PWPF modulator is superior (Song et al., 2001), but difficult to implement since there are many parameters to tune. In fact the Schmitt trigger must be tuned together with the lag filter, which yields four parameters to tune. The greatest advantage of the PWPF modulator, is that it is effective in reducing vibrations in flexible spacecraft structures (Song et al., 2001). It has been used in several satellite control systems, e.g. the Agena satellite, INTELSAT V, INSAT and ARABSAT (Wie, 1998).

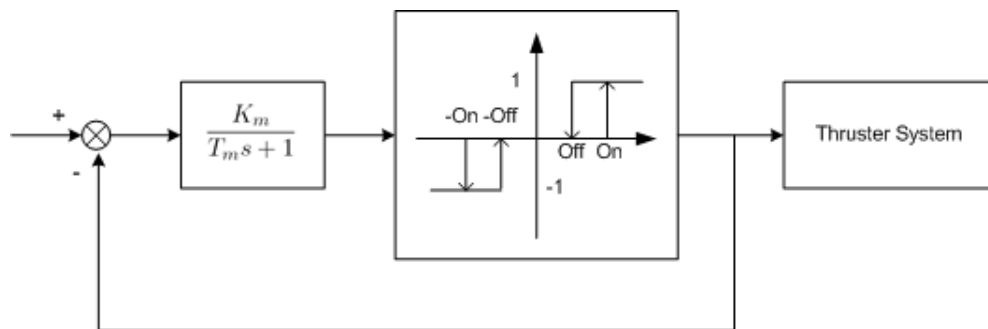


Figure 3.10: PwPF modulator

Chapter 4

Theoretical analysis

4.1 Mathematical modelling

4.1.1 Kinematical model

Because of the possibility of singularities in the mathematical model when using Euler angles, Euler parameters are chosen to describe the orientation of ESEO. This is in accordance with the ESEO AOCS team, which already has made the same choice. Hence the kinematic differential equations are given by the equations in section 3.3.5. Since ESEO will be controlled in reference to the orbit frame \mathcal{F}_o , the kinematic differential equations are given in the body frame \mathcal{F}_b as:

$$\dot{\eta} = -\frac{1}{2}\epsilon^T \omega_{ob}^b \quad (4.1a)$$

$$\dot{\epsilon} = \frac{1}{2}[\eta \mathbf{1} + \epsilon^\times] \omega_{ob}^b \quad (4.1b)$$

4.1.2 Dynamical model

To derive a mathematical model of ESEO's dynamics, the model presented in section 3.4 will be used. Here is a summary of the equations:

$$\mathbf{h}^b = \mathbf{I} \omega_{ib}^b + \mathbf{A} \mathbf{I}_s \omega_s \quad (4.2a)$$

$$\mathbf{h}_a^b = \mathbf{I}_s \mathbf{A}^T \omega_{ib}^b + \mathbf{I}_s \omega_s \quad (4.2b)$$

$$\dot{\mathbf{h}}^b = (\mathbf{h}^b)^\times \omega_{ib}^b + \tau_e \quad (4.2c)$$

$$\dot{\mathbf{h}}_a^b = \tau_a \quad (4.2d)$$

$$\mathbf{J} = \mathbf{I} - \mathbf{A} \mathbf{I}_s \mathbf{A}^T \quad (4.2e)$$

It is desirable to obtain a model describing ESEO in terms of its orientation and its angular velocities. Therefore the above model must be rewritten as a model in angular velocities. According to Hughes (1986), this can be done in the following manner. The equations describing the gyrostatt's angular momentum can be written in matrix form as:

$$\underbrace{\begin{bmatrix} \mathbf{h}^b \\ \mathbf{h}_a^b \end{bmatrix}}_{\mu} = \underbrace{\begin{bmatrix} \mathbf{I} & \mathbf{A}\mathbf{I}_s \\ \mathbf{I}_s\mathbf{A}^T & \mathbf{I}_s \end{bmatrix}}_{\Lambda} \underbrace{\begin{bmatrix} \omega_{ib}^b \\ \omega_s \end{bmatrix}}_{\nu} \quad (4.3)$$

It is now sufficient to transform this model from $\mu = \Lambda\nu$ to $\nu = \Lambda^{-1}\mu$. This is done by inverting the matrix Λ using (A.10). Since Λ is a constant matrix, so is Λ^{-1} . The time derivative of the transformed model is thus:

$$\underbrace{\begin{bmatrix} \dot{\omega}_{ib}^b \\ \dot{\omega}_s \end{bmatrix}}_{\dot{\nu}} = \underbrace{\begin{bmatrix} \mathbf{J}^{-1} & -\mathbf{J}^{-1}\mathbf{A} \\ -\mathbf{A}^T\mathbf{J}^{-1} & \mathbf{I}_s^{-1} + \mathbf{A}^T\mathbf{J}^{-1}\mathbf{A} \end{bmatrix}}_{\Lambda^{-1}} \underbrace{\begin{bmatrix} \dot{\mathbf{h}}^b \\ \dot{\mathbf{h}}_a^b \end{bmatrix}}_{\dot{\mu}} \quad (4.4)$$

Inserting the expressions for $\dot{\mathbf{h}}^b$ and $\dot{\mathbf{h}}_a^b$ yields the following model for the dynamics of the system:

$$\dot{\omega}_{ib}^b = \mathbf{J}^{-1} \left[-\left(\omega_{ib}^b\right)^\times \left(\mathbf{I}\omega_{ib}^b + \mathbf{A}\mathbf{I}_s\omega_s\right) + \tau_e \right] - \mathbf{J}^{-1}\mathbf{A}\tau_a \quad (4.5a)$$

$$\begin{aligned} \dot{\omega}_s &= -\mathbf{A}^T\mathbf{J}^{-1} \left[-\left(\omega_{ib}^b\right)^\times \left(\mathbf{I}\omega_{ib}^b + \mathbf{A}\mathbf{I}_s\omega_s\right) + \tau_e \right] \\ &\quad + \left[\mathbf{A}^T\mathbf{J}^{-1}\mathbf{A} + \mathbf{I}_s^{-1}\right] \tau_a \end{aligned} \quad (4.5b)$$

The complete mathematical model of ESEO consists of the dynamical equations above and the kinematical equations (4.1). Since the angular velocity of ESEO is given in reference to \mathcal{F}_o in (4.1), we need to express the dynamical equations in reference to \mathcal{F}_o . The angular velocity ω_{ib}^b and its time derivative can be expressed as:

$$\omega_{ib}^b = \omega_{ob}^b + \omega_{io}^b = \omega_{ob}^b + \mathbf{R}_o^b\omega_{io}^o \quad (4.6a)$$

$$\dot{\omega}_{ib}^b = \dot{\omega}_{ob}^b + \dot{\mathbf{R}}_o^b\omega_{io}^o + \mathbf{R}_o^b\dot{\omega}_{io}^o = \dot{\omega}_{ob}^b - \left(\omega_{ob}^b\right)^\times \mathbf{R}_o^b\omega_{io}^o + \mathbf{R}_o^b\dot{\omega}_{io}^o \quad (4.6b)$$

In (4.6b), (3.12) has been used. Inserting (4.6a) and (4.6b) into (4.5) yields:

$$\begin{aligned} \dot{\omega}_{ob}^b &= \mathbf{J}^{-1} \left[-\left(\omega_{ob}^b + \mathbf{R}_o^b\omega_{io}^o\right)^\times \left(\mathbf{I}\left[\omega_{ob}^b + \mathbf{R}_o^b\omega_{io}^o\right] + \mathbf{A}\mathbf{I}_s\omega_s\right) + \tau_e \right] \\ &\quad - \mathbf{J}^{-1}\mathbf{A}\tau_a + \left(\omega_{ob}^b\right)^\times \mathbf{R}_o^b\omega_{io}^o - \mathbf{R}_o^b\dot{\omega}_{io}^o \end{aligned} \quad (4.7a)$$

$$\begin{aligned} \dot{\omega}_s &= -\mathbf{A}^T\mathbf{J}^{-1} \left[-\left(\omega_{ob}^b + \mathbf{R}_o^b\omega_{io}^o\right)^\times \left(\mathbf{I}\left[\omega_{ob}^b + \mathbf{R}_o^b\omega_{io}^o\right] + \mathbf{A}\mathbf{I}_s\omega_s\right) + \tau_e \right] \\ &\quad + \left[\mathbf{A}^T\mathbf{J}^{-1}\mathbf{A} + \mathbf{I}_s^{-1}\right] \tau_a \end{aligned} \quad (4.7b)$$

The equations (4.7) and (4.1) represent a complete mathematical model of the system.

4.1.3 Model assumptions

The model presented in (4.7) and (4.1) will now be simplified, based on several model assumptions. These are listed below.

Assumption 4.1. The origin of \mathcal{F}_b coincides with the origin of \mathcal{F}_o , which is the center of mass of the rigid body.

Assumption 4.2. \mathcal{F}_b is oriented along the principal axes of inertia of the rigid body, which implies that the inertia matrix \mathbf{I} is diagonal:

$$\mathbf{I} = \begin{bmatrix} i_x & 0 & 0 \\ 0 & i_y & 0 \\ 0 & 0 & i_z \end{bmatrix} \quad (4.8)$$

Assumption 4.3. The satellite has one reaction wheel, giving a control torque about the y -axis of \mathcal{F}_b . This means that $\mathbf{A} = [0, 1, 0]^T$ and $\mathbf{I}_s = i_s$.

Assumption 4.4. The external torques τ_e affecting the satellite are thruster torques τ_c about all axes of \mathcal{F}_b and the gravity torque τ_g . Thus: $\tau_e = \tau_c + \tau_g$

Assumption 4.5. The angular velocity ω_{io}^o is assumed constant, $\omega_{io}^o = [0, -\omega_0, 0]^T$. This means that $\omega_c = -\omega_0$ in (3.58).

Assumption 4.6. The reaction wheel has a maximum speed, i.e. $|\omega_s| \leq \sigma$.

From these assumptions we get the final mathematical model of ESEO, by simplifying (4.7). We write the complete model as:

$$\dot{\omega}_{ob}^b = \hat{f}_{inert} + \hat{f}_\tau + \hat{f}_g + \hat{f}_{add} \quad (4.9a)$$

$$\dot{\omega}_s = \bar{f}_{inert} + \bar{f}_\tau + \bar{f}_g \quad (4.9b)$$

$$\dot{\eta} = -\frac{1}{2}\epsilon^T \omega_{ob}^b \quad (4.9c)$$

$$\dot{\epsilon} = \frac{1}{2} [\eta \mathbf{1} + \epsilon^\times] \omega_{ob}^b \quad (4.9d)$$

The terms in (4.9) are given as

$$\hat{f}_{inert} = \mathbf{J}^{-1} \left[-(\omega_{ob}^b - \omega_0 \mathbf{c}_2)^\times (\mathbf{I} [\omega_{ob}^b - \omega_0 \mathbf{c}_2] + \mathbf{A} i_s \omega_s) \right] \quad (4.10a)$$

$$\bar{f}_{inert} = \mathbf{A}^T \mathbf{J}^{-1} \left[(\omega_{ob}^b - \omega_0 \mathbf{c}_2)^\times (\mathbf{I} [\omega_{ob}^b - \omega_0 \mathbf{c}_2] + \mathbf{A} i_s \omega_s) \right] \quad (4.10b)$$

$$\hat{f}_\tau = \mathbf{J}^{-1} \tau_c - \mathbf{J}^{-1} \mathbf{A} \tau_a \quad (4.10c)$$

$$\bar{f}_\tau = -\mathbf{A}^T \mathbf{J}^{-1} \tau_c + [\mathbf{A}^T \mathbf{J}^{-1} \mathbf{A} + i_s^{-1}] \tau_a \quad (4.10d)$$

$$\hat{f}_g = \mathbf{J}^{-1} [3\omega_0^2 (\mathbf{c}_3)^\times \mathbf{I} \mathbf{c}_3] \quad (4.10e)$$

$$\bar{f}_g = -\mathbf{A}^T \mathbf{J}^{-1} [3\omega_0^2 (\mathbf{c}_3)^\times \mathbf{I} \mathbf{c}_3] \quad (4.10f)$$

$$\hat{f}_{add} = \omega_0 \dot{\mathbf{c}}_2 \quad (4.10g)$$

where \mathbf{c}_i is the i 'th column vector of the rotation matrix \mathbf{R}_o^b .

4.1.4 Linearized model

Our nonlinear model is quite complex. A way to make it much simpler is to linearize it. Note that a linearized model is only valid close to its operating point. Linearization is done by differentiating the nonlinear system with respect to the total state vector $\mathbf{x} = [(\omega_{ob}^b)^T, \omega_s, \eta, \epsilon^T]^T$, and the input torque vector $\mathbf{u} = [\tau_c^T, \tau_a]^T$. This results in the following linearized model about the point p (Egeland et al., 2001):

$$\Delta \dot{\mathbf{x}} = \mathbf{A} \Delta \mathbf{x} + \mathbf{B} \Delta \mathbf{u} \quad (4.11a)$$

$$\mathbf{A} = \left. \frac{\delta \dot{\mathbf{x}}}{\delta \mathbf{x}} \right|_{\mathbf{x}_p, \mathbf{u}_p}, \quad \mathbf{B} = \left. \frac{\delta \dot{\mathbf{x}}}{\delta \mathbf{u}} \right|_{\mathbf{x}_p, \mathbf{u}_p} \quad (4.11b)$$

Choosing the point p such that $\mathbf{x}_p = [0, 0, 0, 0, 1, 0, 0, 0]$ and $\mathbf{u}_p = [0, 0, 0, 0]$, we get the following system matrices for the linearized system of (4.9):

$$\mathbf{A} = \begin{bmatrix} 0 & 0 & (1 - k_x) \omega_0 & 0 & 0 & -8k_x \omega_0^2 & 0 & 0 \\ 0 & 0 & 0 & 0 & 0 & 0 & \frac{-6k_y i_y \omega_0^2}{k_s} & 0 \\ (k_z - 1) \omega_0 & 0 & 0 & 0 & 0 & 0 & 0 & -2k_z \omega_0^2 \\ 0 & 0 & 0 & 0 & 0 & 0 & \frac{6k_y i_y \omega_0^2}{k_s} & 0 \\ 0 & 0 & 0 & 0 & 0 & 0 & 0 & 0 \\ \frac{1}{2} & 0 & 0 & 0 & 0 & 0 & 0 & 0 \\ 0 & \frac{1}{2} & 0 & 0 & 0 & 0 & 0 & 0 \\ 0 & 0 & \frac{1}{2} & 0 & 0 & 0 & 0 & 0 \end{bmatrix} \quad (4.12a)$$

$$\mathbf{B} = \begin{bmatrix} \frac{1}{i_x} & 0 & 0 & 0 \\ 0 & \frac{1}{k_s} & 0 & -\frac{1}{k_s} \\ 0 & 0 & \frac{1}{i_z} & 0 \\ 0 & -\frac{1}{k_s} & 0 & \frac{i_y}{k_s i_s} \\ 0 & 0 & 0 & 0 \\ 0 & 0 & 0 & 0 \\ 0 & 0 & 0 & 0 \\ 0 & 0 & 0 & 0 \end{bmatrix} \quad (4.12b)$$

$$k_x = \frac{i_y - i_z}{i_x}, \quad k_y = \frac{i_x - i_z}{i_y}, \quad k_z = \frac{i_y - i_x}{i_z}, \quad k_s = i_y - i_s \quad (4.12c)$$

Note that $\dot{\eta} = 0$ in the linearized model, so the number of equations is reduced by one.

4.2 Linear control

In this section we will derive linear controllers for the attitude control of ESEO. When designing controllers, it is common to define an error which will be driven to zero by an appropriate controller. The attitude error dynamics are given by (3.37):

$$\dot{\tilde{\eta}} = -\frac{1}{2} \tilde{\epsilon}^T \tilde{\omega} \quad (4.13a)$$

$$\dot{\tilde{\epsilon}} = -\frac{1}{2} [\tilde{\eta} \mathbf{1} + \tilde{\epsilon}^\times] \tilde{\omega} \quad (4.13b)$$

The angular velocity error is given by (3.39). A mathematical model of the error dynamics as a function of the error in angular velocity can be derived from (4.2) and (3.39). This results in the following model:

$$\mathbf{h}^b = \mathbf{I} \left(\tilde{\omega} + \mathbf{R}_d^b \omega_{id}^d \right) + \mathbf{A} \mathbf{I}_s \omega_s \quad (4.14a)$$

$$\mathbf{h}_a^b = \mathbf{I}_s \mathbf{A}^T \left(\tilde{\omega} + \mathbf{R}_d^b \omega_{id}^d \right) + \mathbf{I}_s \omega_s \quad (4.14b)$$

$$\dot{\mathbf{h}}^b = (\mathbf{h}^b)^\times \left(\tilde{\omega} + \mathbf{R}_d^b \omega_{id}^d \right) + \tau_e \quad (4.14c)$$

$$\dot{\mathbf{h}}_a^b = \tau_a \quad (4.14d)$$

$$\mathbf{J} = \mathbf{I} - \mathbf{A} \mathbf{I}_s \mathbf{A}^T \quad (4.14e)$$

It is shown in appendix A.2.4 that:

$$\mathbf{J} \tilde{\omega} = \mathbf{h}^b - \mathbf{A} \mathbf{h}_a^b - \mathbf{J} \mathbf{R}_d^b \omega_{id}^d \quad (4.15)$$

The control objective is to drive the attitude error and the angular velocity error to zero:

$$\tilde{\omega} \rightarrow 0, \tilde{\epsilon} \rightarrow 0 \quad (4.16)$$

We will now apply the assumptions in 4.1.3, except for assumption 4.3. This means that the number of reaction wheels is arbitrary. Furthermore, we state that the desired frame equals the orbit frame, i.e. $\mathcal{F}_d = \mathcal{F}_o$. Thus:

$$\tilde{\omega} = \omega_{ob}^b \quad (4.17a)$$

$$\mathbf{R}_d^b \omega_{id}^d = -\omega_0 \mathbf{c}_2 \quad (4.17b)$$

$$\tau_e = \tau_c + \tau_g \quad (4.17c)$$

where τ_g is defined by (3.58). From (4.7) and (4.17) we can obtain an expression for $\mathbf{J} \dot{\tilde{\omega}}$ in function of $\tilde{\omega}$ and ω_s :

$$\begin{aligned} \mathbf{J} \dot{\tilde{\omega}} &= \omega_0 \mathbf{J} (\mathbf{c}_2)^\times \tilde{\omega} - \tilde{\omega}^\times \mathbf{I} \tilde{\omega} + \omega_0 \tilde{\omega}^\times \mathbf{I} \mathbf{c}_2 - \tilde{\omega}^\times \mathbf{A} \mathbf{I}_s \omega_s + \omega_0 (\mathbf{c}_2)^\times \mathbf{I} \tilde{\omega} \\ &\quad - \omega_0^2 (\mathbf{c}_2)^\times \mathbf{I} \mathbf{c}_2 + \omega_0 (\mathbf{c}_2)^\times \mathbf{A} \mathbf{I}_s \omega_s + \tau_g + \tau_c - \mathbf{A} \tau_a \end{aligned} \quad (4.18)$$

4.2.1 Local stabilization

An alternative to trying to prove global stabilization for a controller on a nonlinear system, is to linearize the system about an operating point. It is then possible to apply linear control laws to control the system, like the ones described in (3.67). Since the linearized model is only valid close to the operating point, the control law may not stabilize the system when it is far away from this point. A way to deal with this problem is to linearize about several operating points, and switch between them as the system changes states. This kind of control strategy is called *gain scheduling*, and is treated in Khalil (2000). In this thesis we will limit ourselves to one operating point, the origin. Hence, we will use the linearized model given by (4.11) and (4.12).

Using this model implies that $\tilde{\omega} = \omega_{ob}^b$ and $\tilde{\mathbf{q}} = \mathbf{q}$. We will now rewrite the system since the control objective is to drive $\tilde{\omega}$ and $\tilde{\epsilon}$ to zero. In addition we will choose $\Delta\tau_a = 0$, hence the input torque vector is $\Delta\tau_c$.

$$\Delta\dot{\tilde{\omega}} = \mathbf{A}_\omega\Delta\tilde{\omega} + \mathbf{A}_\epsilon\Delta\tilde{\epsilon} + \mathbf{B}\Delta\tau_c \quad (4.19a)$$

$$\Delta\dot{\omega}_s = a\epsilon_2 + \mathbf{b}^T\Delta\tau_c \quad (4.19b)$$

$$\Delta\dot{\eta} = 0 \quad (4.19c)$$

$$\Delta\dot{\tilde{\epsilon}} = \frac{1}{2}\tilde{\omega} \quad (4.19d)$$

From (4.12), we see that \mathbf{A}_ω , \mathbf{A}_ϵ , \mathbf{B} , a and \mathbf{b} are given by:

$$\mathbf{A}_\omega = \begin{bmatrix} 0 & 0 & (1 - k_x)\omega_0 \\ 0 & 0 & 0 \\ (k_z - 1)\omega_0 & 0 & 0 \end{bmatrix} \quad (4.20a)$$

$$\mathbf{A}_\epsilon = \begin{bmatrix} -8k_x\omega_0^2 & 0 & 0 \\ 0 & \frac{-6k_y i_y \omega_0^2}{k_s} & 0 \\ 0 & 0 & -2k_z\omega_0^2 \end{bmatrix} \quad (4.20b)$$

$$\mathbf{B} = \begin{bmatrix} \frac{1}{i_x} & 0 & 0 \\ 0 & \frac{1}{k_s} & 0 \\ 0 & 0 & \frac{1}{i_z} \end{bmatrix} \quad (4.20c)$$

$$a = \frac{6k_y i_y \omega_0^2}{k_s} \quad (4.20d)$$

$$\mathbf{b} = \left[0, -\frac{1}{k_s}, 0, \frac{i_y}{k_s i_s} \right]^T \quad (4.20e)$$

$$k_x = \frac{i_y - i_z}{i_x}, k_y = \frac{i_x - i_z}{i_y}, k_z = \frac{i_y - i_x}{i_z}, k_s = i_y - i_s \quad (4.20f)$$

To derive a linear controller, we will use Lyapunov analysis. Consider the following Lyapunov function candidate (LFC) V :

$$V = \frac{1}{2}(\Delta\tilde{\omega})^T \Delta\tilde{\omega} + k_0 \Delta(\tilde{\epsilon})^T \Delta\tilde{\epsilon} \quad (4.21)$$

$$\dot{V} = (\Delta\tilde{\omega})^T (\mathbf{A}_\omega\Delta\tilde{\omega} + \mathbf{A}_\epsilon\Delta\tilde{\epsilon} + \mathbf{B}\Delta\tau_c) + k_0(\Delta\tilde{\omega})^T \Delta\tilde{\epsilon} \quad (4.22)$$

We choose the following controller

$$\Delta\tau_c = -\mathbf{K}_\epsilon\Delta\tilde{\epsilon} - \mathbf{K}_\omega\Delta\tilde{\omega} \quad (4.23)$$

where the constant matrices $\mathbf{K}_\epsilon > 0$ and $\mathbf{K}_\omega > 0$. Inserting (4.23) into (4.22), we get:

$$\dot{V} = (\Delta\tilde{\omega})^T (\mathbf{A}_\omega - \mathbf{B}\mathbf{K}_\omega) \Delta\tilde{\omega} + (\Delta\tilde{\omega})^T (\mathbf{A}_\epsilon + k_0\mathbf{1} - \mathbf{B}\mathbf{K}_\epsilon) \Delta\tilde{\epsilon} \quad (4.24)$$

We want to remove the second term. Therefore, we make the following choice for \mathbf{K}_ϵ :

$$\mathbf{BK}_\epsilon = \mathbf{A}_\epsilon + k_0 \mathbf{1} \quad (4.25)$$

Consequently:

$$\dot{V} = (\Delta\tilde{\omega})^T (\mathbf{A}_\omega - \mathbf{BK}_\omega) \Delta\tilde{\omega} \quad (4.26)$$

Choosing \mathbf{K}_ω such that $(\mathbf{A}_\omega - \mathbf{BK}_\omega) < 0$ yields $\Delta\tilde{\omega} \rightarrow 0 \Rightarrow \Delta\dot{\tilde{\omega}} \rightarrow 0 \Rightarrow \Delta\dot{\tilde{\epsilon}} \rightarrow 0$ and $\Delta\tilde{\epsilon} \rightarrow 0$. Thus, the controlled system is asymptotically stable. Our linear control law actually corresponds to a PD controller with respect to $\tilde{\epsilon}$, since $\tilde{\omega}$ represents the time derivative of $\tilde{\epsilon}$, although it is not equal to it. Note that $\tau_a = 0$ with this controller. The reaction wheel is not used by the controller, and is left to spin on its own. In appendix A.2.5, the following gain matrices are found to stabilize the system:

$$\mathbf{K}_\epsilon = k_\epsilon \mathbf{I} \quad (4.27a)$$

$$\mathbf{K}_\omega = k_\omega \mathbf{1} \quad (4.27b)$$

$$k_\epsilon \gg \max \{8\omega_0^2, i_s\} \quad (4.27c)$$

$$k_\omega > 0 \quad (4.27d)$$

$$k_\omega^2 > \omega_0^2 \left(i_z [2i_y - 2i_x - i_z] - [i_y - i_x]^2 \right) \quad (4.27e)$$

4.2.2 Global stabilization

We will now analyze how a linear controller can stabilize ESEO globally. To do this, we will use Lyapunov analysis. We choose the following LFC V :

$$V = \overbrace{\frac{1}{2} [\tilde{\omega}^T, \omega_s^T] \begin{bmatrix} \mathbf{I} & \mathbf{A}\mathbf{I}_s \\ \mathbf{I}_s \mathbf{A}^T & \mathbf{I}_s \end{bmatrix} \begin{bmatrix} \tilde{\omega} \\ \omega_s \end{bmatrix}}^{V_a} - \frac{1}{2} \omega_0^2 \mathbf{c}_2^T \mathbf{I} \mathbf{c}_2 \quad (4.28)$$

$$+ k_0 \left(\tilde{\epsilon}^T \tilde{\epsilon} + [\tilde{\eta} - 1]^2 \right) + \frac{3}{2} \omega_0^2 \mathbf{c}_3^T \mathbf{I} \mathbf{c}_3 + \frac{1}{2} \omega_0^2 (i_y - 3i_z)$$

$$V = \frac{1}{2} \tilde{\omega}^T \mathbf{I} \tilde{\omega} + \omega_s \mathbf{I}_s \mathbf{A}^T \tilde{\omega} + \frac{1}{2} \omega_s^T \mathbf{I}_s \omega_s - \frac{1}{2} \omega_0^2 \mathbf{c}_2^T \mathbf{I} \mathbf{c}_2 \quad (4.29)$$

$$+ 2k_0 (1 - \tilde{\eta}) + \frac{3}{2} \omega_0^2 \mathbf{c}_3^T \mathbf{I} \mathbf{c}_3 + \frac{1}{2} \omega_0^2 (i_y - 3i_z)$$

The state vector is $\mathbf{x} = [\tilde{\omega}^T, \omega_s, \tilde{\mathbf{q}}^T, c_{12}, c_{32}, c_{13}, c_{23}]^T$ where c_{12} , c_{32} , c_{13} and c_{23} are the respective components of the vectors \mathbf{c}_2 and \mathbf{c}_3 defined in (3.8). The desired state vector is $\mathbf{x}^* = [0^3, 0^N, 1, 0^3, 0, 0, 0, 0]^T$. The first three terms (V_a) and the fourth term in V represents the kinetic energy of the satellite, although it is not equal to its total kinetic energy. Note that the expression for V_a has the same structure as the expression for the kinetic energy of a one wheel gyostat (3.52). The fifth term comes from the attitude error where k_0 is a positive constant. These terms represent the same idea as in choosing the LFC in example 3.1, i.e. a choice which corresponds to the kinetic energy, and a kinematic term. The sixth term

represents the potential energy of the satellite (3.59). The last term is constant in order to make V a true Lyapunov function, i.e. $V > 0$ and $V(\mathbf{x}^*) = 0$. In fact, V meets these requirements only when $i_y > i_x > i_z$. For details see A.2.1 and A.2.2, or Kristiansen (2000). It is shown in appendix A.2.3 that the time derivative of V_a is given by:

$$\dot{V}_a = \tilde{\omega}^T \tau_e + \omega_s^T \tau_a - \omega_0^2 \tilde{\omega}^T (\mathbf{c}_2)^\times \mathbf{I} \mathbf{c}_2 \quad (4.30)$$

The time derivative of V along the trajectories of (4.14) thus becomes:

$$\dot{V} = \dot{V}_a - \frac{1}{2} \omega_0^2 \mathbf{c}_2^T \mathbf{I} \dot{\mathbf{c}}_2 - 2k_0 \dot{\eta} + \frac{3}{2} \omega_0^2 \mathbf{c}_3^T \mathbf{I} \dot{\mathbf{c}}_3 \quad (4.31)$$

$$\begin{aligned} &= \tilde{\omega}^T \tau_c + \omega_s^T \tau_a - \omega_0^2 \tilde{\omega}^T (\mathbf{c}_2)^\times \mathbf{I} \mathbf{c}_2 + 3\omega_0^2 \tilde{\omega}^T (\mathbf{c}_3)^\times \mathbf{I} \mathbf{c}_3 \\ &\quad - \omega_0^2 \mathbf{c}_2^T \mathbf{I} (\mathbf{c}_2)^\times \tilde{\omega} + k_0 \tilde{\omega}^T \tilde{\epsilon} + 3\omega_0^2 \mathbf{c}_3^T \mathbf{I} (\mathbf{c}_3)^\times \tilde{\omega} \end{aligned} \quad (4.32)$$

Since all the terms are scalars, they can be freely transposed. The following terms are transposed:

$$(-\omega_0^2 \mathbf{c}_2^T \mathbf{I} (\mathbf{c}_2)^\times \tilde{\omega})^T = \omega_0^2 \tilde{\omega}^T (\mathbf{c}_2)^\times \mathbf{I} \mathbf{c}_2 \quad (4.33)$$

$$(3\omega_0^2 \mathbf{c}_3^T \mathbf{I} (\mathbf{c}_3)^\times \tilde{\omega})^T = -3\omega_0^2 \tilde{\omega}^T (\mathbf{c}_3)^\times \mathbf{I} \mathbf{c}_3 \quad (4.34)$$

Note that the change of signs are due to the skew symmetric matrices defined in A.4. We now see that term three and five are the same but with opposite signs. The same goes for term four and six. Thus:

$$\dot{V} = \tilde{\omega}^T \tau_c + \omega_s^T \tau_a + k_0 \tilde{\omega}^T \tilde{\epsilon} \quad (4.35)$$

We now choose the following linear controller

$$\tau_c = -k_0 \tilde{\epsilon} - \mathbf{C} \tilde{\omega} \quad (4.36a)$$

$$\tau_a = \mathbf{D} \tilde{\omega} - \mathbf{E} \omega_s \quad (4.36b)$$

where \mathbf{C} , \mathbf{D} and \mathbf{E} are constant matrices. The control law for the thrusters τ_c corresponds to a PD controller with respect to the satellite's attitude. The control law for the reaction wheels τ_a controls the angular velocity of the spacecraft and the spin of the wheels. Combining (4.36) with (4.35), we get:

$$\dot{V} = -\tilde{\omega}^T \mathbf{C} \tilde{\omega} + \omega_s^T \mathbf{D} \tilde{\omega} - \omega_s^T \mathbf{E} \omega_s \quad (4.37)$$

$$= - \underbrace{[\tilde{\omega}^T, \omega_s^T]}_{\Omega^T} \underbrace{\begin{bmatrix} \mathbf{C} & -\mathbf{D}/2 \\ -\mathbf{D}^T/2 & \mathbf{E} \end{bmatrix}}_{\mathbf{P}} \underbrace{\begin{bmatrix} \tilde{\omega} \\ \omega_s \end{bmatrix}}_{\Omega} \quad (4.38)$$

Choosing $\mathbf{P} > 0$ will make $\dot{V} \leq 0$. An obvious choice is $\mathbf{C} = k_\omega \mathbf{1} > 0$, $\mathbf{E} = k_s \mathbf{1} > 0$ and $\mathbf{D} = 0$ where k_ω and k_s are constants. However this means that the reaction wheels are not

used as actuators to control the attitude of the satellite. The wheels control themselves. It is desirable to see if a linear control law for the wheels which helps to control the spacecraft may yield an asymptotically stable system. Intuitively, this should be possible by choosing $\mathbf{D} \neq 0$ and choosing the positive definite matrices \mathbf{C} and \mathbf{E} large enough to make $\mathbf{P} > 0$. However choosing $\mathbf{D} = 0$ should make \mathbf{P} "more" positive definite, and hence the rate of convergence of $\boldsymbol{\Omega}$ would be greater. Showing this analytically is complicated since \mathbf{P} is a $(3 + N) \times (3 + N)$ matrix. Instead we will use Young's inequality on the following term:

$$\omega_s^T \mathbf{D} \tilde{\omega} = \tilde{\omega}^T \mathbf{D} \omega_s \leq \|\tilde{\omega}\| \|\mathbf{D} \omega_s\| \quad (4.39)$$

Applying Young's inequality (A.12) with $p = 2$, we obtain:

$$\|\tilde{\omega}\| \|\mathbf{D} \omega_s\| \leq \frac{\|\tilde{\omega}\|^2}{2} + \frac{\|\mathbf{D} \omega_s\|^2}{2} \quad (4.40)$$

The vector norms are given by the 2-norm defined in (A.5), thus:

$$\|\tilde{\omega}\|^2 = \tilde{\omega}^T \tilde{\omega} \quad (4.41)$$

$$\|\mathbf{D} \omega_s\|^2 = \omega_s^T \mathbf{D}^T \mathbf{D} \omega_s \quad (4.42)$$

It is possible to use these results to define an upper bound on \dot{V} :

$$\dot{V} \leq -\tilde{\omega}^T \mathbf{C} \tilde{\omega} + \frac{1}{2} \tilde{\omega}^T \tilde{\omega} + \frac{1}{2} \omega_s^T \mathbf{D}^T \mathbf{D} \omega_s - \omega_s^T \mathbf{E} \omega_s \quad (4.43)$$

$$\leq -\tilde{\omega}^T \left(\mathbf{C} - \frac{1}{2} \mathbf{1} \right) \tilde{\omega} - \omega_s^T \left(\mathbf{E} - \frac{1}{2} \mathbf{D}^T \mathbf{D} \right) \omega_s \quad (4.44)$$

We now see that choosing $\mathbf{D} = 0$ gives the greatest rate of convergence of $\boldsymbol{\Omega}$. So choosing $\mathbf{C} > 0$, $\mathbf{E} > 0$ and $\mathbf{D} = 0$ makes $\dot{V} \leq 0$. Thus $\boldsymbol{\Omega} \rightarrow 0 \Rightarrow \dot{\boldsymbol{\Omega}} = 0$, and (4.18) becomes:

$$0 = -\omega_0^2 (\mathbf{c}_2)^\times \mathbf{I} \mathbf{c}_2 + 3\omega_0^2 (\mathbf{c}_3)^\times \mathbf{I} \mathbf{c}_3 - k_0 \tilde{\epsilon} \quad (4.45)$$

Since all of the terms to the right are bounded, there should be a large enough choice of k_0 which makes $\tilde{\epsilon} = 0$ the only solution of (4.45) (Soglo, 1994). The terms are bounded because \mathbf{c}_i is a unit vector and $\|\tilde{\epsilon}\| \leq 1$. To find this value, we will apply Assumption 4.3 and rewrite the equation on component form where $\tilde{\epsilon} = [\tilde{\epsilon}_1, \tilde{\epsilon}_2, \tilde{\epsilon}_3]^T$:

$$k_0 \tilde{\epsilon}_1 = \omega_0^2 (i_y - i_z) (c_{22} c_{32} - 3c_{23} c_{33}) \quad (4.46a)$$

$$k_0 \tilde{\epsilon}_2 = \omega_0^2 (i_z - i_x) (c_{12} c_{32} - 3c_{13} c_{33}) \quad (4.46b)$$

$$k_0 \tilde{\epsilon}_3 = \omega_0^2 (i_x - i_y) (c_{12} c_{22} - 3c_{13} c_{23}) \quad (4.46c)$$

The constant k_0 must be chosen in a way such that $k_0 \tilde{\epsilon}_i$ is larger than the maximum value of all the right hand sides of the above equations. If this is the case, then $\tilde{\epsilon} = 0$ and $c_{k2} c_{l2} = c_{k3} c_{l3} = 0$ are the only solutions. The maximum value of the product $c_{k_i} c_{l_i}$ is $1/2$. This comes from the

relation (3.10), i.e. $c_{1i}^2 + c_{2i}^2 + c_{3i}^2 = 1$. If a product of two directional cosines is to have its maximum value, then the third directional cosine associated with the same vector \mathbf{c}_i must be zero. The product will have its largest value when the two directional cosines have the same value. This value is $\sqrt{1/2}$. Since i_z is the smallest element in \mathbf{I} and i_y is the largest, (4.46a) has the largest right hand side. The largest value is obtained when:

$$\mathbf{c}_3 = \begin{bmatrix} c_{13} \\ c_{23} \\ c_{33} \end{bmatrix} = \begin{bmatrix} 0 \\ \sqrt{1/2} \\ \sqrt{1/2} \end{bmatrix} \quad (4.47a)$$

$$c_{22}c_{32} = 0 \quad (4.47b)$$

This problem has several solutions, and is solved in appendix A.2.6. We are interested in the worst case scenario, i.e. the smallest nonzero solution for $\tilde{\epsilon}_1$ when the right hand side has its maximum value. In fact, the solution must be negative. To see this, consider (4.46a) in our worst case scenario:

$$k_0 \tilde{\epsilon}_1 = -\frac{3}{2} \omega_0^2 (i_y - i_z) \quad (4.48)$$

The right hand side of the above equation is negative, which means that $\tilde{\epsilon}_1$ must be negative. The smallest negative solution is:

$$\tilde{\epsilon}_1 = -0.2706 \quad (4.49)$$

The solutions are shown in figure A.1. Inserting this value into (4.48), yields:

$$0.2706 k_0 = \frac{3}{2} \omega_0^2 (i_y - i_z) \quad (4.50)$$

This expression yields a value for k_0 . If k_0 is chosen greater than this value, then the only possible solution for (4.46a) is that both sides of the equation are zero, i.e. $\tilde{\epsilon}_1 = 0$. Since (4.46b) and (4.46c) have smaller right hand sides, this choice of k_0 will ensure that $\tilde{\epsilon}_2 = 0$ and $\tilde{\epsilon}_3 = 0$. Thus:

$$k_0 > 5.5432 \omega_0^2 (i_y - i_z) \Rightarrow \tilde{\epsilon} \rightarrow 0 \quad (4.51)$$

Corollary 3.2 is now applicable, which means that we have global asymptotic stability for the proposed linear controller.

4.3 Nonlinear control

Using the same model as in section 4.2, we will now find nonlinear controllers to control ESEO's attitude.

4.3.1 Lyapunov controller 1

In the linear controller in section 4.2.2, there was a restriction on the inertia matrix of the satellite. In case such restrictions are not met by a satellite, we will derive a nonlinear controller which does not have these restrictions. Consider the following LFC, which is almost the same LFC as (4.28):

$$V = V_a + 2k_1(1 - \tilde{\eta}) \quad (4.52)$$

where k_1 is a positive constant. The time derivative of V along the trajectories of (4.14) is given by:

$$\dot{V} = \tilde{\omega}^T \tau_c + \omega_s^T \tau_a - \omega_0^2 \tilde{\omega}^T (\mathbf{c}_2)^\times \mathbf{I} \mathbf{c}_2 + 3\omega_0^2 \tilde{\omega}^T (\mathbf{c}_3)^\times \mathbf{I} \mathbf{c}_3 + k_1 \tilde{\omega}^T \tilde{\epsilon} \quad (4.53)$$

We now choose:

$$\tau_c = -k_1 \tilde{\epsilon} - \mathbf{C} \tilde{\omega} + \omega_0^2 (\mathbf{c}_2)^\times \mathbf{I} \mathbf{c}_2 - 3\omega_0^2 (\mathbf{c}_3)^\times \mathbf{I} \mathbf{c}_3 \quad (4.54a)$$

$$\tau_a = -\mathbf{E} \omega_s \quad (4.54b)$$

Consequently:

$$\dot{V} = -\tilde{\omega}^T \mathbf{C} \tilde{\omega} - \omega_s^T \mathbf{E} \omega_s \quad (4.55)$$

Choosing $\mathbf{C} > 0$ and $\mathbf{E} > 0$ makes $\dot{V} \leq 0$. An obvious choice is $\mathbf{C} = k_\omega \mathbf{1}$ and $\mathbf{E} = k_s \mathbf{1}$ where $k_\omega > 0$ and $k_s > 0$ are constants. Thus $\tilde{\omega} \rightarrow 0 \Rightarrow \dot{\tilde{\omega}} \rightarrow 0$ and $\omega_s \rightarrow 0 \Rightarrow \dot{\omega}_s \rightarrow 0$. Hence (4.18) becomes $k_0 \tilde{\epsilon} = 0 \Rightarrow \tilde{\epsilon} \rightarrow 0$. Thus corollary 3.2 states that the system is globally asymptotically stable.

4.3.2 Lyapunov controller 2

It would be desirable to use the reaction wheels as actuators in the same way as the thrusters. This motivates an LFC where we omit ω_s from the state vector, and treat it as an external signal. Consider the LFC

$$V = \frac{1}{2} \tilde{\omega}^T \mathbf{J} \tilde{\omega} - \frac{1}{2} \omega_0^2 \mathbf{c}_2^T \mathbf{I} \mathbf{c}_2 + 2k_2(1 - \tilde{\eta}) + \frac{3}{2} \omega_0^2 \mathbf{c}_3^T \mathbf{I} \mathbf{c}_3 + \frac{1}{2} \omega_0^2 (i_y - 3i_z) \quad (4.56)$$

where k_2 is a positive constant. The state vector is $\mathbf{x} = [\tilde{\omega}^T, \tilde{\mathbf{q}}^T, c_{12}, c_{32}, c_{13}, c_{23}]^T$, and the desired state vector is $\mathbf{x}^* = [0^3, 1, 0^3, 0, 0, 0]^T$. The first and second term in V represents the kinetic energy of the satellite, although it is not equal to its total kinetic energy. The other terms are the same as in the LFC (4.28). This means that V is a Lyapunov function if $i_y > i_x > i_z$. To calculate \dot{V} , we will use (4.18):

$$\dot{V} = \tilde{\omega}^T \mathbf{J} \dot{\tilde{\omega}} - \frac{1}{2} \omega_0^2 \mathbf{c}_2^T \mathbf{I} \dot{\tilde{\omega}} - 2k_2 \dot{\tilde{\omega}} + \frac{3}{2} \omega_0^2 \mathbf{c}_3^T \mathbf{I} \dot{\tilde{\omega}} \quad (4.57)$$

$$\begin{aligned} \dot{V} &= \omega_0 \tilde{\omega}^T \mathbf{J}(\mathbf{c}_2)^\times \tilde{\omega} + \omega_0 \tilde{\omega}^T (\mathbf{c}_2)^\times \mathbf{I} \tilde{\omega} - \omega_0^2 \tilde{\omega}^T (\mathbf{c}_2)^\times \mathbf{I} \mathbf{c}_2 \\ &\quad + \omega_0 \tilde{\omega}^T (\mathbf{c}_2)^\times \mathbf{A} \mathbf{I}_s \omega_s + \tilde{\omega}^T \tau_g + \tilde{\omega}^T \tau_c - \tilde{\omega}^T \mathbf{A} \tau_a \\ &\quad - \omega_0^2 \mathbf{c}_2^T \mathbf{I} (\mathbf{c}_2)^\times \tilde{\omega} + k_2 \tilde{\omega}^T \tilde{\epsilon} + 3\omega_0^2 \mathbf{c}_3^T \mathbf{I} (\mathbf{c}_3)^\times \tilde{\omega} \end{aligned} \quad (4.58)$$

Note that several terms have disappeared since $\tilde{\omega}^T \tilde{\omega}^\times = 0$. These terms will be transposed:

$$(\omega_0 \tilde{\omega}^T \mathbf{J}(\mathbf{c}_2)^\times \tilde{\omega})^T = -\omega_0 \tilde{\omega}^T (\mathbf{c}_2)^\times \mathbf{J} \tilde{\omega} \quad (4.59)$$

$$(-\omega_0^2 \mathbf{c}_2^T \mathbf{I} (\mathbf{c}_2)^\times \tilde{\omega})^T = \omega_0^2 \tilde{\omega}^T (\mathbf{c}_2)^\times \mathbf{I} \mathbf{c}_2 \quad (4.60)$$

$$(3\omega_0^2 \mathbf{c}_3^T \mathbf{I} (\mathbf{c}_3)^\times \tilde{\omega})^T = -3\omega_0^2 \tilde{\omega}^T (\mathbf{c}_3)^\times \mathbf{I} \mathbf{c}_3 \quad (4.61)$$

Observe that term three and eight are the same but with opposite signs. The same goes for term five and ten. Thus:

$$\dot{V} = \omega_0 \tilde{\omega}^T (\mathbf{c}_2)^\times (\mathbf{I} \tilde{\omega} - \mathbf{J} \tilde{\omega} + \mathbf{A} \mathbf{I}_s \omega_s) + \tilde{\omega}^T \tau_c - \tilde{\omega}^T \mathbf{A} \tau_a + k_0 \tilde{\omega}^T \tilde{\epsilon} \quad (4.62)$$

$$= \omega_0 \tilde{\omega}^T (\mathbf{c}_2)^\times \mathbf{A} \mathbf{I}_s (\mathbf{A}^T \tilde{\omega} + \omega_s) + \tilde{\omega}^T \tau_c - \tilde{\omega}^T \mathbf{A} \tau_a + k_2 \tilde{\omega}^T \tilde{\epsilon} \quad (4.63)$$

We now choose the following control laws, applying the principle of section 3.8.1:

$$\tau_c = -k_{\epsilon,1} \tilde{\epsilon} - \mathbf{C} \tilde{\omega} \quad (4.64a)$$

$$\begin{aligned} \mathbf{A} \tau_a &= k_{\epsilon,2} \tilde{\epsilon} + \mathbf{D} \tilde{\omega} \\ &\quad + \omega_0 (\mathbf{c}_2)^\times \mathbf{A} \mathbf{I}_s (\mathbf{A}^T \tilde{\omega} + \omega_s) \end{aligned} \quad (4.64b)$$

where \mathbf{C} and \mathbf{D} are constant matrices, and $k_{\epsilon,i}$ ($i = 1, 2$) is a constant. Note that the control law for τ_a cancels the nonlinearities in \dot{V} . This is only possible if the reaction wheels are able to give torques about all three axes of rotation. If this is not the case, the thrusters should be used. We will get the same result for \dot{V} , if we choose to cancel them with τ_c instead. Inserting (4.64) into (4.63), we get:

$$\dot{V} = (k_2 - k_{\epsilon,1} - k_{\epsilon,2}) \tilde{\omega}^T \tilde{\epsilon} - \tilde{\omega}^T (\mathbf{C} + \mathbf{D}) \tilde{\omega} \quad (4.65)$$

We choose $k_2 = k_{\epsilon,1} + k_{\epsilon,2}$, hence:

$$\dot{V} = -\tilde{\omega}^T (\mathbf{C} + \mathbf{D}) \tilde{\omega} \quad (4.66)$$

If $(\mathbf{C} + \mathbf{D}) > 0$ then $\dot{V} \leq 0$. An obvious choice which ensures this is $\mathbf{C} = k_{\omega,1} \mathbf{1}$ and $\mathbf{D} = k_{\omega,2} \mathbf{1}$ where $k_{\omega,i}$ ($i = 1, 2$) is a constant and $(k_{\omega,1} + k_{\omega,2}) > 0$. Thus we have proved that $\tilde{\omega} \rightarrow 0 \Rightarrow \tilde{\epsilon} \rightarrow 0$. We will now apply corollary 3.2. When $\dot{\tilde{\omega}} = \tilde{\omega} = 0$, (4.18) becomes:

$$0 = -\omega_0^2 (\mathbf{c}_2)^\times \mathbf{I} \mathbf{c}_2 + 3\omega_0^2 (\mathbf{c}_3)^\times \mathbf{I} \mathbf{c}_3 - k_2 \tilde{\epsilon} \quad (4.67)$$

The constant k_2 must be chosen large enough to make $\tilde{\epsilon} = 0$ the only possible solution to this equation. Since this is the same equation as (4.45) choosing $k_2 > 5.5432 \omega_0^2 (i_y - i_z)$ yields a globally asymptotically stable system according to corollary 3.2.

4.3.3 Lyapunov controller 3

In section 4.3.2 there is a restriction on the inertia matrix of the satellite. The next controller will not have such restrictions. We will consider the following LFC V where k_3 is a positive constant:

$$V = \frac{1}{2} \tilde{\omega}^T \mathbf{J} \tilde{\omega} + 2k_3 (1 - \tilde{\eta}) \quad (4.68a)$$

This LFC is almost the same as (4.56), but two terms are removed. \dot{V} becomes:

$$\dot{V} = \tilde{\omega}^T \mathbf{J} \dot{\tilde{\omega}} - 2k_3 \dot{\tilde{\eta}} \quad (4.69)$$

$$\begin{aligned} \dot{V} = & \omega_0 \tilde{\omega}^T \mathbf{J} (\mathbf{c}_2)^\times \tilde{\omega} + \omega_0 \tilde{\omega}^T (\mathbf{c}_2)^\times \mathbf{I} \tilde{\omega} - \omega_0^2 \tilde{\omega}^T (\mathbf{c}_2)^\times \mathbf{I} \mathbf{c}_2 \\ & + \omega_0 \tilde{\omega}^T (\mathbf{c}_2)^\times \mathbf{A} \mathbf{I}_s \omega_s + 3\omega_0^2 \tilde{\omega}^T (\mathbf{c}_3)^\times \mathbf{I} \mathbf{c}_3 \\ & + \tilde{\omega}^T \tau_c - \tilde{\omega}^T \mathbf{A} \tau_a + k_3 \tilde{\omega}^T \tilde{\epsilon} \end{aligned} \quad (4.70)$$

Transposing the first term, and using the definition of \mathbf{J} in (4.14), we get:

$$\begin{aligned} \dot{V} = & \omega_0 \tilde{\omega}^T (\mathbf{c}_2)^\times \mathbf{A} \mathbf{I}_s (\mathbf{A}^T \tilde{\omega} + \omega_s) - \omega_0^2 \tilde{\omega}^T (\mathbf{c}_2)^\times \mathbf{I} \mathbf{c}_2 \\ & + 3\omega_0^2 \tilde{\omega}^T (\mathbf{c}_3)^\times \mathbf{I} \mathbf{c}_3 + \tilde{\omega}^T \tau_c - \tilde{\omega}^T \mathbf{A} \tau_a + k_3 \tilde{\omega}^T \tilde{\epsilon} \end{aligned} \quad (4.71)$$

We now choose the following control laws, applying the principle of section 3.8.1:

$$\tau_c = -k_{\epsilon,1} \tilde{\epsilon} - \mathbf{C} \tilde{\omega} \quad (4.72a)$$

$$\begin{aligned} \mathbf{A} \tau_a = & k_{\epsilon,2} \tilde{\epsilon} + \mathbf{D} \tilde{\omega} + \omega_0 (\mathbf{c}_2)^\times \mathbf{A} \mathbf{I}_s (\mathbf{A}^T \tilde{\omega} + \omega_s) \\ & - \omega_0^2 (\mathbf{c}_2)^\times \mathbf{I} \mathbf{c}_2 + 3\omega_0^2 (\mathbf{c}_3)^\times \mathbf{I} \mathbf{c}_3 \end{aligned} \quad (4.72b)$$

where \mathbf{C} and \mathbf{D} are constant matrices, and $k_{\epsilon,i}$ ($i = 1, 2$) is a constant. The control law for τ_a cancels the nonlinearities in \dot{V} . After inserting (4.72) into (4.71), we get:

$$\dot{V} = (k_3 - k_{\epsilon,1} - k_{\epsilon,2}) \tilde{\omega}^T \tilde{\epsilon} - \tilde{\omega}^T (\mathbf{C} + \mathbf{D}) \tilde{\omega} \quad (4.73)$$

We choose $k_3 = k_{\epsilon,1} + k_{\epsilon,2}$, thus:

$$\dot{V} = -\tilde{\omega}^T (\mathbf{C} + \mathbf{D}) \tilde{\omega} \quad (4.74)$$

If $(\mathbf{C} + \mathbf{D}) > 0$ then $\dot{V} \leq 0$. To ensure this, we choose $\mathbf{C} = k_{\omega,1} \mathbf{1}$ and $\mathbf{D} = k_{\omega,2} \mathbf{1}$ where $k_{\omega,i}$ ($i = 1, 2$) is a constant and $(k_{\omega,1} + k_{\omega,2}) > 0$. Thus $\tilde{\omega} \rightarrow 0 \Rightarrow \dot{\tilde{\omega}} \rightarrow 0$. We will now apply corollary 3.2. When $\dot{\tilde{\omega}} = \tilde{\omega} = 0$, (4.18) becomes $k_0 \tilde{\epsilon} = 0 \Rightarrow \tilde{\epsilon} \rightarrow 0$. Thus corollary 3.2 states that the system is globally asymptotically stable.

4.3.4 Sliding mode controller

The first step in sliding mode control is to design a sliding manifold. Fu, Tsai and Yeh (1999) suggest the following manifold $\mathbf{s} = [s_x, s_y, s_z]^T$, based on the classic dynamical model of a rigid body in motion (3.68) where the kinematics are represented by unit quaternions. Define

$$\mathbf{s} = \tilde{\omega} + \mathbf{P}\tilde{\epsilon} \quad (4.75)$$

where $\mathbf{P} > 0$. It is shown in appendix A.2.7 that when $\mathbf{s} = 0$, $\tilde{\epsilon}$ and $\tilde{\omega}$ tend to zero. We must now design a control law to reach the sliding manifold. Consider the LFC:

$$V = \mathbf{s}^T \mathbf{J} \mathbf{s} \quad (4.76)$$

Its time derivative along the trajectories of (4.14) is given as:

$$\dot{V} = \mathbf{s}^T (\mathbf{J}\dot{\tilde{\omega}} + \mathbf{J}\mathbf{P}\dot{\tilde{\epsilon}}) \quad (4.77)$$

$$\begin{aligned} \dot{V} = \mathbf{s}^T & \left((\mathbf{h}^b)^\times [\tilde{\omega} - \omega_0 \mathbf{c}_2] + \frac{3}{2} \omega_0^2 \mathbf{c}_3^T \mathbf{I} \mathbf{c}_3 + \tau_c - \mathbf{A} \tau_a \right. \\ & \left. + \omega_0 \mathbf{J}(\mathbf{c}_2)^\times \tilde{\omega} + \frac{1}{2} \mathbf{J} \mathbf{P} [\tilde{\eta} \mathbf{1} + (\tilde{\epsilon})^\times] \tilde{\omega} \right) \end{aligned} \quad (4.78)$$

We will now choose a sliding mode control law, where we use the best estimates, or nominal values, of the system parameters. These values are denoted with a hat ($\hat{\cdot}$). The control laws are chosen as:

$$\tau_c = -\tau_{sgn} \quad (4.79a)$$

$$\begin{aligned} \mathbf{A} \tau_a = & (\hat{\mathbf{h}}^b)^\times [\tilde{\omega} + \hat{\omega}_0 \mathbf{c}_2] + \frac{3}{2} \hat{\omega}_0^2 \mathbf{c}_3^T \hat{\mathbf{I}} \mathbf{c}_3 \\ & + \hat{\omega}_0 \hat{\mathbf{J}}(\mathbf{c}_2)^\times \tilde{\omega} + \frac{1}{2} \hat{\mathbf{J}} \mathbf{P} [\tilde{\eta} \mathbf{1} + (\tilde{\epsilon})^\times] \tilde{\omega} + \tau_{sgn,a} \end{aligned} \quad (4.79b)$$

$$\tau_{sgn} = [\beta_x \text{sgn}(s_x), \beta_y \text{sgn}(s_y), \beta_z \text{sgn}(s_z)]^T \quad (4.79c)$$

$$\tau_{sgn,a} = [\beta_{a,x} \text{sgn}(s_x), \beta_{a,y} \text{sgn}(s_y), \beta_{a,z} \text{sgn}(s_z)]^T \quad (4.79d)$$

The sign function $\text{sgn}(\cdot)$ is defined in (3.90c). We will now define the error of a parameter α to be $\Delta\alpha = \alpha - \hat{\alpha}$. Using this notation, and inserting (4.79) into (4.78), we get:

$$\begin{aligned} \dot{V} = \mathbf{s}^T & \left((\Delta \mathbf{h}^b)^\times \tilde{\omega} - (\Delta(\mathbf{h}^b \omega_0))^\times \mathbf{c}_2 + \frac{3}{2} \mathbf{c}_3^T \Delta(\omega_0^2 \mathbf{I}) \mathbf{c}_3 \right. \\ & \left. + \Delta(\omega_0 \mathbf{J})(\mathbf{c}_2)^\times \tilde{\omega} + \frac{1}{2} \Delta \mathbf{J} \mathbf{P} [\tilde{\eta} \mathbf{1} + (\tilde{\epsilon})^\times] \tilde{\omega} \right. \\ & \left. - \tau_{sgn} - \tau_{sgn,a} \right) \end{aligned} \quad (4.80)$$

The details of this calculation is found in appendix A.2.8. To simplify the expression, we will collect all the parameter error terms in the variable $\delta = [\delta_x, \delta_y, \delta_z]^T$:

$$\begin{aligned} \delta &= (\Delta \mathbf{h}^b)^\times \tilde{\omega} - (\Delta(\mathbf{h}^b \omega_0))^\times \mathbf{c}_2 + \frac{3}{2} \mathbf{c}_3^T \Delta(\omega_0^2 \mathbf{I}) \mathbf{c}_3 \\ &\quad + \Delta(\omega_0 \mathbf{J})(\mathbf{c}_2)^\times \tilde{\omega} + \frac{1}{2} \Delta \mathbf{J} \mathbf{P} [\tilde{\eta} \mathbf{1} + (\tilde{\epsilon})^\times] \tilde{\omega} \end{aligned} \quad (4.81)$$

$$\begin{aligned} &\Downarrow \\ \dot{V} &= \mathbf{s}^T (\delta - \tau_{sgn} - \tau_{sgn,a}) \end{aligned} \quad (4.82)$$

If we choose $\beta_i + \beta_{a,i}$ larger than δ_i , i.e.

$$\beta_i + \beta_{a,i} \geq \delta_i + \beta_{0,i} \quad (4.83)$$

where $\beta_{0,i} > 0$ is a constant, we get:

$$\dot{V} \leq -(\beta_{0,x} |s_x| + \beta_{0,y} |s_y| + \beta_{0,z} |s_z|) \quad (4.84)$$

For $\mathbf{s} \neq 0$, $\dot{V} < 0 \Rightarrow \mathbf{s} \rightarrow 0$. Hence, we reach our manifold \mathbf{s} in finite time and the system is globally asymptotically stable.

Chapter 5

Simulation

5.1 SIMULINK model of ESEO

5.1.1 Mathematical model

The mathematical model given by (4.9) and (4.10) has been implemented in SIMULINK. Recall that ESEO only has one reaction wheel, which means that the Lyapunov controllers must be adapted to this situation. Therefore we will define the 3×3 matrix \mathbf{B} which is equal to the identity matrix if there are no reaction wheels. Then, each column represents the three unit vectors of \mathcal{F}_b . If the reaction wheels can give a torque about an axis of \mathcal{F}_b , the corresponding unit vector in \mathbf{B} is zero. $\mathbf{B} = \mathbf{0}$ if the reaction wheels can give torques about all body axes.

$$\mathbf{A} = \begin{bmatrix} 0 \\ 1 \\ 0 \end{bmatrix} \Rightarrow \mathbf{B} = \begin{bmatrix} 1 & 0 & 0 \\ 0 & 0 & 0 \\ 0 & 0 & 1 \end{bmatrix} \quad (5.1)$$

5.1.2 Simulation parameters

For the simulation, we will have a relatively short time frame, i.e. several hundred seconds. A circular orbit is assumed, which is possible since a segment of an ellipse can be approximated to be a part of a circle. The altitude of ESEO in this circular orbit will be its altitude at perigee. The desired position of ESEO at the start of all the simulations is to coincide with the orbit frame \mathcal{F}_o . The controllers are tuned to satisfy an attitude accuracy of $\pm 1^\circ$. All simulation results are found in appendix B.

Step simulation with ideal conditions

The first simulation to be performed is a step simulation with ideal conditions, i.e. perfect measurements of the state vector and correct values of system parameters. After 500 seconds, there is a step in the desired position. All axes of the body frame of ESEO \mathcal{F}_b are commanded to have an angle of 30° with their respective axes in \mathcal{F}_o . These angles are the Euler angles. Even though the simulator uses unit quaternions to calculate ESEO's attitude, the input attitude and output attitude are given in Euler angles, since they have a clearer physical meaning. ESEO's

initial states are given below where $\tilde{\Theta}$ denotes the attitude error in Euler angles.

$$\tilde{\Theta}_{init} = \begin{bmatrix} 60^\circ \\ 60^\circ \\ 60^\circ \end{bmatrix} = \begin{bmatrix} 1.0472 \text{ rad} \\ 1.0472 \text{ rad} \\ 1.0472 \text{ rad} \end{bmatrix} \quad (5.2a)$$

$$\tilde{\omega}_{init} = \begin{bmatrix} 1^\circ/\text{s} \\ 1^\circ/\text{s} \\ 1^\circ/\text{s} \end{bmatrix} = \begin{bmatrix} 0.0175 \text{ rad/s} \\ 0.0175 \text{ rad/s} \\ 0.0175 \text{ rad/s} \end{bmatrix} \quad (5.2b)$$

$$\omega_{s,init} = 0 \quad (5.2c)$$

Regarding thruster control, a bang-bang controller with deadzone is used. The deadzone parameter in figure 3.7 is chosen to be:

$$O_n = 0.001 \quad (5.3)$$

Large initial angular velocity

The second simulation has the same initial states as the first, except for the initial angular velocity, which is changed to a large value:

$$\tilde{\omega}_{init} = \begin{bmatrix} 1 \text{ rad/s} \\ 1 \text{ rad/s} \\ 1 \text{ rad/s} \end{bmatrix} \quad (5.4)$$

There is no step in this simulation, and the desired Euler angles of \mathcal{F}_b are constantly 30° with the respective axes of \mathcal{F}_o .

Step simulation with uncertain inertia

This is the same simulation as the step simulation, but the controllers use estimates of the inertial parameters, rather than the correct ones. The estimates and actual inertial parameters are given below, where the estimates are denoted with a hat ($\hat{\cdot}$).

$$\hat{\mathbf{I}} = \begin{bmatrix} 4.3500 & 0 & 0 \\ 0 & 4.3370 & 0 \\ 0 & 0 & 3.6640 \end{bmatrix} \quad (5.5a)$$

$$\mathbf{I} = 0.8\hat{\mathbf{I}} \quad (5.5b)$$

$$\hat{i}_s = 4 \times 10^{-5} \text{ kgm}^2 \quad (5.5c)$$

$$i_s = 0.8\hat{i}_s \quad (5.5d)$$

Step simulation with noise

This fourth simulation has the same initial conditions as the first, and the same step is performed. The difference is that white noise is added to the state vector which is fed to the controllers. The motivation for this simulation, is that ESEO will receive estimates of its state

vector from an estimator, usually a Kalman filter. These estimates are not necessarily correct, but should be close to the real values. Secondly, they will not be updated continuously, but with a certain frequency. The added white noise simulates this behavior. More precisely, the white noise has a frequency of 10 Hz, and the noise vector's amplitude is approximately 5 percent of the vector $\chi = [\chi_\omega^T, \chi_s, \chi_q^T]^T$:

$$\chi_\omega = \tilde{\omega}_{init}/2 \quad (5.6a)$$

$$\chi_s = 1 \text{ rad/s} \quad (5.6b)$$

$$\chi_q = 1/2 [1, 1, 1, 1]^T \quad (5.6c)$$

5.2 Linear control

The global controller has been proved to stabilize ESEO if $i_y > i_x > i_z$. However this restriction is not met by ESEO, because $i_x > i_y > i_z$. Hence only the local controller is simulated.

5.2.1 Local controller

The controller below is based on the linearized model of ESEO:

$$\tau_c = -k_\epsilon \mathbf{I}\tilde{\epsilon} - k_\omega \tilde{\omega} \quad (5.7a)$$

$$\tau_a = 0 \quad (5.7b)$$

The controller parameters satisfy

$$k_\epsilon \gg i_s = 4 \times 10^{-5} \quad (5.8a)$$

$$k_\omega > 0 \quad (5.8b)$$

$$k_\omega^2 > \omega_0^2 \left(i_z [2i_y - 2i_x - i_z] - [i_y - i_x]^2 \right) = -1.8597 \times 10^{-5} \quad (5.8c)$$

and the following parameters were chosen for the simulation:

$$k_\epsilon = 0.05 \quad (5.9)$$

$$k_\omega = 3 \quad (5.10)$$

The simulation results for this local controller can be found in figure B.1, figure B.5, figure B.9 and figure B.10. For the noise simulation, the bang-bang dead-zone was changed to $O_n = 0.007$.

5.3 Nonlinear control

Lyapunov controller 2 has been proved to stabilize ESEO if $i_y > i_x > i_z$, but this is not the case for ESEO. Therefore, we will only simulate the performance of Lyapunov controller 1 and 3.

5.3.1 Lyapunov controller 1

The first Lyapunov controller is given by

$$\tau_c = -k_\epsilon \tilde{\epsilon} - k_\omega \tilde{\omega} + \omega_0^2(\mathbf{c}_2)^\times \mathbf{I}\mathbf{c}_2 - 3\omega_0^2(\mathbf{c}_3)^\times \mathbf{I}\mathbf{c}_3 \quad (5.11a)$$

$$\tau_a = -k_s \omega_s \quad (5.11b)$$

where the controller parameters satisfy

$$k_\epsilon > 0 \quad (5.12a)$$

$$k_\omega > 0 \quad (5.12b)$$

$$k_s > 0 \quad (5.12c)$$

They are chosen as:

$$k_\epsilon = 0.2 \quad (5.13a)$$

$$k_\omega = 3 \quad (5.13b)$$

$$k_s = 0.001 \quad (5.13c)$$

The results from the simulations are presented in figure B.2, figure B.6, figure B.9 and figure B.11. For the noise simulation, the bang-bang dead-zone was changed to $\text{On} = 0.006$.

5.3.2 Lyapunov controller 3

Since ESEO only has one reaction wheel, the control laws for Lyapunov controller 3 are rewritten as

$$\begin{aligned} \tau_c = & -k_{\epsilon,1} \tilde{\epsilon} - k_{\omega,1} \tilde{\omega} - \omega_0 \mathbf{B}(\mathbf{c}_2)^\times \mathbf{A}\mathbf{I}_s (\mathbf{A}^T \tilde{\omega} + \omega_s) \\ & + \omega_0^2 \mathbf{B}(\mathbf{c}_2)^\times \mathbf{I}\mathbf{c}_2 - 3\omega_0^2 \mathbf{B}(\mathbf{c}_3)^\times \mathbf{I}\mathbf{c}_3 \tilde{\omega} \end{aligned} \quad (5.14a)$$

$$\begin{aligned} \mathbf{A}\tau_a = & k_{\epsilon,2} \tilde{\epsilon} + k_{\omega,2} \tilde{\omega} + \omega_0(\mathbf{c}_2)^\times \mathbf{A}\mathbf{I}_s (\mathbf{A}^T \tilde{\omega} + \omega_s) \\ & - \omega_0^2(\mathbf{c}_2)^\times \mathbf{I}\mathbf{c}_2 + 3\omega_0^2(\mathbf{c}_3)^\times \mathbf{I}\mathbf{c}_3 \end{aligned} \quad (5.14b)$$

where the controller parameters satisfy:

$$k_{\epsilon,1} + k_{\epsilon,2} > 0 \quad (5.15a)$$

$$k_{\omega,1} + k_{\omega,2} > 0 \quad (5.15b)$$

By introducing \mathbf{B} , the thrusters will compensate for the nonlinear terms about the x axis and the z axis of \mathcal{F}_b . For the step simulation, the following parameters were chosen:

$$k_{\epsilon,1} = 0.2 \quad (5.16a)$$

$$k_{\epsilon,2} = 0.2 \quad (5.16b)$$

$$k_{\omega,1} = 3 \quad (5.16c)$$

$$k_{\omega,2} = 3 \quad (5.16d)$$

The step simulation results for this controller can be found in figure B.3. When simulating with a large initial angular velocity, the gains were changed because it gave better performance:

$$k_{\epsilon,1} = 0.1 \quad (5.17a)$$

$$k_{\epsilon,2} = 0.1 \quad (5.17b)$$

$$k_{\omega,1} = 2 \quad (5.17c)$$

$$k_{\omega,2} = 2 \quad (5.17d)$$

Figure B.7 shows the results of this simulation. The last two simulations are presented in figure B.9 and figure B.12. The bang-bang dead-zone was changed to $\text{On} = 0.006$ in the noise simulation.

5.3.3 Sliding mode controller

The Lyapunov controllers are not designed to be robust to parameter uncertainties, like the sliding mode controller. Therefore we will compare the controllers when assuming that the system parameters are correct. Thus, the nonlinearities are canceled, and the gains β_i and $\beta_{a,i}$ can be chosen constant. The rewritten sliding mode controller becomes

$$\begin{aligned} \tau_c = & -\mathbf{B}(\mathbf{h}^b)^\times [\tilde{\omega} - \omega_0 \mathbf{c}_2] - \frac{3}{2} \omega_0^2 \mathbf{B} \mathbf{c}_3^T \mathbf{I} \mathbf{c}_3 \\ & - \omega_0 \mathbf{B} \mathbf{J}(\mathbf{c}_2)^\times \tilde{\omega} - \frac{1}{2} \mathbf{B} \mathbf{J} \mathbf{P} [\tilde{\eta} \mathbf{1} + (\tilde{\epsilon})^\times] \tilde{\omega} \\ & - \tau_{sgn} \end{aligned} \quad (5.18a)$$

$$\begin{aligned} \mathbf{A} \tau_a = & (\mathbf{h}^b)^\times [\tilde{\omega} - \omega_0 \mathbf{c}_2] + \frac{3}{2} \omega_0^2 \mathbf{c}_3^T \mathbf{I} \mathbf{c}_3 \\ & + \omega_0 \mathbf{J}(\mathbf{c}_2)^\times \tilde{\omega} + \frac{1}{2} \mathbf{J} \mathbf{P} [\tilde{\eta} \mathbf{1} + (\tilde{\epsilon})^\times] \tilde{\omega} \\ & + \tau_{sgn,a} \end{aligned} \quad (5.18b)$$

$$\tau_{sgn} = [\beta_x \text{sgn}(s_x), \beta_y \text{sgn}(s_y), \beta_z \text{sgn}(s_z)]^T \quad (5.18c)$$

$$\tau_{sgn,a} = [\beta_{a,x} \text{sgn}(s_x), \beta_{a,y} \text{sgn}(s_y), \beta_{a,z} \text{sgn}(s_z)]^T \quad (5.18d)$$

where

$$\beta_i + \beta_{a,i} > 0 \quad (5.19)$$

To avoid chattering, the sign function is replaced with the saturation function (figure 3.4). The

parameters for the sliding mode controller were chosen as follows:

$$\gamma = 0.05 \quad (5.20a)$$

$$\mathbf{P} = 0.1 \mathbf{1} \quad (5.20b)$$

$$\beta_x = 0.2 \quad (5.20c)$$

$$\beta_y = 0.1 \quad (5.20d)$$

$$\beta_z = 0.2 \quad (5.20e)$$

$$\beta_{a,y} = 0.1 \quad (5.20f)$$

$$\beta_{a,x} = \beta_{a,z} = 0 \quad (5.20g)$$

Note that since ESEO only has a reaction wheel about its y -axis, $\beta_{a,x}$ and $\beta_{a,z}$ can be chosen arbitrarily. This controller's simulation results can be found in figure B.4, figure B.8, figure B.9 and figure B.13. For the noise simulation, the bang-bang dead-zone was changed to $O_n = 0.010$.

Chapter 6

Discussion and conclusion

6.1 Discussion

6.1.1 Theoretical analysis

Mathematical model

Regarding the kinematical model in chapter 4, Euler parameters are chosen for the angular parametrization, since they do not introduce singularities in the model. It is however possible to use a three parameter representation with singularities. Fossen (2002) suggests using two representations of Euler angles with different singularities, and switching between them. There are other possible representations with three parameters, like the Euler-Rodrigues parameters (Egeland et al., 2001), but four parameters are needed to avoid singularities (Hughes, 1986). Another advantage of the Euler parameters is that they are computationally efficient (Hughes, 1986). Euler angles can be demanding to compute because of the trigonometric functions associated with them.

In the mathematical model developed in chapter 4 for the system dynamics, the system states are chosen as the angular velocities of ESEO and the reaction wheel. An alternative would have been to use the angular momenta as states. There are several explanations for this decision. One of them is that angular momenta can not be observed or measured directly. They must be calculated from the angular velocities. Another reason is that the error dynamics of such a system would have introduced more equations in the satellite model, as in Hall et al. (2002). On the other hand, such a model representation would have had simpler equations than the one used here.

Linear control

The advantage of the linear controllers is that they are easy to implement, and computationally simple. However, neither the local PD controller nor the global linear controller use reaction wheels to control the spacecraft's attitude. The global controller uses the reaction wheels to control themselves. Thus, if one wishes to use a linear controller, the reaction wheel may not serve any purpose and can be removed from the spacecraft. This would yield a simpler mathematical model, i.e. the classical spacecraft model which is treated in example 3.1.

Nonlinear control

The Lyapunov controllers presented in this thesis are found by canceling nonlinearities, to obtain asymptotic stability. The alternative to this approach is to dominate the nonlinear terms, i.e. choosing large controller gains to make sure that $\dot{V} \leq 0$ regardless of the nonlinear term's value. This is often possible if the nonlinear terms are bounded. This technique will often yield simpler controllers, while the advantage of canceling nonlinearities is that it gives greater freedom when selecting controller gains. A disadvantage of canceling nonlinearities, is that the technique is vulnerable to parameter uncertainties. Dominating them yields more robust controllers.

It is important to note, that the sliding mode controller together with Lyapunov controller 2 and 3 are the only controllers which use the reaction wheels actively to control the spacecraft's attitude. In fact, they permit to only use reaction wheels for attitude control if the reaction wheels can produce torques about all axes of the spacecraft body frame. Lyapunov controller 1 cannot control the spacecraft's attitude without the thrusters.

6.1.2 Simulation

When viewing the simulation results, it is easily seen that the attitude is never exactly equal to the desired attitude. This is because of the thruster torques generated by the bang-bang controller with dead-zone. Since the thrusters are not capable of delivering exact torques, the attitude error never reaches exactly zero. Instead the attitude converges to an interval close to the desired attitude. Another interesting observation, is that the Euler angle representing rotation about the y -axis converges slightly faster than the two other Euler angles, and it has a higher degree of accuracy. This applies to all the controllers in the step simulations. Since Lyapunov controller 3 and the sliding mode controller use the wheel actively to help controlling θ , it makes sense that θ converges faster and is closer to the desired value than the other Euler angles. However, in the simulation with large initial angular velocity, θ is the fastest converging Euler angle only for the local PD controller and Lyapunov controller 1. Another explanation is that the reaction wheel has a damping effect on the rotation about the y -axis, and this helps θ to converge. This makes sense, because if the satellite body starts to spin in one direction about the y -axis, the reaction wheel will spin in the opposite direction. It is probable that both explanations are valid, but when using the reaction wheel actively at large initial spin, other effects arise.

Step simulation with ideal conditions

In the step simulation with ideal conditions, all the controllers, including the local PD controller, obtain an accuracy of $\pm 1^\circ$, and they converge close to the desired attitude after approximately 100 seconds. Thus, the local PD controller works, even though it does not operate close to its operating point. From a theoretical point of view this can be explained. It is shown in appendix A.2.9 that the local PD controller is stable close to the origin, but will never reach it. The local PD controller is not globally asymptotically stable. We have already observed that the attitude error converges to an interval because of the thruster controller. It seems that this interval contains the interval which the local PD controller converges to. Thus, the fact that the controller does not converge to an attitude error of zero has no effect on the controller's performance.

Concerning the reaction wheel, the local PD controller lets it spin on its own (figure B.1), while Lyapunov controller 1 makes $\omega_s \rightarrow 0$ (figure B.2). The latter seems to be a disadvantage, since this causes a disturbance torque with respect to the attitude control of ESEO. The reason for this is that the control law for the reaction wheel only cares about the wheel spin, not the satellite's other states. Thus, increased thrusting is needed to compensate. Figure B.2 shows that Lyapunov controller 1 has more thruster firings than the other controllers. Lyapunov controller 3 and the sliding mode controller both use the reaction wheel actively to reach the desired attitude. When the simulation starts, the desired attitude is far from the actual attitude. Thus, a large torque is put on the reaction wheel. It quickly reaches saturation, and is then unable to provide torques, unless it is commanded to spin the other way. From figure B.3 we see that the wheel stays saturated when Lyapunov controller 3 is used. Thus the reaction wheel only gives one large torque in the beginning of the simulation. Afterwards, only the thrusters are used to control ESEO's attitude. This is not the case for the sliding mode controller. The reaction wheel delivers a large torque in the beginning, and when the step is performed. Hence, it can be concluded that the sliding mode controller uses the reaction wheel in a better way than Lyapunov controller 3.

Large initial angular velocity

As in the former simulation, the controllers converge with the desired accuracy. It is interesting to see that the local PD controller performs as well as the other controllers. The explanations are the same as in the preceding section. Although all controllers converge, the sliding mode controller and Lyapunov controller 3 are about 50 seconds slower than the other controllers. In addition, they have considerably more thruster firings than the other controllers. It is natural to assume that this is related to the use of the reaction wheel. Note that when the satellite rotates several times about its own axes, the P term of the linear controllers and the Lyapunov controllers, i.e. typically $-k_0\tilde{e}$, changes sign often. What is needed is to reduce the angular velocity, but the P term will always try to get to a certain point in space, and does not care about angular velocity. The D term contributes greatly to reduce the rotation, and when it is reduced considerably, the P term will bring ESEO into its final position. This means that for a large initial angular velocity, it could be a good idea to have a controller which only slows down the satellite's rotation, since the P term actually will accelerate the rotation periodically. This is the idea behind the modified PD controller in figure 2.3. When the angular velocity is sufficiently low, one could switch to one of the controllers suggested in this thesis.

Step simulation with uncertain inertia

Figure B.9 shows that differences between the nominal inertial parameters of the satellite and the actual inertial parameters, yields almost the same results as in the step simulation with ideal conditions. The only difference is that the spacecraft attitude converges approximately 10 to 30 seconds later. Thus, all controllers seem to be robust with respect to uncertain inertial parameters. It is known that sliding mode controllers are robust to such uncertainties, but more surprising that the Lyapunov controllers perform well. These controllers cancel nonlinearities which are functions of inertial parameters. An explanation to this, might be that the nonlinearities are so small in magnitude that they do not come into play before the system states have converged to the convergence interval induced by the thruster controller. The local PD controller performs well because it is sufficient that $k_e\mathbf{I} \gg 4.1979 \cdot 10^{-5}$ to approach the origin.

This is shown in appendix A.2.9.

Step simulation with noise

Because of the added noise, all controllers use more thruster firings, which is natural since the feedback states never converge to constant values. In fact, the deadzone of the bang-bang controller had to be enlarged, since the controllers fired the thrusters constantly.

6.1.3 Implementation issues

Implementation of the control laws suggested in this thesis depends on two important subjects. The first is computational resources. The nonlinear controllers require more resources in every time step to compute the control torques, compared to the linear controllers. Especially the Lyapunov controllers, since they rely on cancellation of nonlinearities. Regarding the sliding mode controller, it will often be possible to choose the gain β constant, like in our simulations, which will make the controller simpler to implement. The second important subject is the availability of measurements of the system states and the system parameters. System state measurements will typically be estimates coming from a Kalman filter, which is the case for ESEO. It is evident that these measurements should be available and as accurate as possible. Regarding the actual system parameters, the Lyapunov controllers require more parameters to work than the other controllers because of the nonlinearity cancellation. The linear controllers do not require such knowledge, and neither does the sliding mode controller if the gain β can be chosen constant. The simulation with uncertain inertial parameters shows that all controllers work well, but if some parameters are unknown, it could be wise to avoid the Lyapunov controllers.

6.2 Conclusion

In this thesis, linear and nonlinear control methods are developed to control the attitude of a satellite. Except for the local PD controller, the controllers can be used to control any satellite using thrusters and reaction wheels as actuators. Two linear control laws are developed. The local PD controller is based on a linearized satellite model of ESEO, which means that it does not apply to a general spacecraft. It does not use the reaction wheel when controlling ESEO. The global linear controller stabilizes a spacecraft if its diagonal inertia matrix satisfies the constraint $i_y > i_x > i_z$. This controller controls the spin of the reaction wheels to zero. Four nonlinear control laws have been developed. Three of them, the Lyapunov controllers, have been found through Lyapunov stability analysis. They are based on different LFCs, and work by canceling system nonlinearities. The fourth controller is a sliding mode controller. Lyapunov controller 2 and 3, and the sliding mode controller, use the reaction wheels actively to control the spacecraft's attitude. This is not achieved with the linear controllers, nor Lyapunov controller 1. It is worth noting that the inertia matrix constraint $i_y > i_x > i_z$ simplifies the Lyapunov controllers.

To simulate the performance of the developed controllers, a nonlinear mathematical model is developed and implemented in MATLAB/SIMULINK. Data for the micro-satellite ESEO is used as model parameters in the simulations, and a bang-bang controller with dead-zone is used for thruster control. The performance of two controllers is not simulated, since ESEO's

inertia matrix does not meet the constraint $i_y > i_x > i_z$. The controllers are tested in four different simulations. The first is a basic step simulation with perfect measurements of the state vector. The second is a test of convergence when the spacecraft has a large initial spin. Controller performance with uncertain inertial parameters is the objective of the third simulation. In the last simulation, noise is added to the measured state vector. The simulations show that the developed controllers perform well regarding attitude control of ESEO. An important observation is that the controllers which actively use the reaction wheel of ESEO as an actuator to control its attitude, does not produce better results than the local PD controller which do not use it, or Lyapunov controller 1 which controls the reaction wheel spin to zero. The presence of the reaction wheel seems to help convergence to the origin for these controllers as well. In fact, the Euler angle representing rotation about the y -axis converges slightly faster than the two other Euler angles, and it has a higher degree of accuracy. This suggests that the reaction wheel has a stabilizing effect on ESEO, even when it is not used actively.

6.3 Recommendations

A natural suggestion for further work is to develop a model of a Kalman filter to provide the measured state vector to the controllers, which produces realistic noise and accuracy. The white noise vector χ presented here is not chosen from any experimental data.

Regarding thruster control, it would be interesting to see the performance of a PWPF modulator compared to the implemented bang-bang controller. A PWPF modulator should in theory provide more accurate control, but it poses a tuning problem, since it has several tunable parameters.

The simulations suggest that using reaction wheels as actuators provides a challenge. It would be interesting to see if control allocation (Fossen, 2002) could be used to obtain better performance. The idea of control allocation is to first compute a torque to be commanded, and then find the best way to produce that torque using the available actuators. With this approach, the reaction wheels could be used actively for attitude control, regardless of control method. Another challenge regarding the reaction wheels is to develop a control algorithm to unload the reaction wheels, i.e. to slow them down when they reach saturation, in order to use them again. They cannot provide any torques while spinning at constant speed.

The controllers presented in this thesis are shown to bring the spacecraft's attitude to the error quaternion $\tilde{\mathbf{q}}_1 = [1, 0, 0, 0]^T$ which is a stable equilibrium point of the system. The error quaternion $\tilde{\mathbf{q}}_2 = [-1, 0, 0, 0]^T$ represents an unstable equilibrium point, but from the definition of unit quaternions, it is clear that $\tilde{\mathbf{q}}_2$ represents the same attitude as $\tilde{\mathbf{q}}_1$. It would be interesting to design controllers in such a way that both of these equilibrium points are stable. This is done for underwater vehicles in Fjellstad et. al (1994).

An important assumption of the development of the controllers in this thesis, is that the gravity gradient of the Earth is the only external disturbance torque which affects the satellite. This assumption will be violated if the satellite should go into moon orbit, which is the objective of the ESMO mission, and hence the controllers using system parameters to calculate control torques will need to be modified. Secondly, other disturbance torques may become significant for a satellite far from the Earth. This should be investigated for the ESMO mission.

Bibliography

Balchen, J. G., Andresen, T. and Foss, B. A., *Reguleringsteknikk*. Trondheim, Norway: Department of Engineering Cybernetics, Norwegian University of Science and Technology, 2001.

Egeland, O. and Gravdahl, J. T., *Modeling and Simulation for Control*. Trondheim, Norway: Department of Engineering Cybernetics, Norwegian University of Science and Technology, 2001.

Fauske, K. M., NCUBE Attitude Control. (Master thesis, Department of Engineering Cybernetics, Norwegian University of Science and Technology, 2002).

Fjellstad, O. and Fossen, T. I., *Quaternion Feedback Regulation of Underwater Vehicles*. *Proceedings of the Third IEEE Conference on Control Applications, Glasgow, UK, 1994*.

Fossen, T. I., *Marine Control Systems*. Trondheim, Norway: Marine Cybernetics, 2002.

Fu, L-C., Tsai, C-W. and Yeh, F-K. *A Nonlinear Missile Guidance Controller with Pulse Type Input Devices*. *Proceedings of the American Control Conference, San Diego, California, USA, 1999*.

Gravdahl, J. T., Eide, E., Skavhaug, A., Svartveit, K., Fauske, K. M. and Indergaard, F. M., *Three axis Attitude Determination and Control System for a picosatellite: Design and implementation*. *Proceedings of the 54th International Astronautical Congress, Bremen, Germany, 2003*.

Hall, C. D., *High Speed Flywheels for Integrated Energy Storage and Attitude Control*. *Proceedings of the American Control Conference, Albuquerque, New Mexico, USA, 1997*.

Hall, C. D., *Attitude Dynamics of Orbiting Gyrostats*. Invited Paper at the US - European Celestial Mechanics Workshop, Adam Mickiewicz University, Poznan, Poland, July 2000.

Hall C. D., Tsiotras, P. and Shen H., *Satellite Attitude Control and Power Tracking with Energy/Momentum Wheels*. *Journal of Guidance, Control and Dynamics*, Vol. 24, No. 1, 2001.

Hall C. D., Tsiotras, P. and Shen H., *Tracking Rigid Body Motion Using Thrusters and Momentum Wheels*. *Journal of the Astronautical Sciences*, Vol. 50, No. 3, 2002.

Hegrenæs, Ø., *Attitude Control by means of Explicit Model Predictive Control, via Multi-Parametric Quadratic Programming*. (Master thesis, Department of Engineering Cybernetics, Norwegian University of Science and Technology, 2004).

Hughes, P. C., *Spacecraft Attitude Dynamics*. USA: John Wiley & Sons, Inc., 1986.

Khalil, H. K., *Nonlinear Systems*. Upper Saddle River, New Jersey, USA: Pearson Education International Inc., 2000.

Kristiansen, R., Attitude Control of a Microsatellite. (Master thesis, Department of Engineering Cybernetics, Norwegian University of Science and Technology, 2000).

Lee, J. G., Park, C. G. and Park, H. W., Sliding-Mode Controller Design for Spacecraft Attitude Tracking Maneuvers. *IEEE Transactions on aerospace and electronic systems*, Vol. 29, No. 4, 1993.

Ogata, K., *Discrete-Time Control Systems*. Upper Saddle River, New Jersey, USA: Prentice-Hall Inc., 1995.

Riise, Å-R., Samuelsen, B., Sokolova, N., Cederblad, H., Fasseland, J., Nordin, C., Otterstad, J., Fauske, K., Eriksen, O., Indergaard, F., Svartveit, K., Furebotten, P., Sæther, E., and Eide, E., *Ncube: The First Norwegian Student Satellite. Proceedings of The 17th AIAA/USU Conference on Small Satellites, Logan, Utah, USA, 2003*.

Show, L-L., Juang, J-C. and Jan, Y-W., An LMI-Based Nonlinear Attitude Control Approach. *IEEE Transactions on control systems technology*, Vol. 11, No. 1, 2003.

Soglo, P. K., 3-aksestyring av gravitasjonsstabilisert satelitt ved bruk av magnetpoler. (Master thesis, Department of Engineering Cybernetics, Norwegian University of Science and Technology, 1994).

Song, G. and Agrawal, B. N., Vibration Suppression during Attitude Control. *Acta Astronautica*, Vol. 49, No. 2, 2001.

SSETI ESEO AOCS team, *Subsystem Requirements Document Phase - B*. (Issue 3, 2004a, ESA/ESTEC, Noordwijk, The Netherlands).

SSETI ESEO AOCS team, *Reaction Wheel Design Justification Document Phase - B*. (Issue 4, 2004b, ESA/ESTEC, Noordwijk, The Netherlands).

SSETI ESEO AOCS team, *Attitude Estimation and Control Design Justification Document Phase - B*. (Issue 3, 2004c, ESA/ESTEC, Noordwijk, The Netherlands).

SSETI ESEO MIAS team, *Mission Analysis Phase C Report*. (Issue 1, 2003, ESA/ESTEC, Noordwijk, The Netherlands).

SSETI ESEO PROP team, *Operations Plan*. (Issue 9, 2003, ESA/ESTEC, Noordwijk, The Netherlands).

SSETI PR team, 2004. *SSETI* [Online]. Available from: URL <http://sseti.gte.tuwien.ac.at/WSW4/> [Accessed 24 May 2004].

Trottemant, E. J. and SSETI teams, *ESEO European Student Earth Orbiter Phase-A Study Report*. (2001, ESA/ESTEC, Noordwijk, The Netherlands).

Weisstein, E. W., 2004a. *Schwarz's Inequality* [Online]. Available from: MathWorld - A Wolfram Web Resource. URL <http://mathworld.wolfram.com/SchwarzsInequality.html> [Accessed 9 June 2004].

Weisstein, E. W., 2004b. *Young's Inequality* [Online]. Available from: MathWorld - A Wolfram Web Resource. URL <http://mathworld.wolfram.com/YoungsInequality.html> [Accessed 9 June 2004].

Weisstein, E. W., 2004c. *Matrix Norm* [Online]. Available from: MathWorld - A Wolfram Web Resource. URL <http://mathworld.wolfram.com/MatrixNorm.html> [Accessed 9 June 2004].

Wertz, J. R. and Larson, W. J., *Space Mission Analysis and Design*. Dordrecht, The Netherlands: Kluwer Academic Publishers Group, 1999.

Wie, B., *Space Vehicle Dynamics and Control*. Reston, Virginia, USA: American Institute of Aeronautics and Astronautics, Inc., 1998.

Wie, B., Weiss, H. and Arapostathis, A., Quaternion Feedback Regulator for Spacecraft Eigenaxis Rotations. *Journal of Guidance, Control and Dynamics*, Vol. 12, No. 3, 1989.

Appendix A

Mathematical appendix

A.1 Calculus

A.1.1 Definitions

Definition A.1. A scalar function $V(\mathbf{x})$ where $\mathbf{x} \in \mathbb{R}^n$ is said to be positive definite if:

$$V(\mathbf{x}) > 0, \forall \mathbf{x} \neq 0 \quad (\text{A.1a})$$

$$V(\mathbf{x}) = 0 \Leftrightarrow \mathbf{x} = 0 \quad (\text{A.1b})$$

If $-V(\mathbf{x})$ is positive definite, then $V(\mathbf{x})$ is negative definite.

Definition A.2. A scalar function $V(\mathbf{x})$ where $\mathbf{x} \in \mathbb{R}^n$ is said to be positive semidefinite if:

$$V(\mathbf{x}) \geq 0, \forall \mathbf{x} \neq 0 \quad (\text{A.2a})$$

$$V(\mathbf{x}) = 0 \Leftrightarrow \mathbf{x} = 0 \quad (\text{A.2b})$$

If $-V(\mathbf{x})$ is positive semidefinite, then $V(\mathbf{x})$ is negative semidefinite.

Definition A.3. A real square matrix \mathbf{A} is symmetric if $\mathbf{A} = \mathbf{A}^T$.

Definition A.4. A real square matrix \mathbf{A} is skew-symmetric if $\mathbf{A} = -\mathbf{A}^T$. It has the following properties:

- The eigenvalues of a real skew-symmetric matrix are all zero.
- If \mathbf{A} is real, then $\mathbf{x}^T \mathbf{A} \mathbf{x} = 0$

Definition A.5. A real square symmetric matrix \mathbf{A} is said to be positive definite ($\mathbf{A} > 0$) if:

$$\mathbf{x}^T \mathbf{A} \mathbf{x} > 0, \forall \mathbf{x} \neq 0 \quad (\text{A.3a})$$

$$\mathbf{x}^T \mathbf{A} \mathbf{x} = 0 \Leftrightarrow \mathbf{x} = 0 \quad (\text{A.3b})$$

\mathbf{A} is negative definite ($\mathbf{A} < 0$) if $-\mathbf{A}$ is positive definite.

Definition A.6. A real square symmetric matrix \mathbf{A} is said to be positive semidefinite ($\mathbf{A} \geq 0$) if:

$$\mathbf{x}^T \mathbf{A} \mathbf{x} \geq 0, \forall \mathbf{x} \neq 0 \quad (\text{A.4a})$$

$$\mathbf{x}^T \mathbf{A} \mathbf{x} = 0 \Leftrightarrow \mathbf{x} = 0 \quad (\text{A.4b})$$

\mathbf{A} is negative semidefinite ($\mathbf{A} \leq 0$) if $-\mathbf{A}$ is positive semidefinite.

A.1.2 Vector and matrix norm properties

The norm $\|\cdot\|$ of a vector or matrix is a scalar, a kind of absolute value. There are several definitions of the vector and matrix norm (Ogata, 1995), but they all have the same properties. A widely used vector norm is the 2-norm:

$$\|\mathbf{x}\|_2 = \sqrt{\langle \mathbf{x}, \mathbf{x} \rangle} \quad (\text{A.5})$$

$\langle \cdot, \cdot \rangle$ denotes the inner product of a vector. The inner product of \mathbf{x} and \mathbf{y} in \mathbb{R}^n is given by (Ogata, 1995):

$$\langle \mathbf{x}, \mathbf{y} \rangle = \mathbf{x}^T \mathbf{y} = \mathbf{y}^T \mathbf{x} \quad (\text{A.6})$$

Note that the inner product is a scalar. The matrix 2-norm is defined by (Weisstein, 2004c):

$$\|\mathbf{A}\|_2 = \max_{\|\mathbf{x}\|_2=1} \|\mathbf{A}\mathbf{x}\|_2 \quad (\text{A.7})$$

If \mathbf{A} and \mathbf{B} are real $n \times n$ matrices and \mathbf{x} an n -dimensional vector, these properties apply (Ogata, 1995):

$$\|\mathbf{x}\| = 0, \forall \mathbf{x} \neq 0 \quad (\text{A.8a})$$

$$\|\mathbf{x}\| = 0 \Leftrightarrow \mathbf{x} = 0 \quad (\text{A.8b})$$

$$\|c\mathbf{x}\| = |k| \|\mathbf{x}\|, k \text{ is a scalar} \quad (\text{A.8c})$$

$$\|\mathbf{x} + \mathbf{y}\| \leq \|\mathbf{x}\| + \|\mathbf{y}\| \quad (\text{A.8d})$$

$$|\langle \mathbf{x}, \mathbf{y} \rangle| \leq \|\mathbf{x}\| \|\mathbf{y}\| \quad (\text{A.8e})$$

$$\|\mathbf{A}\| = \|\mathbf{A}^T\| \quad (\text{A.8f})$$

$$\|\mathbf{A} + \mathbf{B}\| \leq \|\mathbf{A}\| + \|\mathbf{B}\| \quad (\text{A.8g})$$

$$\|\mathbf{A}\mathbf{B}\| \leq \|\mathbf{A}\| \|\mathbf{B}\| \quad (\text{A.8h})$$

$$\|\mathbf{A}\mathbf{x}\| \leq \|\mathbf{A}\| \|\mathbf{x}\| \text{ (Schwartz's inequality)} \quad (\text{A.8i})$$

A.1.3 Matrix inversion

The following formulas for matrix inversion are found in the appendix of Ogata (1995). If \mathbf{A} , \mathbf{B} , \mathbf{C} and \mathbf{D} are, respectively, an $n \times n$, an $n \times m$, and $m \times n$, and and $m \times m$ matrix, and $|\mathbf{A}| \neq 0$ and $|\mathbf{S}_A| \neq 0$ where $\mathbf{S}_A = \mathbf{D} - \mathbf{C}\mathbf{A}^{-1}\mathbf{B}$, we have:

$$\begin{bmatrix} \mathbf{A} & \mathbf{B} \\ \mathbf{C} & \mathbf{D} \end{bmatrix}^{-1} = \begin{bmatrix} \mathbf{A}^{-1} + \mathbf{A}^{-1}\mathbf{B}\mathbf{S}_A^{-1}\mathbf{C}\mathbf{A}^{-1} & -\mathbf{A}^{-1}\mathbf{B}\mathbf{S}_A^{-1} \\ -\mathbf{S}_A^{-1}\mathbf{C}\mathbf{A}^{-1} & \mathbf{S}_A^{-1} \end{bmatrix} \quad (\text{A.9})$$

Alternatively, if $|\mathbf{D}| \neq 0$ and $|\mathbf{S}_D| \neq 0$ where $\mathbf{S}_D = \mathbf{A} - \mathbf{B}\mathbf{D}^{-1}\mathbf{C}$, we have:

$$\begin{bmatrix} \mathbf{A} & \mathbf{B} \\ \mathbf{C} & \mathbf{D} \end{bmatrix}^{-1} = \begin{bmatrix} \mathbf{S}_D^{-1} & -\mathbf{S}_D^{-1}\mathbf{B}\mathbf{D}^{-1} \\ -\mathbf{D}^{-1}\mathbf{C}\mathbf{S}_D^{-1} & \mathbf{D}^{-1}\mathbf{C}\mathbf{S}_D^{-1}\mathbf{B}\mathbf{D}^{-1} + \mathbf{D}^{-1} \end{bmatrix} \quad (\text{A.10})$$

A.1.4 Inequalities

Schwartz's inequality

Schwartz's inequality can be found in Weisstein (2004a), where it is expressed using the inner product $\langle \cdot, \cdot \rangle$ and the real functions f and g :

$$|\langle f, g \rangle|^2 \leq \langle f, f \rangle \langle g, g \rangle \quad (\text{A.11})$$

Young's inequality

Young's inequality can be found in Weisstein (2004b). It can be written like this:

$$\frac{a^p}{p} + \frac{b^q}{q} \geq ab \quad (\text{A.12a})$$

$$\frac{1}{p} + \frac{1}{q} = 1 \quad (\text{A.12b})$$

$$a \geq 0, b \geq 0, p > 1 \quad (\text{A.12c})$$

A.2 Theoretical analysis

A.2.1 Positive definiteness of V_r

Consider the function V_r :

$$V_r = -\frac{1}{2}\omega_0^2 \mathbf{c}_2^T \mathbf{I} \mathbf{c}_2 + \frac{1}{2}\omega_0^2 i_y \quad (\text{A.13})$$

We will now find the conditions for this function to be positive definite. In component form, V_r can be written as:

$$V_r = -\frac{1}{2}\omega_0^2 (i_x c_{12}^2 + i_y [c_{22}^2 - 1] + i_z c_{32}^2) \quad (\text{A.14})$$

Since the \mathbf{c}_2 is a unit vector, $c_{12}^2 + c_{22}^2 + c_{32}^2 = 1$. Inserting this into V_r yields:

$$V_r = \frac{1}{2}\omega_0^2 (i_y - i_x) c_{12}^2 + \frac{1}{2}\omega_0^2 (i_y - i_z) c_{23}^2 \quad (\text{A.15})$$

Thus:

$$i_y > i_x, i_y > i_z \Rightarrow V_r > 0 \quad (\text{A.16})$$

A.2.2 Positive definiteness of V_g

Consider the function V_g :

$$V_g = \frac{3}{2}\omega_0^2 \mathbf{c}_3^T \mathbf{I} \mathbf{c}_3 - \frac{3}{2}\omega_0^2 i_z \quad (\text{A.17})$$

We will now find the conditions for this function to be positive definite. V_g can be written as:

$$V_g = \frac{3}{2}\omega_0^2 (i_x c_{13}^2 + i_y c_{23}^2 + i_z [c_{33}^2 - 1]) \quad (\text{A.18})$$

The directional cosines are unit vectors, i.e. $c_{13}^2 + c_{23}^2 + c_{33}^2 = 1$. Inserting this into V_g yields:

$$V_g = \frac{3}{2}\omega_0^2 (i_x - i_z) c_{13}^2 + \frac{3}{2}\omega_0^2 (i_y - i_z) c_{23}^2 \quad (\text{A.19})$$

It is now clear that:

$$i_x > i_z, i_y > i_z \Rightarrow V_g > 0 \quad (\text{A.20})$$

A.2.3 Time derivative of V_a

Consider the function V_a :

$$V_a = \frac{1}{2}\tilde{\omega}^T \mathbf{I} \tilde{\omega} + \omega_s^T \mathbf{I}_s \mathbf{A}^T \tilde{\omega} + \frac{1}{2}\omega_s^T \mathbf{I}_s \omega_s \quad (\text{A.21})$$

To calculate \dot{V}_a we need expressions for $\dot{\tilde{\omega}}$ and $\dot{\omega}_s$. First we will define:

$$\begin{aligned} \nu = & \tilde{\omega}^\times \mathbf{I} \tilde{\omega} - \omega_0 \tilde{\omega}^\times \mathbf{I} \mathbf{c}_2 + \tilde{\omega}^\times \mathbf{A} \mathbf{I}_s \omega_s - \omega_0 (\mathbf{c}_2)^\times \mathbf{I} \tilde{\omega} \\ & + \omega_0^2 (\mathbf{c}_2)^\times \mathbf{I} \mathbf{c}_2 - \omega_0 (\mathbf{c}_2)^\times \mathbf{A} \mathbf{I}_s \omega_s \end{aligned} \quad (\text{A.22})$$

From (4.18) we obtain:

$$\dot{\tilde{\omega}} = \omega_0 (\mathbf{c}_2)^\times \tilde{\omega} - \mathbf{J}^{-1} (\nu + \tau_e - \mathbf{A} \tau_a) \quad (\text{A.23})$$

$$\dot{\omega}_s = \mathbf{A}^T \mathbf{J}^{-1} \nu - \mathbf{A}^T \mathbf{J}^{-1} \tau_e + (\mathbf{A}^T \mathbf{J}^{-1} \mathbf{A} + \mathbf{I}_s^{-1}) \tau_a \quad (\text{A.24})$$

The time derivative of V is given by:

$$\dot{V} = \underbrace{\tilde{\omega}^T \mathbf{I} \dot{\tilde{\omega}}}_{\dot{V}_1} + \underbrace{\tilde{\omega}^T \mathbf{A} \mathbf{I}_s \dot{\omega}_s}_{\dot{V}_2} + \underbrace{\omega_s^T \mathbf{I}_s \mathbf{A}^T \dot{\tilde{\omega}}}_{\dot{V}_3} + \underbrace{\omega_s^T \mathbf{I}_s \dot{\omega}_s}_{\dot{V}_4} \quad (\text{A.25})$$

Note that \dot{V}_2 has been transposed. Since it is a scalar, transposing it will not change its value. We will now calculate the time derivatives \dot{V}_i ($i = 1, \dots, 4$) along the system trajectories:

$$\dot{V}_1 = \tilde{\omega}^T \mathbf{I} (\omega_0(\mathbf{c}_2)^\times \tilde{\omega} - \mathbf{J}^{-1} \nu + \mathbf{J}^{-1} \tau_e - \mathbf{J}^{-1} \mathbf{A} \tau_a) \quad (\text{A.26})$$

$$\dot{V}_2 = \tilde{\omega}^T \mathbf{A} \mathbf{I}_s \mathbf{A}^T \mathbf{J}^{-1} \nu - \tilde{\omega}^T \mathbf{A} \mathbf{I}_s \mathbf{A}^T \mathbf{J}^{-1} \tau_e + \tilde{\omega}^T \mathbf{A} \mathbf{I}_s (\mathbf{A}^T \mathbf{J}^{-1} \mathbf{A} + \mathbf{I}_s^{-1}) \tau_a \quad (\text{A.27})$$

$$\begin{aligned} &= \tilde{\omega}^T \mathbf{I} \mathbf{J}^{-1} \nu - \tilde{\omega}^T \mathbf{I} \mathbf{J}^{-1} \tau_e + \tilde{\omega}^T \mathbf{I} \mathbf{J}^{-1} \mathbf{A} \tau_a + \tilde{\omega}^T \mathbf{A} \tau_a \\ &\quad - \tilde{\omega}^T \nu + \tilde{\omega}^T \tau_e - \tilde{\omega}^T \mathbf{A} \tau_a \end{aligned} \quad (\text{A.28})$$

In the last passage, the relation $\mathbf{J} = \mathbf{I} - \mathbf{A} \mathbf{I} \mathbf{A}^T$ is used. We see that the sum of these two become:

$$\dot{V}_1 + \dot{V}_2 = \omega_0 \tilde{\omega}^T \mathbf{I}(\mathbf{c}_2)^\times \tilde{\omega} - \tilde{\omega}^T \nu + \tilde{\omega}^T \tau_e \quad (\text{A.29})$$

Continuing with the time derivatives, we have:

$$\dot{V}_3 = \omega_s^T \mathbf{I}_s \mathbf{A}^T (\omega_0(\mathbf{c}_2)^\times \tilde{\omega} - \mathbf{J}^{-1} \nu + \mathbf{J}^{-1} \tau_e - \mathbf{J}^{-1} \mathbf{A} \tau_a) \quad (\text{A.30})$$

$$\dot{V}_4 = \omega_s^T \mathbf{I}_s \mathbf{A}^T \mathbf{J}^{-1} \nu - \omega_s^T \mathbf{I}_s \mathbf{A}^T \mathbf{J}^{-1} \tau_e + \omega_s^T \mathbf{I}_s (\mathbf{A}^T \mathbf{J}^{-1} \mathbf{A} + \mathbf{I}_s^{-1}) \tau_a \quad (\text{A.31})$$

$$= \omega_s^T \mathbf{I}_s \mathbf{A}^T \mathbf{J}^{-1} \nu - \omega_s^T \mathbf{I}_s \mathbf{A}^T \mathbf{J}^{-1} \tau_e + \omega_s^T \mathbf{I}_s \mathbf{A}^T \mathbf{J}^{-1} \mathbf{A} \tau_a + \omega_s^T \tau_a \quad (\text{A.32})$$

The sum of these two expressions become:

$$\dot{V}_3 + \dot{V}_4 = \omega_0 \omega_s^T \mathbf{I}_s \mathbf{A}^T (\mathbf{c}_2)^\times \tilde{\omega} + \omega_s^T \tau_a \quad (\text{A.33})$$

Thus:

$$\dot{V}_a = \omega_0 \tilde{\omega}^T \mathbf{I}(\mathbf{c}_2)^\times \tilde{\omega} - \tilde{\omega}^T \nu + \tilde{\omega}^T \tau_e + \omega_0 \omega_s^T \mathbf{I}_s \mathbf{A}^T (\mathbf{c}_2)^\times \tilde{\omega} + \omega_s^T \tau_a \quad (\text{A.34})$$

We now calculate:

$$\tilde{\omega}^T \nu = -\omega_0 \tilde{\omega}^T (\mathbf{c}_2)^\times \tilde{\omega} + \omega_0^2 \tilde{\omega}^T (\mathbf{c}_2)^\times \mathbf{I} \mathbf{c}_2 - \omega_0 \tilde{\omega}^T (\mathbf{c}_2)^\times \mathbf{A} \mathbf{I}_s \omega_s \quad (\text{A.35})$$

$$= \omega_0 \tilde{\omega}^T \mathbf{I}(\mathbf{c}_2)^\times \tilde{\omega} + \omega_0^2 \tilde{\omega}^T (\mathbf{c}_2)^\times \mathbf{I} \mathbf{c}_2 + \omega_0 \omega_s^T \mathbf{I}_s \mathbf{A}^T (\mathbf{c}_2)^\times \tilde{\omega} \quad (\text{A.36})$$

Note that $\tilde{\omega}^T \tilde{\omega}^\times = 0$. Hence:

$$\dot{V}_a = \tilde{\omega}^T \tau_e + \omega_s^T \tau_a - \omega_0^2 \tilde{\omega}^T (\mathbf{c}_2)^\times \mathbf{I} \mathbf{c}_2 \quad (\text{A.37})$$

A.2.4 Calculation of $\mathbf{J} \tilde{\omega}$

From (4.14) we have expressions for \mathbf{h}^b , \mathbf{h}_a^b and \mathbf{J} . We start by substituting for $\mathbf{I}_s \omega_s$:

$$\mathbf{h}^b = \mathbf{I} (\tilde{\omega} + \mathbf{R}_d^b \omega_{id}^d) + \mathbf{A} \mathbf{h}_a - \mathbf{A} \mathbf{I}_s \mathbf{A}^T (\tilde{\omega} + \mathbf{R}_d^b \omega_{id}^d) \quad (\text{A.38})$$

Since $\mathbf{J} = \mathbf{I} - \mathbf{A}\mathbf{I}_s\mathbf{A}^T$, we get:

$$\mathbf{h}^b = \mathbf{J} \left(\tilde{\omega} + \mathbf{R}_d^b \omega_{id}^d \right) + \mathbf{A}\mathbf{h}_a^b \quad (\text{A.39})$$

$$\mathbf{J}\tilde{\omega} = \mathbf{h}^b - \mathbf{A}\mathbf{h}_a^b - \mathbf{J}\mathbf{R}_d^b \omega_{id}^d \quad (\text{A.40})$$

A.2.5 Gain selection for linear controller

We recall that to stabilize the linearized system, the gain matrices had to be chosen in the following way:

$$\mathbf{B}\mathbf{K}_\epsilon = \mathbf{A}_\epsilon + k_0\mathbf{1} \quad (\text{A.41})$$

$$(\mathbf{A}_\omega - \mathbf{B}\mathbf{K}_\omega) < 0 \quad (\text{A.42})$$

The gain matrices will be chosen to be diagonal:

$$\mathbf{K}_\epsilon = \begin{bmatrix} k_{\epsilon 1} & 0 & 0 \\ 0 & k_{\epsilon 2} & 0 \\ 0 & 0 & k_{\epsilon 3} \end{bmatrix}, \quad \mathbf{K}_\omega = \begin{bmatrix} k_{\omega 1} & 0 & 0 \\ 0 & k_{\omega 2} & 0 \\ 0 & 0 & k_{\omega 3} \end{bmatrix} \quad (\text{A.43})$$

We will start by examining equation (A.41):

$$\begin{bmatrix} \frac{k_{\epsilon 1}}{i_x} & 0 & 0 \\ 0 & \frac{k_{\epsilon 2}}{i_y - i_s} & 0 \\ 0 & 0 & \frac{k_{\epsilon 1}}{i_z} \end{bmatrix} = \begin{bmatrix} \frac{8\omega_0^2(i_y - i_z) + k_0 i_x}{i_x} & 0 & 0 \\ 0 & \frac{6\omega_0^2(i_x - i_z) + k_0(i_y - i_s)}{i_y - i_s} & 0 \\ 0 & 0 & \frac{2\omega_0^2(i_y - i_x) + k_0 i_z}{i_z} \end{bmatrix} \quad (\text{A.44})$$

The constant ω_0 has its largest value at the spacecraft's perigee altitude. At perigee, $\omega_0 = 0.0012 \Rightarrow \omega_0^2 = 1.3755 \cdot 10^{-6}$. The constant $i_s = 4 \cdot 10^{-5}$. Choosing k_0 much larger than $8\omega_0^2$ and i_s will make them negligible. This is true because i_x , i_y and i_z have the same order of magnitude. Note that $i_y \gg i_s$. So if we choose $k_0 \gg \max\{8\omega_0^2, i_s\} = i_s$ we can approximate the above matrix equation to:

$$\begin{bmatrix} \frac{k_{\epsilon 1}}{i_x} & 0 & 0 \\ 0 & \frac{k_{\epsilon 2}}{i_y} & 0 \\ 0 & 0 & \frac{k_{\epsilon 1}}{i_z} \end{bmatrix} = \begin{bmatrix} \frac{k_0 i_x}{i_x} & 0 & 0 \\ 0 & \frac{k_0 i_y}{i_y} & 0 \\ 0 & 0 & \frac{k_0 i_z}{i_z} \end{bmatrix} \quad (\text{A.45})$$

This leads to the following choices for the elements of \mathbf{K}_ϵ :

$$k_{\epsilon 1} = k_0 i_x \quad (\text{A.46a})$$

$$k_{\epsilon 2} = k_0 i_y \quad (\text{A.46b})$$

$$k_{\epsilon 3} = k_0 i_z \quad (\text{A.46c})$$

Secondly, we will look at equation (A.42). We have:

$$(\mathbf{A}_\omega - \mathbf{BK}_\omega) = \begin{bmatrix} -\frac{k_{\omega 1}}{i_x} & 0 & \frac{\omega_0(i_z - i_y + i_x)}{i_x} \\ 0 & -\frac{k_{\omega 2}}{i_y - i_s} & 0 \\ -\frac{\omega_0(i_z - i_y + i_x)}{i_x} & 0 & -\frac{k_{\omega 3}}{i_z} \end{bmatrix} \quad (\text{A.47})$$

This matrix will be negative definite if the diagonal elements of \mathbf{K}_ω are chosen large enough. A negative definite matrix is a matrix with eigenvalues which have negative real parts. To find how to choose the elements of \mathbf{K}_ω , we will compute the eigenvalues of the above matrix. The characteristic polynomial of $(\mathbf{A}_\omega - \mathbf{BK}_\omega)$ is:

$$\det(\mathbf{A}_\omega - \mathbf{BK}_\omega - \lambda \mathbf{1}) = \frac{-\lambda(i_y - i_s) - k_{\omega 2}}{i_x(i_y - i_s)i_z} (i_x i_z \lambda^2 + [k_{\omega 3} i_x + k_{\omega 1} i_z] \lambda + k_{\omega 1} k_{\omega 3} + \omega_0^2 i_z^2 - 2\omega_0^2 i_z i_y + 2\omega_0^2 i_z i_x) \quad (\text{A.48})$$

$$+ \omega_0^2 i_y^2 - 2\omega_0^2 i_y i_x + \omega_0^2 i_x^2) \\ = \frac{-\lambda(i_y - i_s) - k_{\omega 2}}{i_x(i_y - i_s)i_z} (a\lambda^2 + b\lambda + c) \quad (\text{A.49})$$

The eigenvalues of $(\mathbf{A}_\omega - \mathbf{BK}_\omega)$ are the solutions with respect to λ of:

$$\det(\mathbf{A}_\omega - \mathbf{BK}_\omega - \lambda \mathbf{1}) = 0 \quad (\text{A.50})$$

The first eigenvalue λ_1 is given by

$$-\lambda(i_y - i_s) - k_{\omega 2} = 0 \quad (\text{A.51})$$

↓

$$\lambda_1 = -\frac{k_{\omega 2}}{i_y - i_s} \quad (\text{A.52})$$

where λ_1 is negative if $k_{\omega 2} > 0$. The last two eigenvalues are given by the following equation:

$$a\lambda^2 + b\lambda + c = 0 \quad (\text{A.53})$$

↓

$$\lambda_2 = \frac{-b + \sqrt{b^2 - 4ac}}{2a} \quad (\text{A.54})$$

$$\lambda_3 = \frac{-b - \sqrt{b^2 - 4ac}}{2a} \quad (\text{A.55})$$

The square root returns a positive real value or an imaginary value, thus the real part of λ_3 is negative if $b > 0$, since $a > 0$. This is ensured if $k_{\omega 1} > 0$ and $k_{\omega 3} > 0$. If the square root in the above expression for λ_2 returns a positive real value, λ_2 may get a positive real part. To ensure that the real part of λ_2 is negative, we solve the following equation:

$$b > \sqrt{b^2 - 4ac} \quad (\text{A.56})$$

$$b^2 > b^2 - 4ac \quad (\text{A.57})$$

$$\Downarrow$$

$$c > 0 \quad (\text{A.58})$$

$$\Downarrow$$

$$k_{\omega 1} k_{\omega 3} > \omega_0^2 (2i_z i_y + 2i_y i_x - i_z^2 - 2i_z i_x - i_y^2 - i_x^2) \quad (\text{A.59})$$

$$\Downarrow$$

$$k_{\omega 1} k_{\omega 3} > \omega_0^2 (i_z [2i_y - 2i_x - i_z] - [i_y - i_x]^2) \quad (\text{A.60})$$

A.2.6 Solution to $\mathbf{c}_3 = [0, \sqrt{1/2}, \sqrt{1/2}]^T$, $c_{22}c_{32} = 0$

From the definition of \mathbf{c}_3 in (3.8) applied to the rotation matrix in Euler angles (3.16), we can obtain an equation set to solve. In Euler angles, $\mathbf{c}_3 = [0, \sqrt{1/2}, \sqrt{1/2}]^T$ is written:

$$s\psi s\phi + c\psi c\phi s\theta = 0 \quad (\text{A.61a})$$

$$-c\psi s\phi + s\theta s\psi c\phi = \sqrt{1/2} \quad (\text{A.61b})$$

$$c\theta c\phi = \sqrt{1/2} \quad (\text{A.61c})$$

The second equation is $c_{22}c_{32} = 0 \Rightarrow c_{22} = 0$ or $c_{32} = 0$. Thus:

$$c\psi c\phi + s\phi s\theta s\psi = 0 \quad (\text{A.62a})$$

or

$$c\theta s\phi = 0 \quad (\text{A.62b})$$

We must now solve the equation set consisting of (A.61) and (A.62a), and the set containing (A.61) and (A.62b). The first set has no solutions. The equation set (A.61c) and (A.62b) has 4 solutions, and all of these solutions satisfy (A.61). These solutions are given below.

$$\begin{bmatrix} \phi \\ \theta \\ \psi \end{bmatrix} = \left\{ \begin{bmatrix} 0 \\ \pi/4 \\ \pi/2 \end{bmatrix}, \begin{bmatrix} 0 \\ -\pi/4 \\ -\pi/2 \end{bmatrix}, \begin{bmatrix} \pi \\ 3\pi/4 \\ -\pi/2 \end{bmatrix}, \begin{bmatrix} \pi \\ -3\pi/4 \\ \pi/2 \end{bmatrix} \right\} \quad (\text{A.63})$$

These solutions can be converted to quaternions in MATLAB/SIMULINK. The results are shown in figure A.1 where $\mathbf{q} = [\eta, \epsilon_1, \epsilon_2, \epsilon_3]^T$. Note that it should be possible to solve the equation $\mathbf{c}_3 = [0, \sqrt{1/2}, \sqrt{1/2}]^T$ directly in quaternions using the quaternion expression for \mathbf{c}_3 , but the author was not successful in finding a real solution.

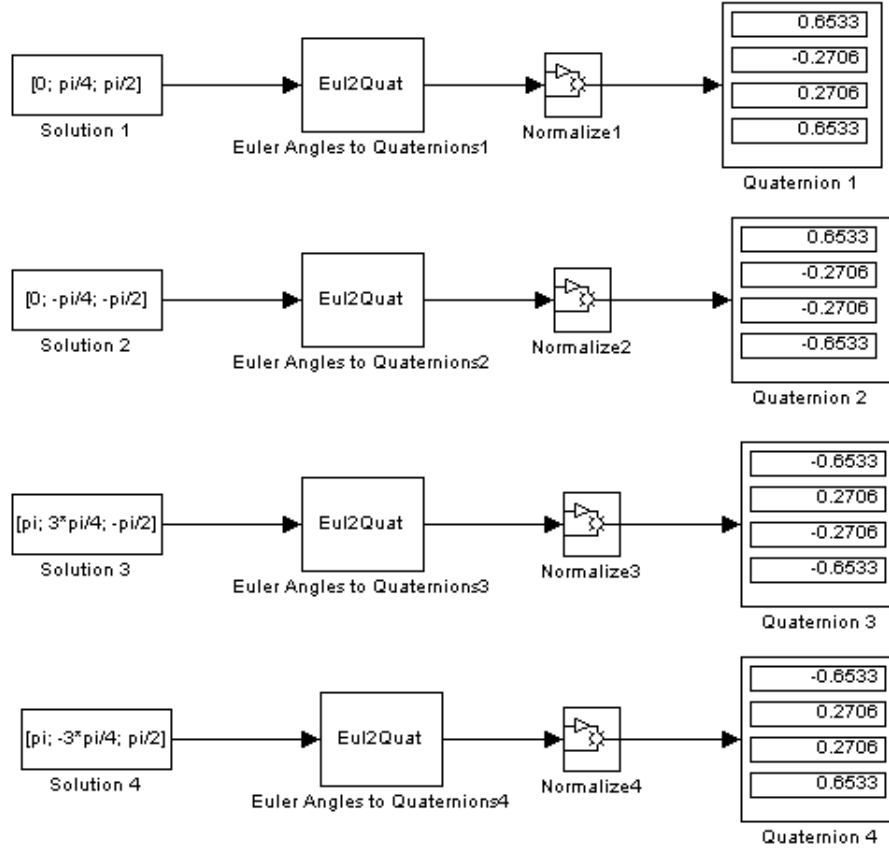


Figure A.1: Conversion of solutions to quaternions

A.2.7 Convergence of sliding manifold

Consider this sliding manifold, where $\mathbf{P} > 0$:

$$\mathbf{s} = \tilde{\omega} + \mathbf{P}\tilde{\epsilon} \quad (\text{A.64})$$

We will now show that when $\mathbf{s} = 0$, $\tilde{\epsilon}$ and $\tilde{\omega}$ converge to zero. This proof can be found in Fu et al. (1999). When $\mathbf{s} = 0$, we get:

$$\tilde{\omega} = -\mathbf{P}\tilde{\epsilon} \quad (\text{A.65})$$

Thus, the equations describing the motion on the manifold $\mathbf{s} = 0$ are given by the above expression inserted into (3.37):

$$\dot{\tilde{\eta}} = \frac{1}{2}\tilde{\epsilon}^T \mathbf{P}\tilde{\epsilon} \quad (\text{A.66a})$$

$$\dot{\tilde{\epsilon}} = -\frac{1}{2}[\tilde{\eta}\mathbf{1} + (\tilde{\epsilon})^\times] \mathbf{P}\tilde{\epsilon} \quad (\text{A.66b})$$

To show convergence we will use Lyapunov analysis. Choosing the LFC

$$V_\epsilon = \tilde{\epsilon}^T \tilde{\epsilon}, \quad (\text{A.67})$$

the time derivative \dot{V}_ϵ is given by:

$$\dot{V}_\epsilon = -\tilde{\eta} \tilde{\epsilon}^T \mathbf{P} \tilde{\epsilon} \quad (\text{A.68})$$

Since $\tilde{\eta}^2 + \tilde{\epsilon}^T \tilde{\epsilon} = 1$, $\tilde{\eta}$ has two possible values whenever $\tilde{\eta} \neq 0$, i.e. a positive value and a negative value. If we choose the positive value, $\tilde{\eta}$ will remain positive since $\dot{\tilde{\eta}}$ is positive. Hence, $\dot{V} < 0$ if $\tilde{\epsilon} \neq 0$. Thus, $\tilde{\epsilon} \rightarrow 0 \Rightarrow \tilde{\eta} \rightarrow 1$. If $\tilde{\eta} = 0$ we cannot conclude, but since the equilibrium points of the kinematic equations are given by $\tilde{\eta} = \pm 1$ and $\tilde{\epsilon} = 0$, the system will not stay in this state. This means that $\tilde{\eta}$ will not remain equal to zero, and thus the above conclusions apply. From (A.65), we see that $\tilde{\epsilon} \rightarrow 0 \Rightarrow \tilde{\omega} \rightarrow 0$. Hence, we have convergence to the origin for the states on the sliding manifold $\mathbf{s} = 0$.

A.2.8 Parameter error terms

The error of a parameter α is defined to be $\Delta\alpha = \alpha - \hat{\alpha}$. We will now apply this notation in calculating several parameter error terms:

$$(\mathbf{h}^b)^\times (\tilde{\omega} - \omega_0 \mathbf{c}_2) - (\hat{\mathbf{h}}^b)^\times (\tilde{\omega} - \hat{\omega}_0 \mathbf{c}_2) = (\mathbf{h}^b)^\times \tilde{\omega} - (\mathbf{h}^b)^\times \omega_0 \mathbf{c}_2 - (\hat{\mathbf{h}}^b)^\times \tilde{\omega} + (\hat{\mathbf{h}}^b)^\times \hat{\omega}_0 \mathbf{c}_2 \quad (\text{A.69a})$$

$$= \left((\mathbf{h}^b)^\times - (\hat{\mathbf{h}}^b)^\times \right) \tilde{\omega} \quad (\text{A.69b})$$

$$- \left((\mathbf{h}^b)^\times \omega_0 - (\hat{\mathbf{h}}^b)^\times \hat{\omega}_0 \right) \mathbf{c}_2 = (\Delta \mathbf{h}^b)^\times \tilde{\omega} - (\Delta (\mathbf{h}^b \omega_0)) \mathbf{c}_2 \quad (\text{A.69c})$$

$$\frac{3}{2} \omega_0^2 \mathbf{c}_3^T \mathbf{I} \mathbf{c}_3 - \frac{3}{2} \hat{\omega}_0^2 \mathbf{c}_3^T \hat{\mathbf{I}} \mathbf{c}_3 = \frac{3}{2} \mathbf{c}_3^T \left(\omega_0^2 \mathbf{I} - \hat{\omega}_0^2 \hat{\mathbf{I}} \right) \mathbf{c}_3 \quad (\text{A.70a})$$

$$= \frac{3}{2} \mathbf{c}_3^T \Delta (\omega_0^2 \mathbf{I}) \mathbf{c}_3 \quad (\text{A.70b})$$

$$\omega_0 \mathbf{J}(\mathbf{c}_2)^\times \tilde{\omega} - \hat{\omega}_0 \hat{\mathbf{J}}(\mathbf{c}_2)^\times \tilde{\omega} = \Delta (\omega_0 \mathbf{J})(\mathbf{c}_2)^\times \tilde{\omega} \quad (\text{A.71})$$

$$\frac{1}{2} \mathbf{J} \mathbf{P} [\tilde{\eta} \mathbf{1} + (\tilde{\epsilon})^\times] \tilde{\omega} - \frac{1}{2} \hat{\mathbf{J}} \mathbf{P} [\tilde{\eta} \mathbf{1} + (\tilde{\epsilon})^\times] \tilde{\omega} = \frac{1}{2} \Delta \mathbf{J} \mathbf{P} [\tilde{\eta} \mathbf{1} + (\tilde{\epsilon})^\times] \tilde{\omega} \quad (\text{A.72})$$

A.2.9 Stability of local PD controller

Consider the LFC used to derive Lyapunov controller 1 and its time derivative along the system trajectories:

$$V = V_a + 2k_1(1 - \tilde{\eta}) \quad (\text{A.73})$$

$$\dot{V} = \tilde{\omega}^T \tau_c + \omega_s^T \tau_a - \omega_0^2 \tilde{\omega}^T (\mathbf{c}_2)^\times \mathbf{I} \mathbf{c}_2 + 3\omega_0^2 \tilde{\omega}^T (\mathbf{c}_3)^\times \mathbf{I} \mathbf{c}_3 + k_1 \tilde{\omega}^T \tilde{\epsilon} \quad (\text{A.74})$$

where k_1 is a positive constant. The local PD controller is given by

$$\tau_c = -k_1 \tilde{\epsilon} - k_\omega \tilde{\omega} \quad (\text{A.75a})$$

$$\tau_a = 0 \quad (\text{A.75b})$$

where k_ω is a positive constant. Thus:

$$\dot{V} = -k_\omega \tilde{\omega}^T \tilde{\omega} - \omega_0^2 \tilde{\omega}^T (\mathbf{c}_2)^\times \mathbf{I} \mathbf{c}_2 + 3\omega_0^2 \tilde{\omega}^T (\mathbf{c}_3)^\times \mathbf{I} \mathbf{c}_3 \quad (\text{A.76})$$

We will now take a closer look at the following terms:

$$\begin{aligned} -\omega_0^2 \tilde{\omega}^T (\mathbf{c}_2)^\times \mathbf{I} \mathbf{c}_2 &= \omega_0^2 \mathbf{c}_2^T \mathbf{I} (\mathbf{c}_2)^\times \tilde{\omega} \\ &\leq \omega_0^2 \|(\mathbf{c}_2)^\times\| \|\mathbf{I}\| \|\tilde{\omega}\| \|\mathbf{c}_2\| \end{aligned} \quad (\text{A.77})$$

$$3\omega_0^2 \tilde{\omega}^T (\mathbf{c}_3)^\times \mathbf{I} \mathbf{c}_3 \leq 3\omega_0^2 \|(\mathbf{c}_3)^\times\| \|\mathbf{I}\| \|\tilde{\omega}\| \|\mathbf{c}_3\| \quad (\text{A.78})$$

Applying Young's inequality (A.12) on $\|\tilde{\omega}\| \|\mathbf{c}_i\|$ with $p = 2$, we obtain:

$$\|\tilde{\omega}\| \|\mathbf{c}_i\| \leq \frac{1}{2} \left(2\|\tilde{\omega}\|^2 + \frac{1}{2}\|\mathbf{c}_i\|^2 \right) \quad (\text{A.79})$$

The vector norms are given by the 2-norm defined in (A.5), thus:

$$\|\tilde{\omega}\|^2 = \tilde{\omega}^T \tilde{\omega} \quad (\text{A.80})$$

$$\|\mathbf{c}_i\|^2 = \mathbf{c}_i^T \mathbf{c}_i \quad (\text{A.81})$$

It is possible to use these results to define an upper bound on \dot{V} :

$$\begin{aligned} \dot{V} &\leq -k_\omega \tilde{\omega}^T \tilde{\omega} + \omega_0^2 \|(\mathbf{c}_2)^\times\| \|\mathbf{I}\| \left(\tilde{\omega}^T \tilde{\omega} + \frac{1}{4} \|\mathbf{c}_2\|^2 \right) \\ &\quad + 3\omega_0^2 \|(\mathbf{c}_3)^\times\| \|\mathbf{I}\| \left(\tilde{\omega}^T \tilde{\omega} + \frac{1}{4} \|\mathbf{c}_3\|^2 \right) \end{aligned} \quad (\text{A.82})$$

$$\begin{aligned} \dot{V} &\leq -\left(k_\omega - \omega_0^2 \|\mathbf{I}\| \left[\|(\mathbf{c}_2)^\times\| + 3\|(\mathbf{c}_3)^\times\| \right]\right) \tilde{\omega}^T \tilde{\omega} \\ &\quad + \frac{1}{4} \omega_0^2 \|\mathbf{I}\| \left[\|(\mathbf{c}_2)^\times\| \|\mathbf{c}_2\|^2 + 3\|(\mathbf{c}_3)^\times\| \|\mathbf{c}_3\|^2 \right] \end{aligned} \quad (\text{A.83})$$

$$\dot{V} \leq -(k_\omega - \zeta_1) \tilde{\omega}^T \tilde{\omega} + \zeta_2 \quad (\text{A.84})$$

Because \mathbf{c}_i is a unit vector, and ω_0 and \mathbf{I} are constants, ζ_1 and ζ_2 are bounded. Hence, choosing $k_\omega > \zeta_1$ will ensure that the quadratic term in $\tilde{\omega}$ is negative when $\tilde{\omega} \neq 0$. However, the presence

of ζ_2 makes sure that the system is not asymptotically stable. We will now calculate ζ_1 and ζ_2 for ESEO using the 2-norms for vectors and matrices:

$$\omega_0 = 0.0012 \Rightarrow \omega_0^2 = 1.3755 \cdot 10^{-6} \quad (\text{A.85})$$

$$\|\mathbf{I}\| = 4.3500 \quad (\text{A.86})$$

$$\|\mathbf{c}_i\| = 1 \quad (\text{A.87})$$

$$\|(\mathbf{c}_i)^\times\| = 1 \quad (\text{A.88})$$

↓

$$\zeta_1 = 2.3934 \times 10^{-5} \quad (\text{A.89})$$

$$\zeta_2 = 5.9835 \times 10^{-6} \quad (\text{A.90})$$

We see that in ESEO's case ζ_2 is close to zero. Thus $V < 0$ for large values of $\tilde{\omega}$, but when $\tilde{\omega}$ gets very close to zero, $V > 0$. Hence, $\tilde{\omega}$ never converges to the origin, but stays close to it. This means that the system is stable. For the rest of the analysis we will assume that $\zeta_2 \approx 0$ in order to investigate what happens to $\tilde{\epsilon}$. Hence, (4.18) becomes:

$$0 = -\omega_0^2 (\mathbf{c}_2)^\times \mathbf{I} \mathbf{c}_2 + \omega_0 (\mathbf{c}_2)^\times \mathbf{A} \mathbf{I}_s \omega_s + 3\omega_0^2 (\mathbf{c}_3)^\times \mathbf{I} \mathbf{c}_3 - k_1 \tilde{\epsilon} \quad (\text{A.91})$$

As in section 4.2.2, k_1 must be chosen large enough to make $\tilde{\epsilon}$ the only possible solution. Rewriting this equation on component form for ESEO, yields:

$$k_1 \tilde{\epsilon}_1 = \omega_0^2 (i_y - i_z) (c_{22}c_{32} - 3c_{23}c_{33}) - \omega_0 c_{32} i_s \omega_s \quad (\text{A.92a})$$

$$k_1 \tilde{\epsilon}_2 = \omega_0^2 (i_z - i_x) (c_{12}c_{32} - 3c_{13}c_{33}) \quad (\text{A.92b})$$

$$k_1 \tilde{\epsilon}_3 = \omega_0^2 (i_x - i_y) (c_{12}c_{22} - 3c_{13}c_{23}) + \omega_0 c_{12} i_s \omega_s \quad (\text{A.92c})$$

In this situation, the largest possible right hand side depends on the wheel spin ω_s , and will be at its maximum when ω_s is at its maximum, i.e. $\omega_s = \sigma$. For ESEO (A.92a) will have the largest right hand side, because $(i_y - i_z) > (i_x - i_y)$. (A.92b) has the smallest since it does not depend on the wheel spin. The maximum value of (A.92a) is:

$$k_1 \tilde{\epsilon}_1 = -\frac{3}{2} \omega_0^2 (i_y - i_z) - \omega_0 c_{32} i_s \sigma \quad (\text{A.93})$$

$$-\frac{3}{2} \omega_0^2 (i_y - i_z) = -1.3886 \cdot 10^{-6} \quad (\text{A.94})$$

$$\omega_0 c_{32} i_s \sigma = -2.9683 \cdot 10^{-5} \quad (\text{A.95})$$

↓

$$k_1 \tilde{\epsilon}_1 = -3.1072 \cdot 10^{-5} \quad (\text{A.96})$$

We see that the term from the wheel spin is approximately ten times larger than the other term.

This maximum value is obtained when:

$$\mathbf{c}_3 = \begin{bmatrix} c_{13} \\ c_{23} \\ c_{33} \end{bmatrix} = \begin{bmatrix} 0 \\ \sqrt{1/2} \\ \sqrt{1/2} \end{bmatrix} \quad (\text{A.97a})$$

$$\mathbf{c}_2 = \begin{bmatrix} c_{12} \\ c_{22} \\ c_{32} \end{bmatrix} = \begin{bmatrix} 0 \\ 0 \\ 1 \end{bmatrix} \quad (\text{A.97b})$$

This equation set has no solutions. Since the term from the wheel spin is much larger than the other, we will assume that the other term can be neglected. Thus the largest right hand side of (A.92a) is:

$$k_1 \tilde{\epsilon}_1 \approx \omega_0 c_{32} i_s \sigma = -2.9683 \times 10^{-5} \quad (\text{A.98})$$

This value is obtained when:

$$\mathbf{c}_2 = \begin{bmatrix} c_{12} \\ c_{22} \\ c_{32} \end{bmatrix} = \begin{bmatrix} 0 \\ 0 \\ 1 \end{bmatrix} \quad (\text{A.99})$$

From the definition of the directional cosines (3.8) applied to the rotation matrix in Euler angles (3.16), this equation set can be written:

$$-s\psi c\theta + c\psi s\theta s\phi = 0 \quad (\text{A.100a})$$

$$c\psi c\phi + s\phi s\theta s\psi = 0 \quad (\text{A.100b})$$

$$c\theta s\phi = 1 \quad (\text{A.100c})$$

Four solutions satisfy these equations:

$$\begin{bmatrix} \phi \\ \theta \\ \psi \end{bmatrix} = \left\{ \begin{bmatrix} \pi/2 \\ 0 \\ 0 \end{bmatrix}, \begin{bmatrix} \pi/2 \\ 0 \\ \pi \end{bmatrix}, \begin{bmatrix} -\pi/2 \\ \pi \\ 0 \end{bmatrix}, \begin{bmatrix} -\pi/2 \\ \pi \\ \pi \end{bmatrix} \right\} \quad (\text{A.101})$$

Figure A.2 shows these solutions converted to unit quaternions in MATLAB/SIMULINK. The smallest negative nonzero solution for $\tilde{\epsilon}_1$ is:

$$\tilde{\epsilon}_1 = -0.7071 \quad (\text{A.102})$$

Inserting this into (A.98) yields an expression for k_1 :

$$k_1 \tilde{\epsilon}_1 \approx \omega_0 c_{32} i_s \sigma \quad (\text{A.103})$$

↓

$$k_1 \approx 4.1979 \cdot 10^{-5} \quad (\text{A.104})$$

Since we have used an estimate for the largest possible right hand side of (A.92a), we should choose $k_1 \gg 4.1979 \times 10^{-5}$ to ensure that $\tilde{\epsilon} = 0$ is the only solution of (A.91). To conclude, we have shown that with this choice of k_1 , $\tilde{\epsilon} \rightarrow 0$ when $\tilde{\omega} \rightarrow 0$. However, $\tilde{\omega}$ only gets close to the origin. This means that $\tilde{\epsilon}$ will approach the origin, but never reach it. This is shown in figure A.3, where the command torques are continuous instead of being thruster pulses. The Euler angles converge close to the desired value, but do not reach it.

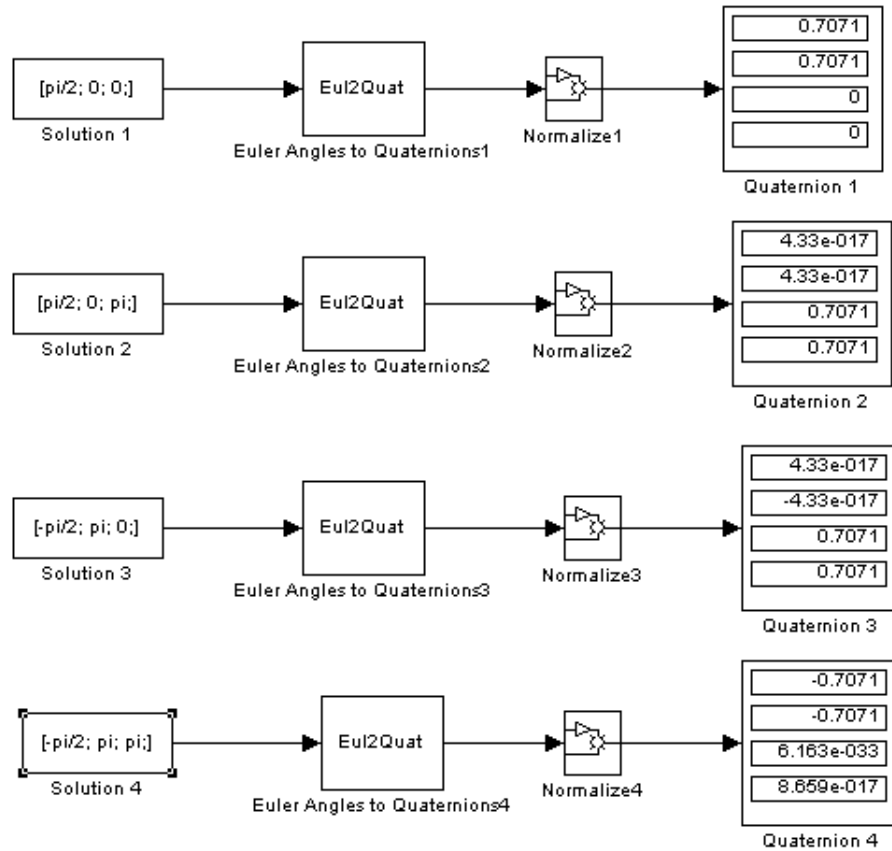


Figure A.2: c_2 -solutions in quaternions

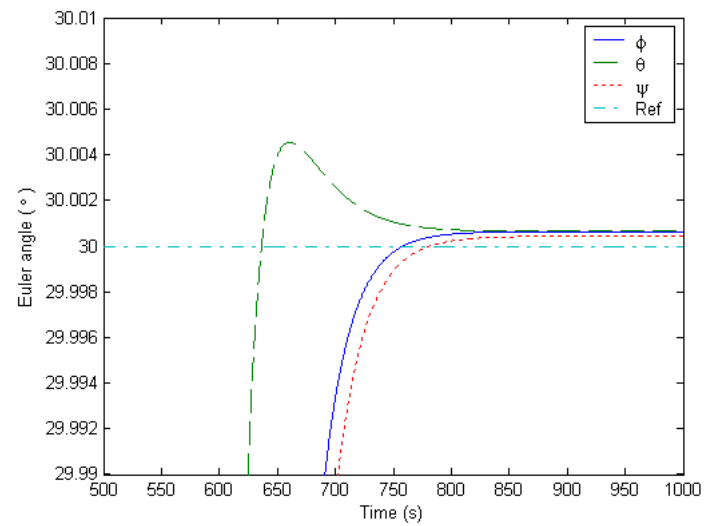
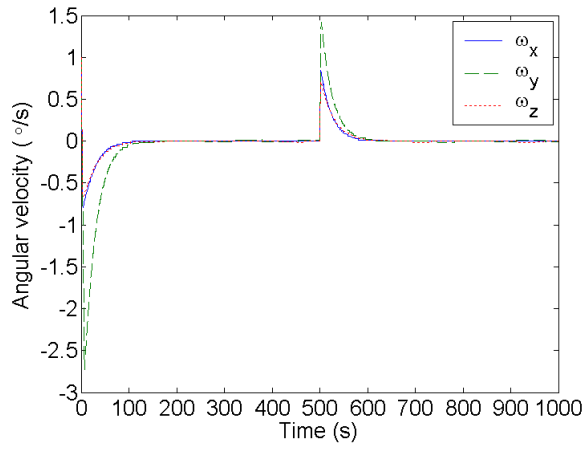


Figure A.3: Convergence of local PD controller with continuous command torques

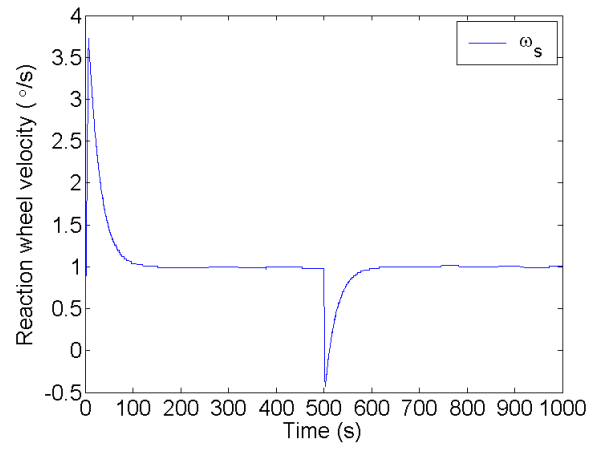
Appendix B

Simulation plots

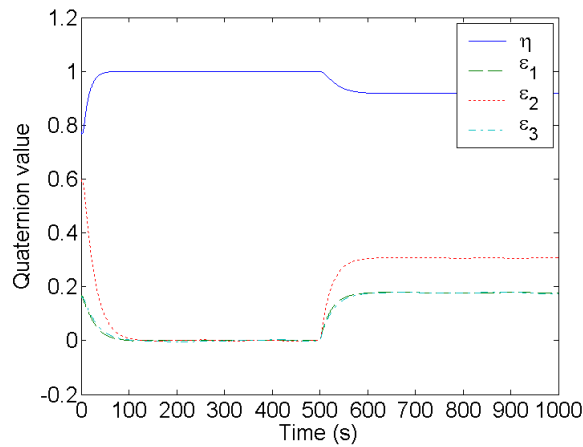
This appendix contains all the plots from the simulations. Figure B.1 to B.4 show the plots from the step simulation with ideal conditions. The results from the simulation with large initial angular velocity is presented in figure B.5 to B.8. Figure B.9 shows the plots from the step simulation with inertia uncertainty, and figure B.10 to B.13 present the results from the step simulation with added white noise.



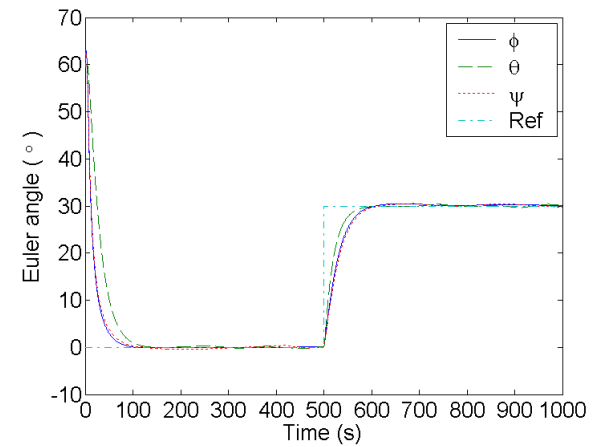
(a) Angular velocity



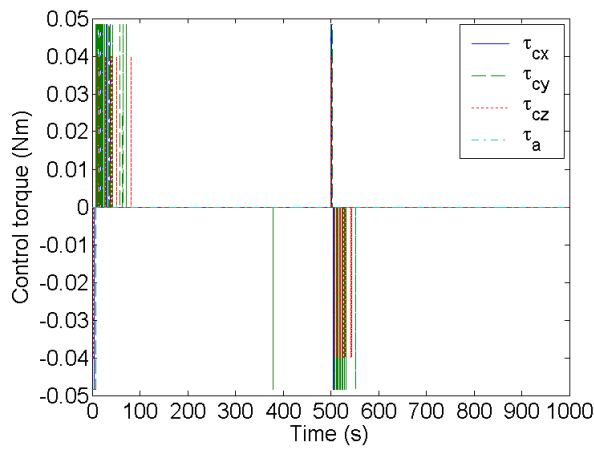
(b) Reaction wheel velocity



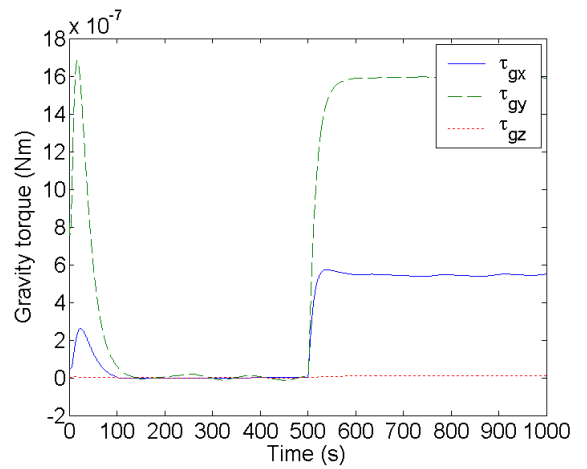
(c) Euler parameters



(d) Euler angles with reference

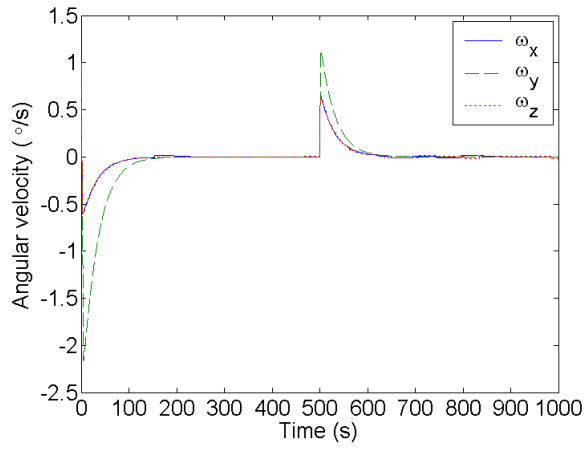


(e) Control torques

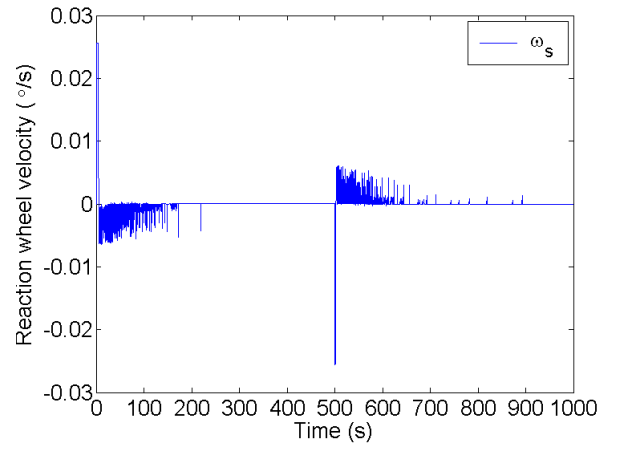


(f) Gravity torque

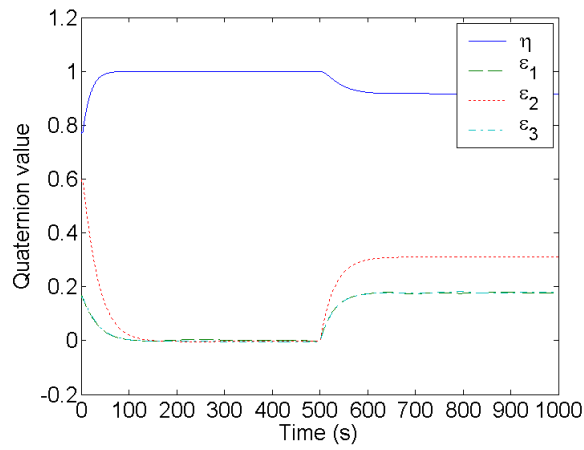
Figure B.1: Step simulation of local controller



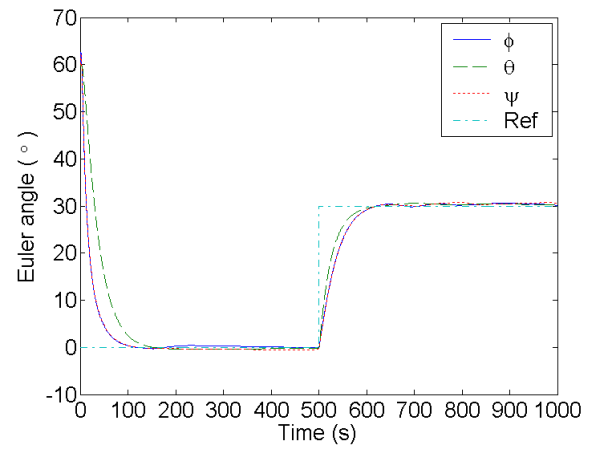
(a) Angular velocity



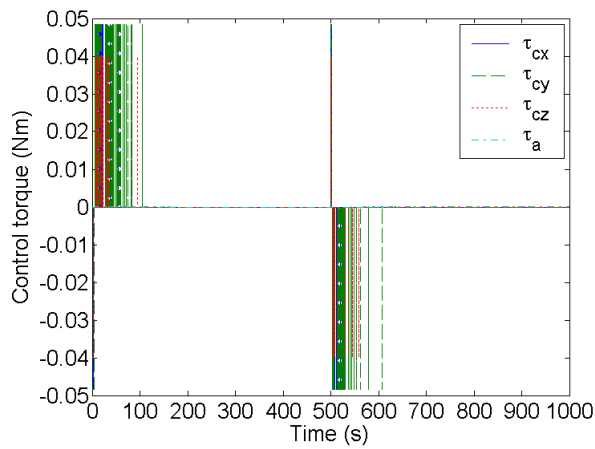
(b) Reaction wheel velocity



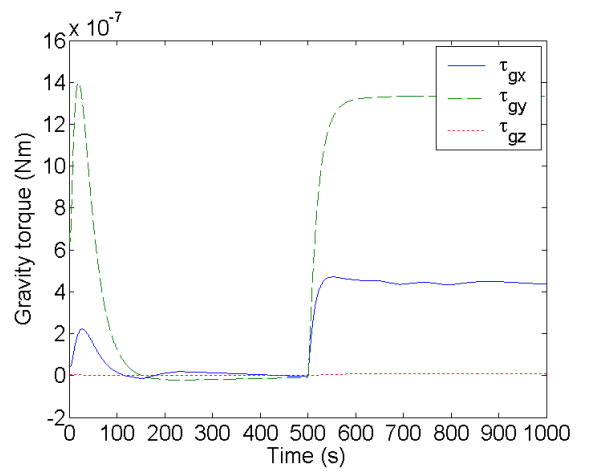
(c) Euler parameters



(d) Euler angles with reference

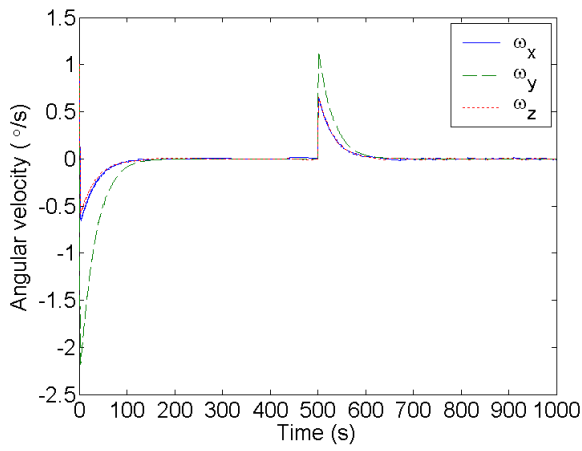


(e) Control torques

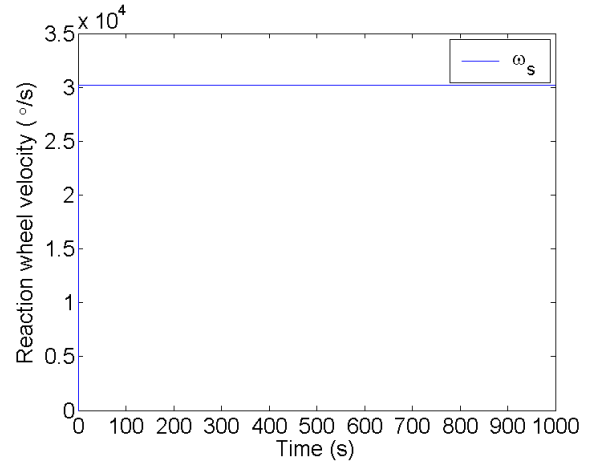


(f) Gravity torque

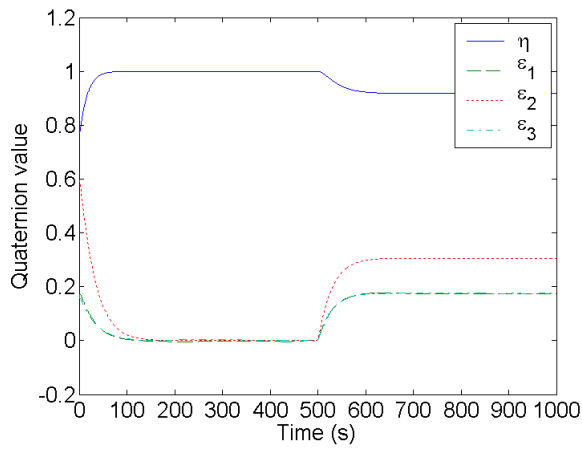
Figure B.2: Step simulation of Lyapunov controller 1



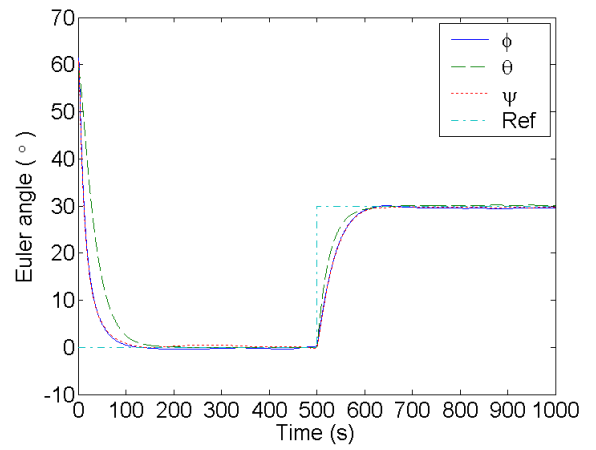
(a) Angular velocity



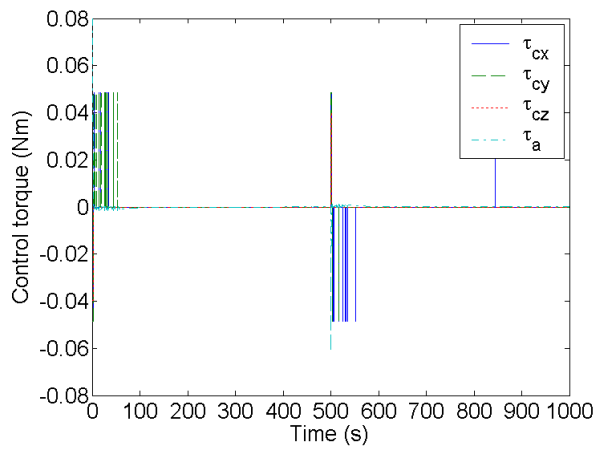
(b) Reaction wheel velocity



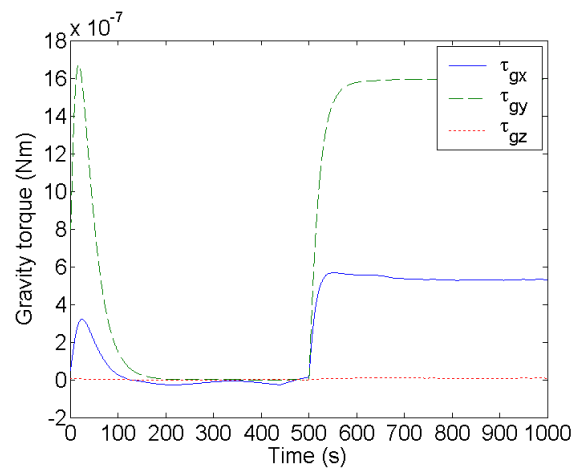
(c) Euler parameters



(d) Euler angles with reference

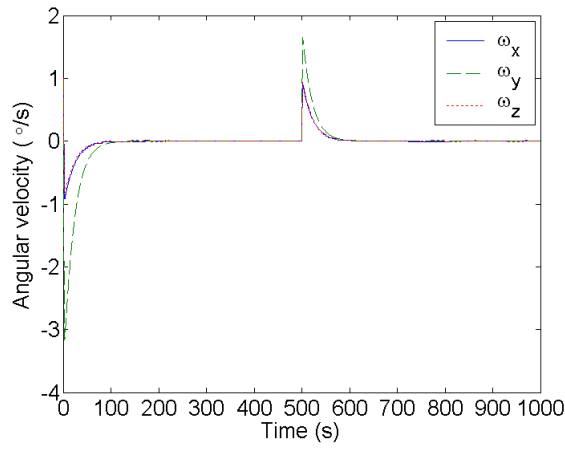


(e) Control torques

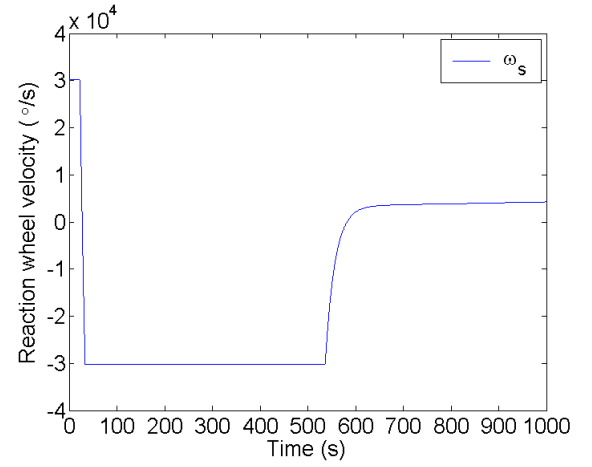


(f) Gravity torque

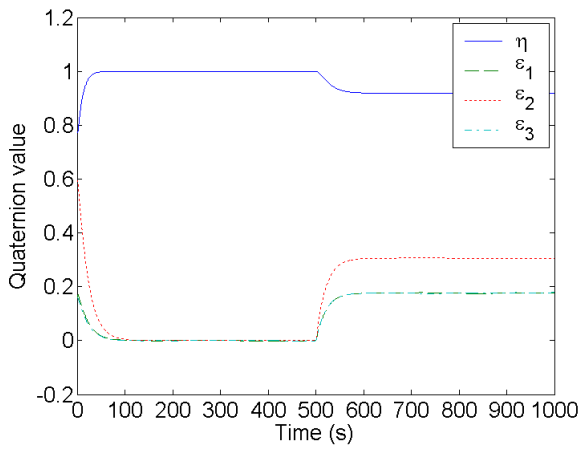
Figure B.3: Step simulation of Lyapunov controller 3



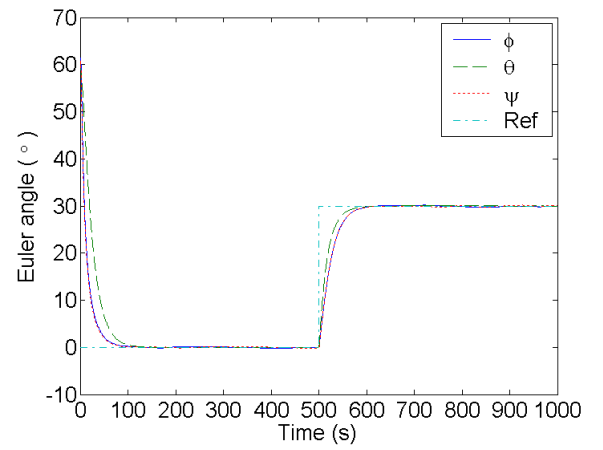
(a) Angular velocity



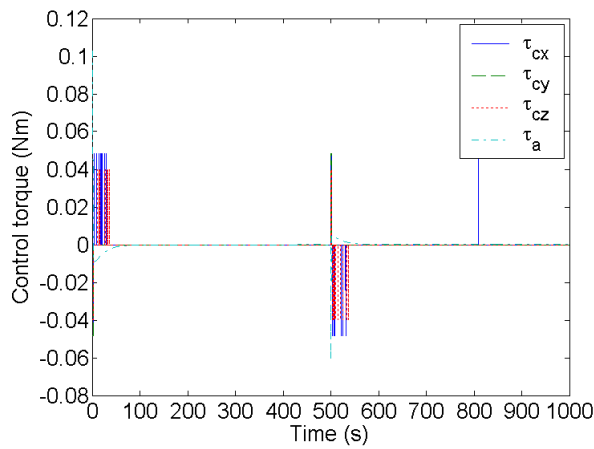
(b) Reaction wheel velocity



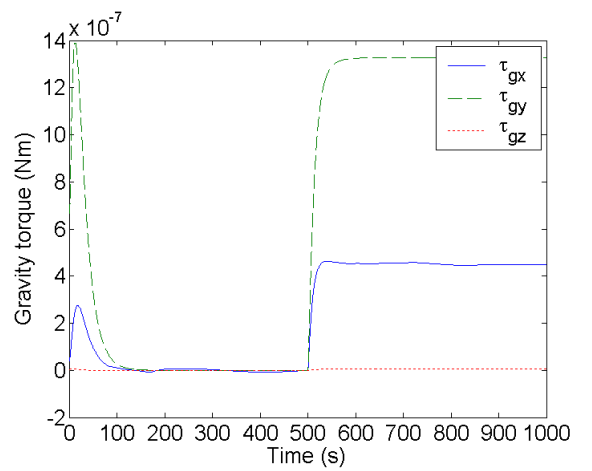
(c) Euler parameters



(d) Euler angles with reference



(e) Control torques



(f) Gravity torque

Figure B.4: Step simulation of sliding mode controller

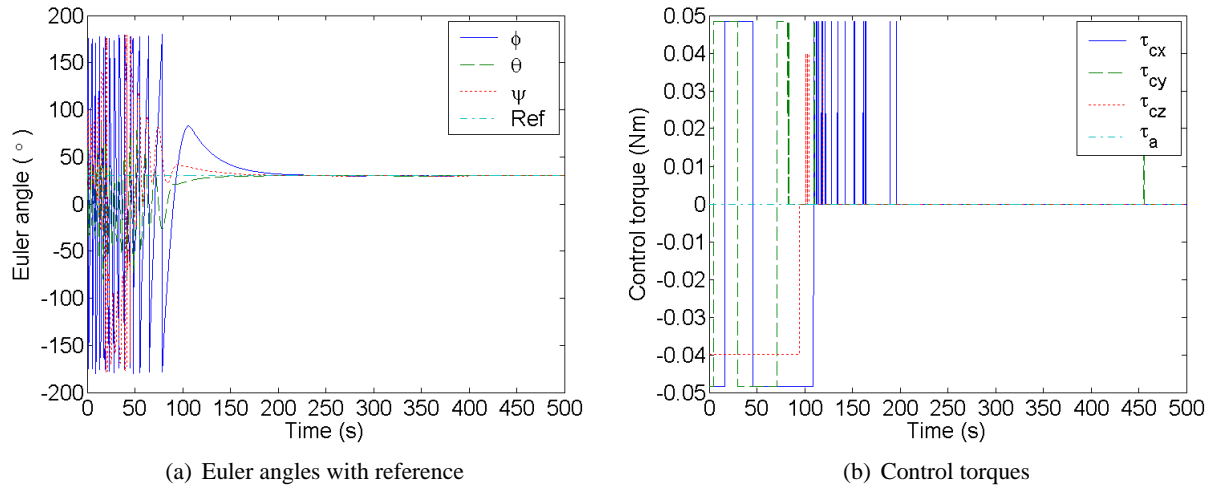


Figure B.5: Simulation of local PD controller with large initial angular velocity

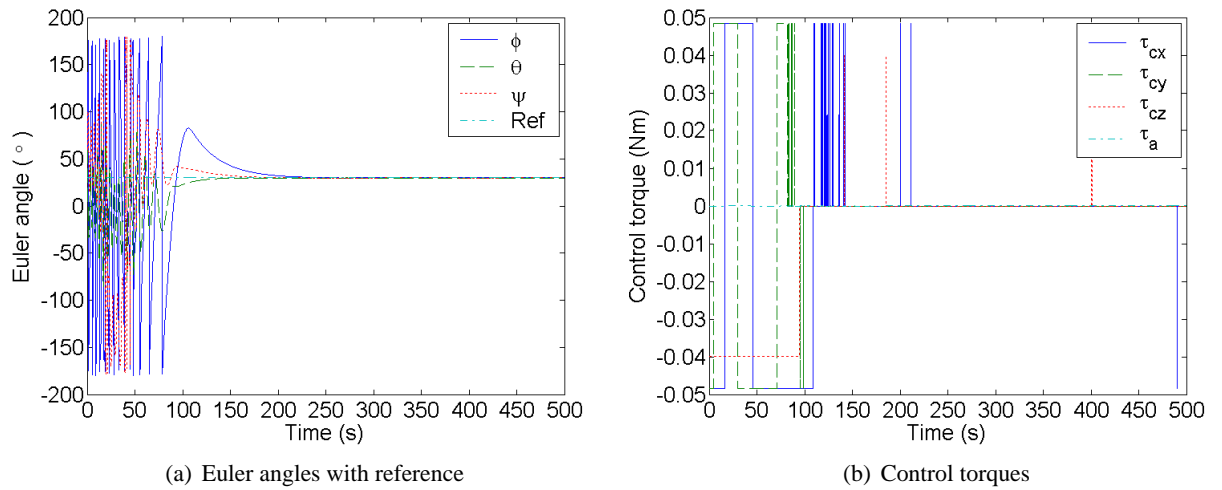


Figure B.6: Simulation of Lyapunov controller 1 with large initial angular velocity

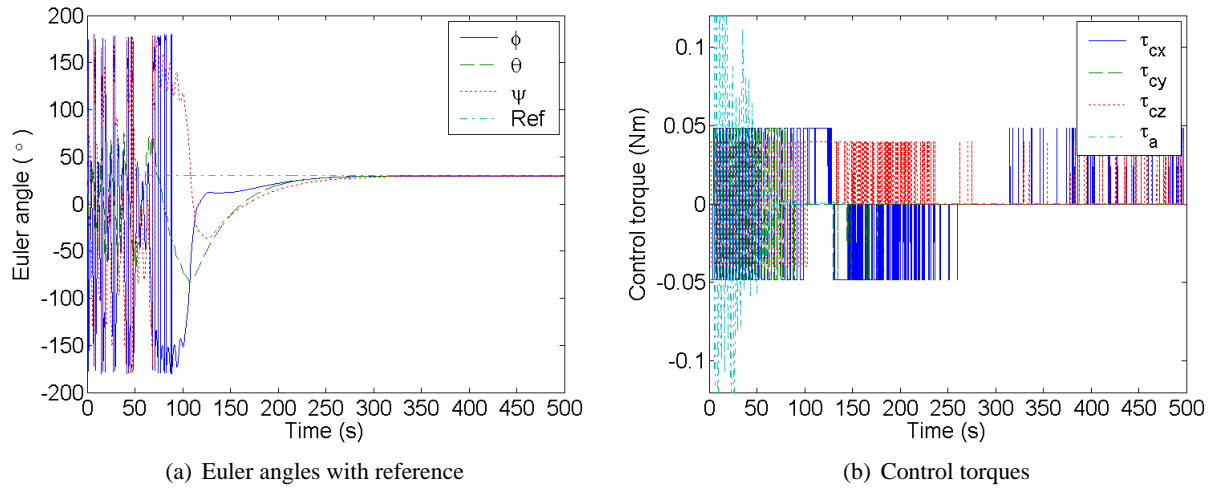


Figure B.7: Simulation of Lyapunov controller 3 with large initial angular velocity

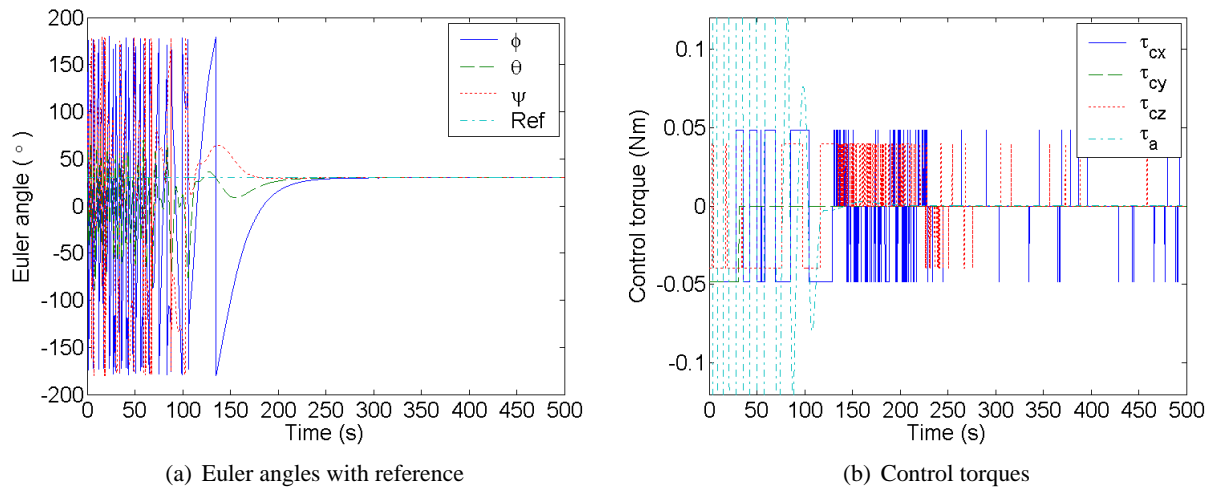


Figure B.8: Simulation of sliding mode controller with large initial angular velocity

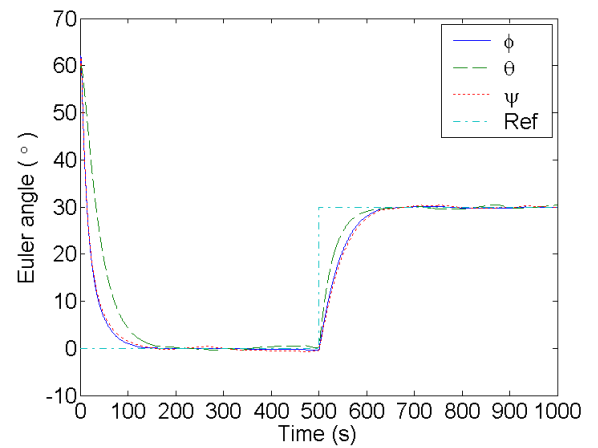
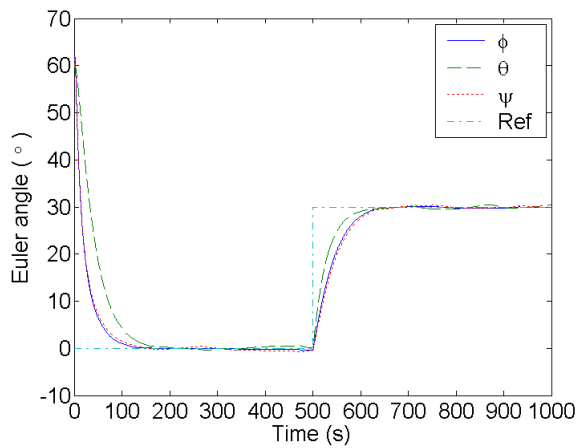
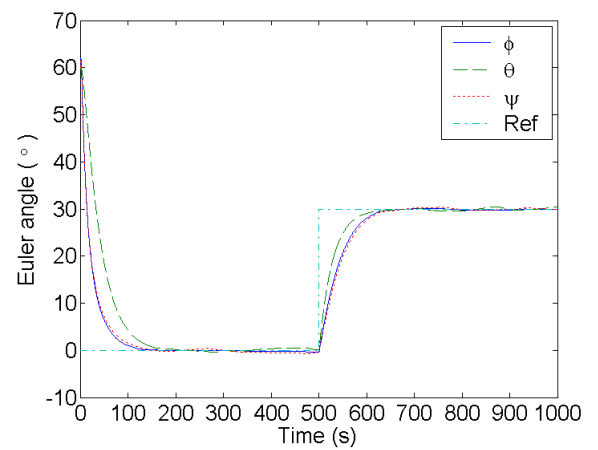
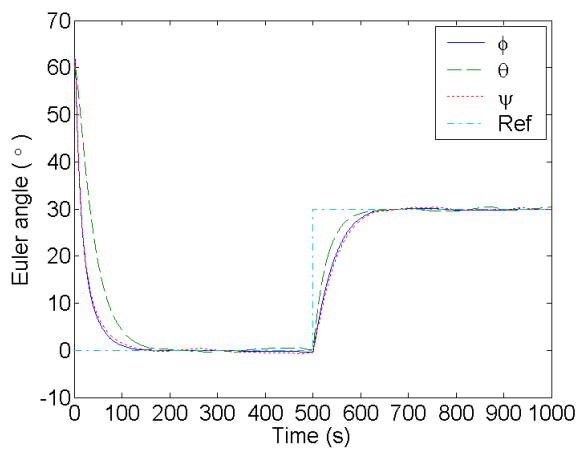


Figure B.9: Simulation of controllers with inertia uncertainty (Euler angles with reference)

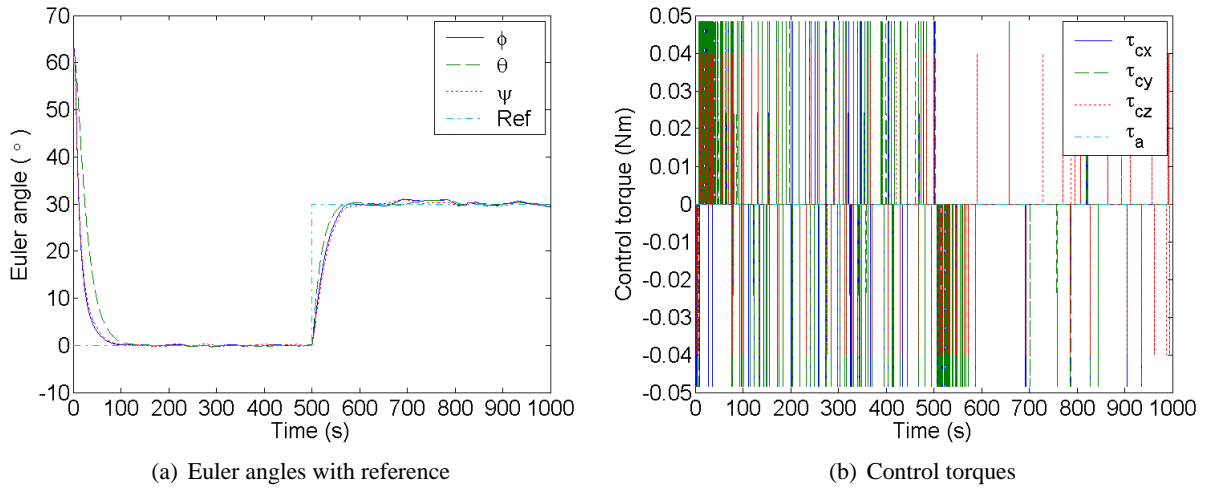


Figure B.10: Simulation of local PD controller with added white noise

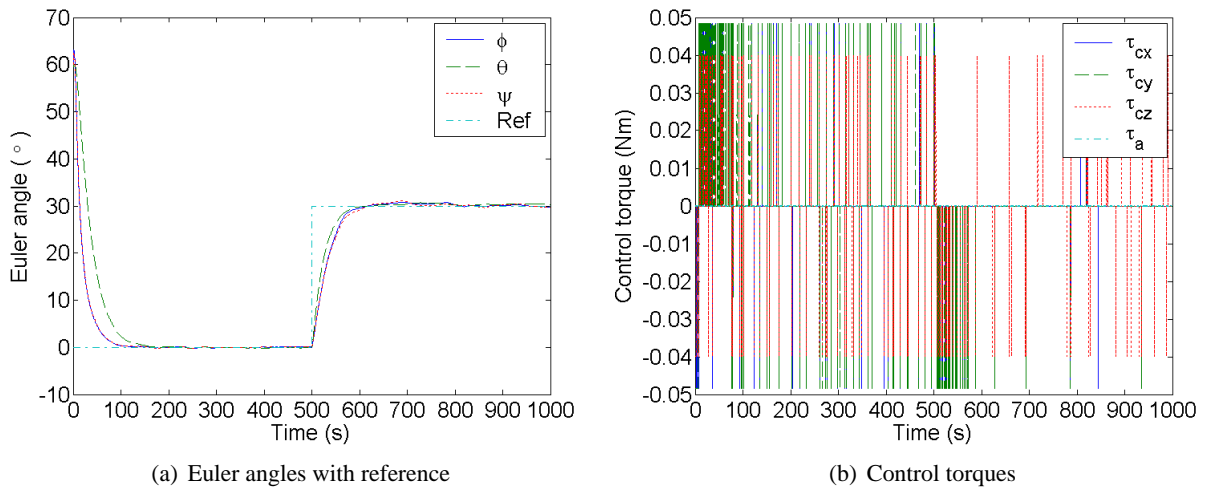


Figure B.11: Simulation of Lyapunov controller 1 with added white noise

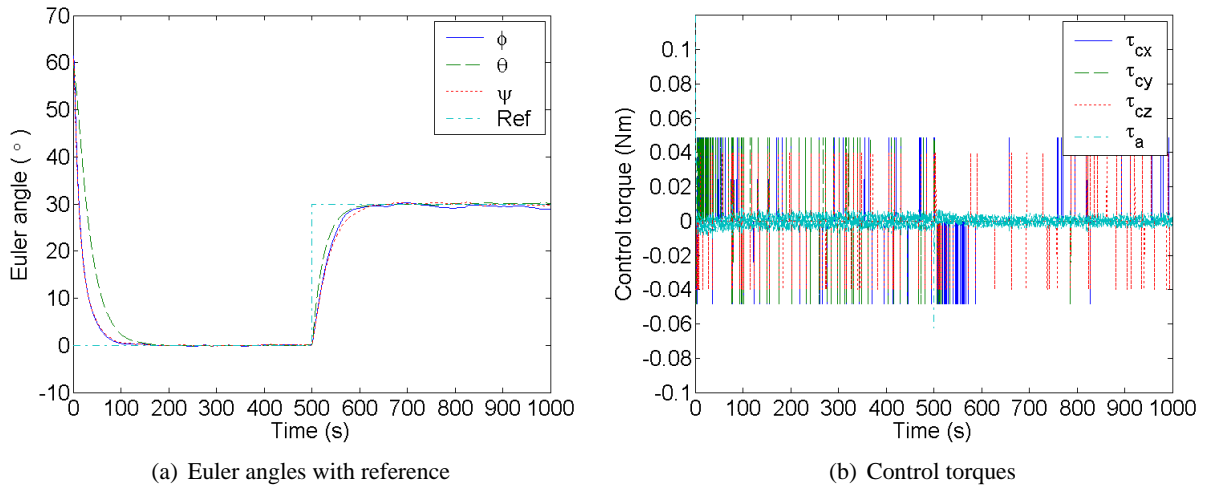


Figure B.12: Simulation of Lyapunov controller 3 with added white noise

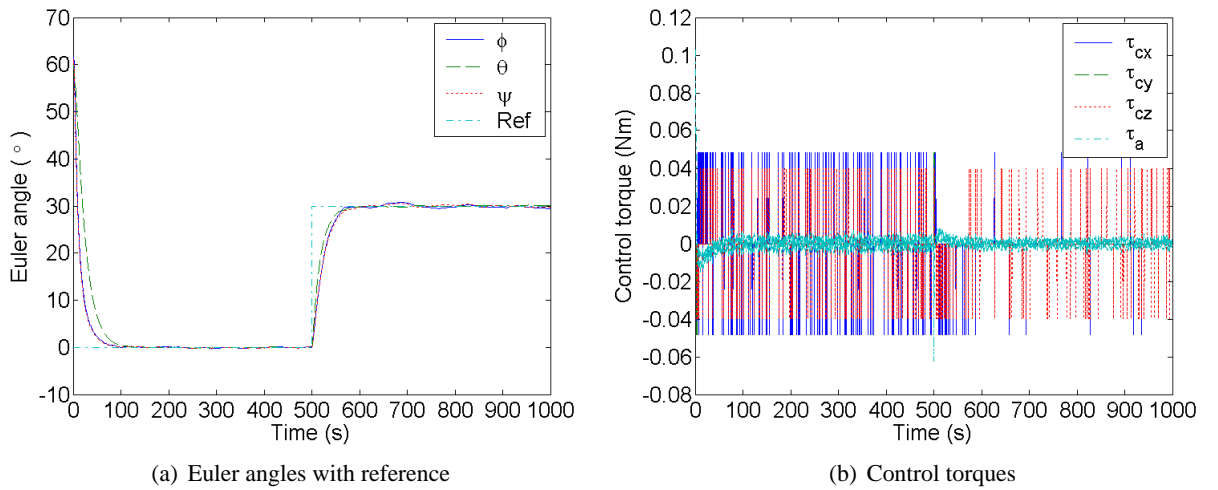


Figure B.13: Simulation of sliding mode controller with added white noise

Appendix C

Maple and MATLAB/SIMULINK input

This appendix contains Maple calculations, MATLAB code and SIMULINK diagrams. It starts with a Maple calculation which results in the linearized model of (4.9) found in (4.11) and (4.12). The MATLAB code which follows is the contents of *init.m* where simulator parameters are initialized. The appendix ends with three SIMULINK diagrams, where the simulator is presented. In the SIMULINK diagram called *SIMULATOR*, an orbit propagator is present. It is used to simulate an elliptical orbit, and has been developed by Hegrenæs (2004). However, in this thesis a circular orbit has been assumed. Hence the orbit propagator is not used. The details of the controller block in *SIMULATOR* is presented in the diagram *CONTROLLER*. It is in this block that the various controllers are plugged in. In *CONTROLLER* the sliding mode controller is inserted. The last diagram shows the blocks for the controllers and thruster controllers. In the accompanying CD, the simulator is located in the file *eseosystem.mdl*. Note that *init.m* must be run before running the simulator. The file *ControllersAndModulation.mdl* contains the various controllers and thruster controllers.

```
> restart;
```

```
MATHEMATICAL MODEL
```

```
> with(LinearAlgebra):Ib:=Matrix(3,3,[[ix,0,0],[0,iy,0],[0,0,iz]]);
```

$$Ib := \begin{bmatrix} ix & 0 & 0 \\ 0 & iy & 0 \\ 0 & 0 & iz \end{bmatrix}$$

```
> A:=Vector(1..3,[0,1,0]);
```

$$A := \begin{bmatrix} 0 \\ 1 \\ 0 \end{bmatrix}$$

```
> J:=Ib-A*Is.Transpose(A);
```

$$J := \begin{bmatrix} ix & 0 & 0 \\ 0 & iy - Is & 0 \\ 0 & 0 & iz \end{bmatrix}$$

```
> wbob:=Vector(1..3,[w1,w2,w3]);
```

$$wbob := \begin{bmatrix} w1 \\ w2 \\ w3 \end{bmatrix}$$

```
> eo:=Vector(1..3,[e1,e2,e3]);
```

$$eo := \begin{bmatrix} e1 \\ e2 \\ e3 \end{bmatrix}$$

```
> Rbo:=Matrix(3,3,[[1-2*(e2^2 + e3^2),2*(e1*e2 - e3*n),2*(e1*e3 + e2*n)],  
[2*(e1*e2 + e3*n),1-2*(e1^2 + e3^2),2*(e2*e3 - e1*n)],  
[2*(e1*e3 - e2*n),2*(e2*e3 + e1*n),1-2*(e1^2 + e2^2)]]);
```

$$Rbo := \begin{bmatrix} 1 - 2e2^2 - 2e3^2 & 2e1e2 - 2e3n & 2e1e3 + 2e2n \\ 2e1e2 + 2e3n & 1 - 2e1^2 - 2e3^2 & 2e2e3 - 2e1n \\ 2e1e3 - 2e2n & 2e2e3 + 2e1n & 1 - 2e1^2 - 2e2^2 \end{bmatrix}$$

```
> c2:=Column(Rbo,2);
```

$$c2 := \begin{bmatrix} 2 e1 e2 - 2 e3 n \\ 1 - 2 e1^2 - 2 e3^2 \\ 2 e2 e3 + 2 e1 n \end{bmatrix}$$

> c3:=Column(Rbo,3);

$$c3 := \begin{bmatrix} 2 e1 e3 + 2 e2 n \\ 2 e2 e3 - 2 e1 n \\ 1 - 2 e1^2 - 2 e2^2 \end{bmatrix}$$

> wbib:=wbob-w0*c2;

$$wbib := \begin{bmatrix} w1 - w0 (2 e1 e2 - 2 e3 n) \\ w2 - w0 (1 - 2 e1^2 - 2 e3^2) \\ w3 - w0 (2 e2 e3 + 2 e1 n) \end{bmatrix}$$

> Jinv:=MatrixInverse(J);

$$Jinv := \begin{bmatrix} \frac{1}{ix} & 0 & 0 \\ 0 & \frac{1}{iy - Is} & 0 \\ 0 & 0 & \frac{1}{iz} \end{bmatrix}$$

> tau:=Vector(1..3,symbol=t);

$$\tau := \begin{bmatrix} t_1 \\ t_2 \\ t_3 \end{bmatrix}$$

> taua:=ta;

$$taua := ta$$

> fhi:=Jinv.(-CrossProduct(wbib,(Ib.wbib+A*Is*ws))):

> fht:=Jinv.tau-Jinv.A*taua:

> fhg:=Jinv.(3*w0^2*CrossProduct(c3,Ib.c3)):

> dotc2:=-CrossProduct(wbob,c2):

> fha:=dotc2*(w0):

> dotwbob:=fhi+fha+fhg+fht:

> fsi:=Transpose(A).Jinv.(CrossProduct(wbib,(Ib.wbib+A*Is*ws))):

```

> fst:=-Transpose(A).Jinv.tau + (Transpose(A).Jinv.A + 1/Is)*taua:
> fsg:=-Transpose(A).Jinv.(3*w0^2*CrossProduct(c3,Ib.c3)):
> dotws:=fsi+fst+fsg:
> M1:=Matrix(3,3,shape=identity);

```

$$M1 := \begin{bmatrix} 1 & 0 & 0 \\ 0 & 1 & 0 \\ 0 & 0 & 1 \end{bmatrix}$$

```

> dote:=1/2*(n*M1.wbob+CrossProduct(eo,wbob)):
> dotn:=-1/2*Transpose(eo).wbob:

```

LINEARIZATION OF MODEL

```

> sysvector:=Vector(1..8,[dotwbob[1],dotwbob[2],dotwbob[3],dotws,dotn,dote[1],dote[2],dote[3]]):
> with(VectorCalculus):jacobisys:=Jacobian(sysvector,[w1,w2,w3,ws,n,e1,e2,e3]):

```

Warning, the names &x, CrossProduct and DotProduct have been rebound

Warning, the assigned names <,> and <|> now have a global binding

Warning, these protected names have been redefined and unprotected: *, +, ., D, Vector, diff, int, limit, series

```

> jacobiinput:=Jacobian(sysvector,[tau[1],tau[2],tau[3],ta]):
> n:=1: e1:=0: e2:=0: e3:=0: w1:=0: w2:=0: w3:=0: ws:=0:
> A_sys := eval(simplify(jacobisys));

```

$$A_{sys} := \begin{bmatrix} \left[0, 0, -\frac{-w0 iz + iy w0 - ix w0}{ix}, 0, 0, -\frac{2 w0 (4 w0 iz - 4 iy w0)}{ix}, 0, 0 \right], \\ \left[0, 0, 0, 0, 0, 0, -\frac{2 w0 (-3 ix w0 + 3 w0 iz)}{iy - Is}, 0 \right], \\ \left[\frac{-w0 iz + iy w0 - ix w0}{iz}, 0, 0, 0, 0, 0, \frac{2 w0 (iy w0 - ix w0)}{iz} \right], \\ \left[0, 0, 0, 0, 0, 0, \frac{2 w0 (-3 ix w0 + 3 w0 iz)}{iy - Is}, 0 \right], [0, 0, 0, 0, 0, 0, 0, 0], \left[\frac{1}{2}, 0, 0, 0, 0, 0, 0, 0 \right], \\ \left[0, \frac{1}{2}, 0, 0, 0, 0, 0, 0 \right], \\ \left[0, 0, \frac{1}{2}, 0, 0, 0, 0, 0 \right] \end{bmatrix}$$

```

> B_sys := eval(simplify(jacobiinput));

```

$$B_{\text{sys}} := \begin{bmatrix} \frac{1}{ix} & 0 & 0 & 0 \\ 0 & \frac{1}{iy - Is} & 0 & -\frac{1}{iy - Is} \\ 0 & 0 & \frac{1}{iz} & 0 \\ 0 & -\frac{1}{iy - Is} & 0 & \frac{iy}{(iy - Is) Is} \\ 0 & 0 & 0 & 0 \\ 0 & 0 & 0 & 0 \\ 0 & 0 & 0 & 0 \\ 0 & 0 & 0 & 0 \end{bmatrix}$$

LINEAR CONTROL

```
> A_w :=
Matrix([[A_sys[1,1], A_sys[1,2], A_sys[1,3]], [A_sys[2,1], A_sys[2,2], A_sys[2,3]], [A_sys[3,1], A_sys[3,2], A_sys[3,3]]]);
```

$$A_w := \begin{bmatrix} 0 & 0 & -\frac{-w0 iz + iy w0 - ix w0}{ix} \\ 0 & 0 & 0 \\ \frac{-w0 iz + iy w0 - ix w0}{iz} & 0 & 0 \end{bmatrix}$$

```
> A_e :=
Matrix([[A_sys[1,6], A_sys[1,7], A_sys[1,8]], [A_sys[2,6], A_sys[2,7], A_sys[2,8]], [A_sys[3,6], A_sys[3,7], A_sys[3,8]]]);
```

$$A_e := \begin{bmatrix} -\frac{2 w0 (4 w0 iz - 4 iy w0)}{ix} & 0 & 0 \\ 0 & -\frac{2 w0 (-3 ix w0 + 3 w0 iz)}{iy - Is} & 0 \\ 0 & 0 & \frac{2 w0 (iy w0 - ix w0)}{iz} \end{bmatrix}$$

```
> K_e := Matrix([[ke1, 0, 0], [0, ke2, 0], [0, 0, ke3]]);
```

$$K_e := \begin{bmatrix} ke1 & 0 & 0 \\ 0 & ke2 & 0 \\ 0 & 0 & ke3 \end{bmatrix}$$

> K_w := Matrix([[kw1,0,0],[0,kw2,0],[0,0,kw3]]);

$$K_w := \begin{bmatrix} kw1 & 0 & 0 \\ 0 & kw2 & 0 \\ 0 & 0 & kw3 \end{bmatrix}$$

> B_w := Matrix([[B_sys[1,1..3]],[B_sys[2,1..3]],[B_sys[3,1..3]]]);

$$B_w := \begin{bmatrix} \frac{1}{ix} & 0 & 0 \\ 0 & \frac{1}{iy - Is} & 0 \\ 0 & 0 & \frac{1}{iz} \end{bmatrix}$$

> B_w.K_e;

$$\begin{bmatrix} \frac{ke1}{ix} & 0 & 0 \\ 0 & \frac{ke2}{iy - Is} & 0 \\ 0 & 0 & \frac{ke3}{iz} \end{bmatrix}$$

> simplify(A_e+M1*k0);

$$\left[\left[\frac{-8 w0^2 iz + 8 w0^2 iy + k0 ix}{ix}, 0, 0 \right], \left[0, \frac{6 w0^2 ix - 6 w0^2 iz + k0 iy - k0 Is}{iy - Is}, 0 \right], \left[0, 0, \frac{2 w0^2 iy - 2 w0^2 ix + k0 iz}{iz} \right] \right]$$

> simplify(A_w - B_w.K_w);

$$\begin{bmatrix} -\frac{kw1}{ix} & 0 & \frac{w0 (iz - iy + ix)}{ix} \\ 0 & -\frac{kw2}{iy - Is} & 0 \\ -\frac{w0 (iz - iy + ix)}{iz} & 0 & -\frac{kw3}{iz} \end{bmatrix}$$

Characteristic polynomial

```
> Determinant(simplify(A_w - B_w.K_w - lambda.M1));
-  $\frac{1}{ix (iy - Is) iz} ((\lambda iy - \lambda Is + kw2) (\lambda^2 ix iz + \lambda ix kw3 + kw1 \lambda iz + kw1 kw3 + w0^2 iz^2 - 2 w0^2 iz iy + 2 w0^2 iz ix + w0^2 iy^2 - 2 w0^2 iy ix + w0^2 ix^2))$ 
```

```
*****
%*
%*   init.m
%*
%*   Author: Oeyvind Hegrenaes and Morten Topland, NTNU 2004
%*
%*   Initialization of different parameters used in Simulink
%*
%*
*****

% Earth Parameters by means of WGS84
mu = 398600.5; % [km^3/s^2]
re = 6378137e-3; % Equatorial Radius of the Earth [km]
f = 1/298.257223563; % Flattering of Earth ellipsoid
rp = re - f*re; % Polar Radius of the Earth [km]

% Orbit parameters for circular orbit
ra = 250; % Spacecraft altitude at perigee [km]
rc = (re + rp)/2 + ra; % Distance from Earth center to spacecraft [km]
w0 = sqrt(mu/rc^3); % Angular velocity of orbit frame about y axis.

% SSETI/ESEO Parameters
i_x = 4.35; i_y = 4.337; i_z = 3.664; % AOCs document 02.04.2004 states: i_x = 4.35; i_y ✓
= 4.337; i_z = 3.664
Ib_hat = [i_x 0 0; 0 i_y 0; 0 0 i_z]; % Nominal inertia matrix
Ib = 1.2*Ib_hat; % Actual inertia matrix
a_vec = [0 1 0]'; % Normalized axis of relative rotation (reaction wheel)
A = a_vec;
B = [1 0 0; 0 0 0; 0 0 1];
Is_hat = 4.0e-5; % Nominal moment of inertia of the wheel about a_vec [kg m^2]
Is = 1.2*Is_hat; % Actual wheel inertia
J = Ib - A*Is*A'; % Inertialike matrix
J_hat = Ib_hat - A*Is_hat*A'; % Nominal inertialike matrix

% Saturation in ACS [Nm]
Tau_thrust_nom = [0.0484, 0.0484, 0.0398]'; % Nominal values from PROP document 24.02.200 ✓
4 [Nm]
Tau_thrust_min = [0.0306, 0.0306, 0.0252]'; % Minimum values from PROP document 24.02.200 ✓
4 [Nm]

% Reaction wheel
Tau_rw_max = 3.7e-3; % Maximum motor torque from AOCs document 04.11.2003 [Nm]
w_s_max = 5035*2*pi/60; % Maximum angular velocity (5035 rpm) from AOCs document 04.11.20 ✓
03 [rad/s]

% Pulse-Width Pulse-Frequency Modulator
Kp = 1; % Song and Agrawal (2000) recommends 1 < Kp < 2
Km = 1; % Song and Agrawal (2000) recommends 1 < Km < 6
Tm = 0.5; % Song and Agrawal (2000) recommends 0.4 < Tm < 0.6
Uon = 0.4; % Song and Agrawal (2000) recommends 0.3 < Uon
Uoff = 0.1*Uon; % Song and Agrawal (2000) recommends Uoff < 0.8*Uon

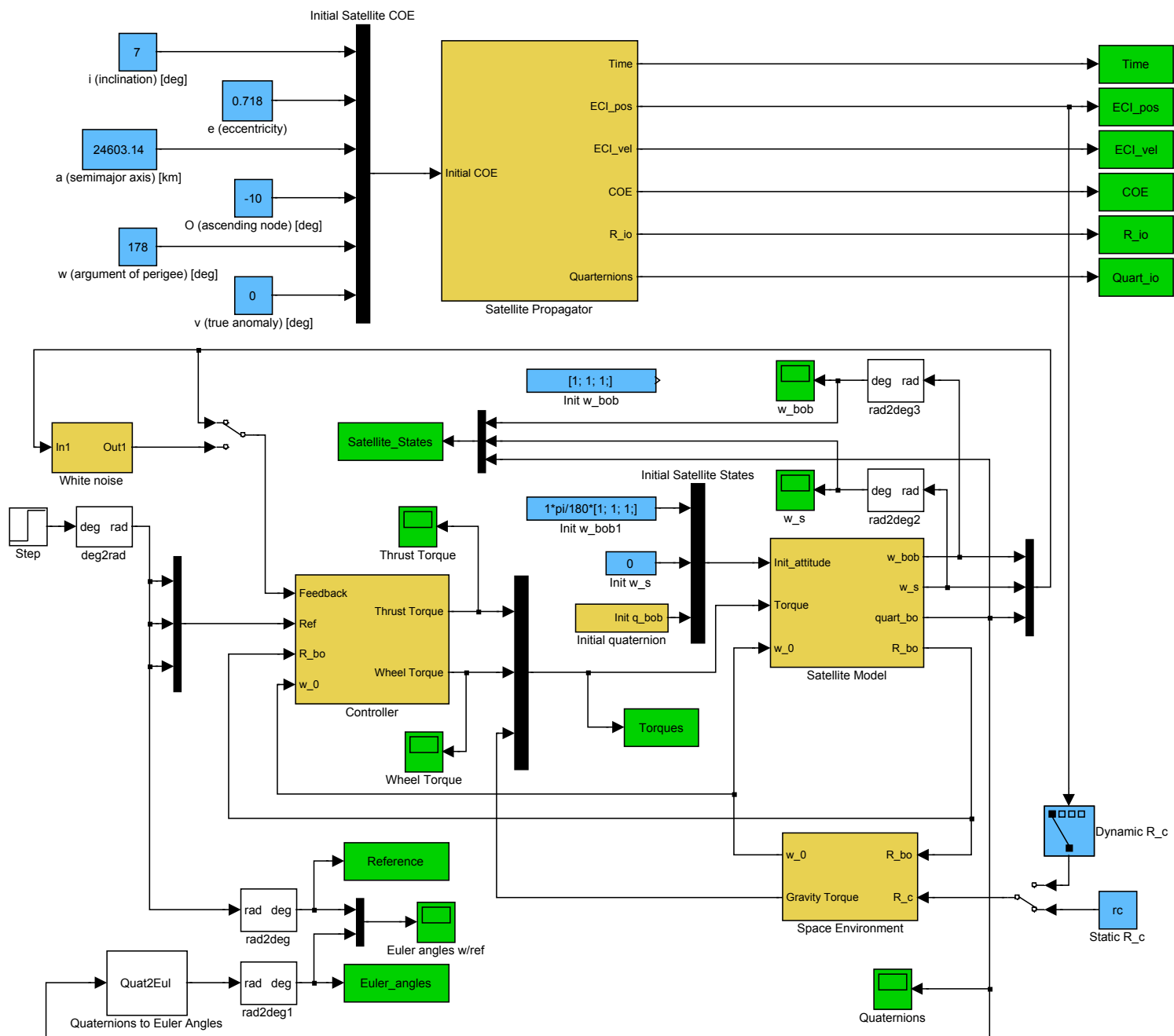
% Schmitt trigger parameters
Son = 0.002;
Soff = 0.2*Son;

% Bangbang control parameter: Dead Zone
```

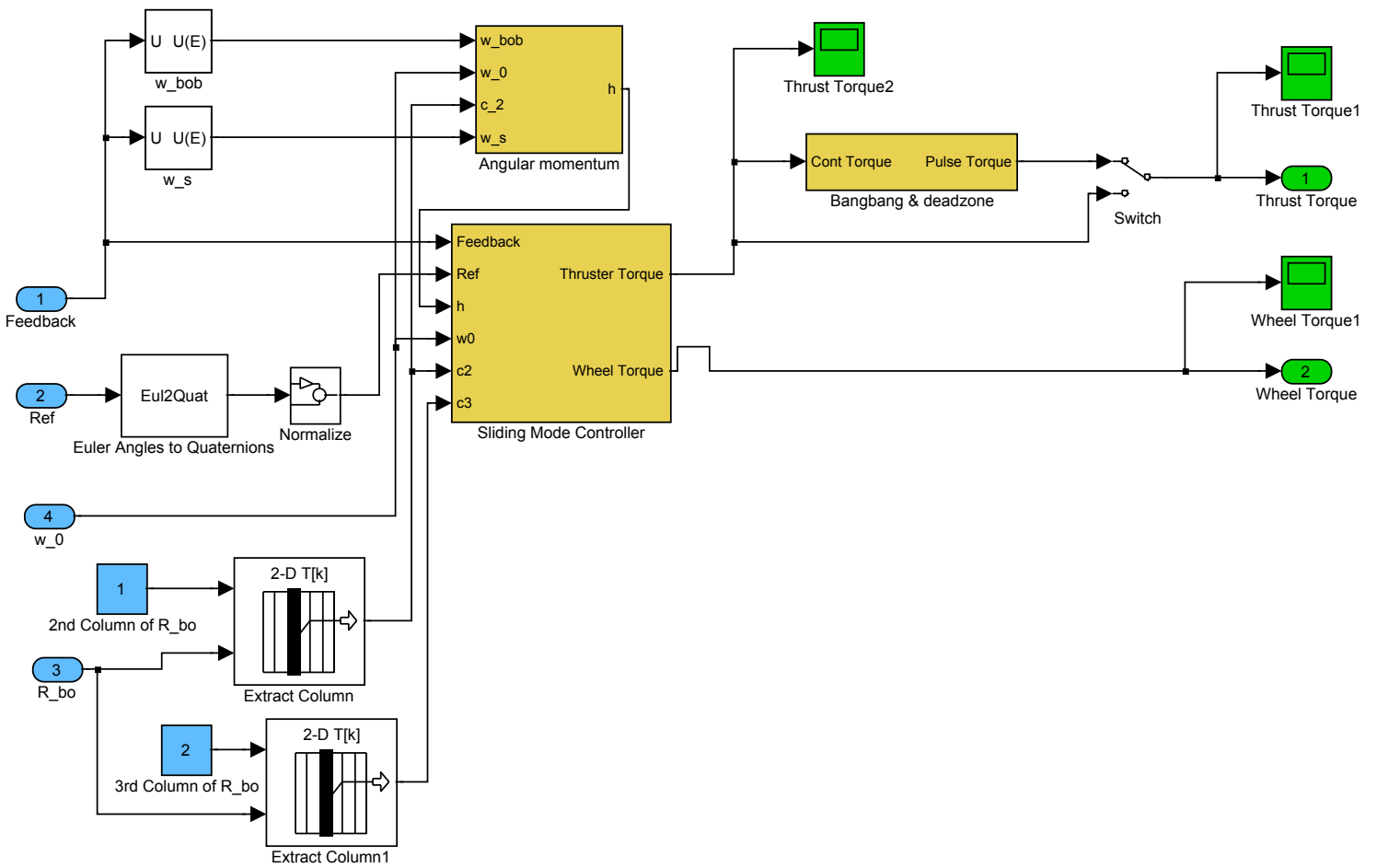
```
dz = 0.001;  
% Excellent accuracy when dz = 0.001.  
% Noise simulation: Good performance for Lyapunov controllers when dz =  
% 0.006. PD controller and Sliding Mode controller performs well at dz =  
% 0.007 and dz = 0.01 respectively.
```

```
whos
```

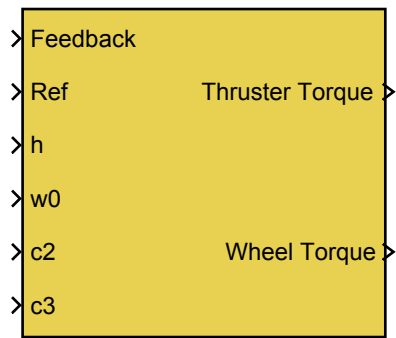
SIMULATOR



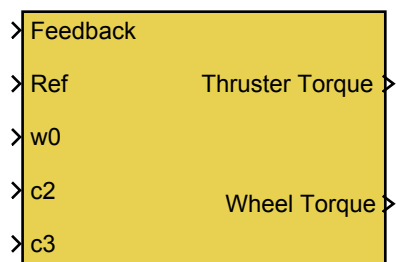
CONTROLLER BLOCK



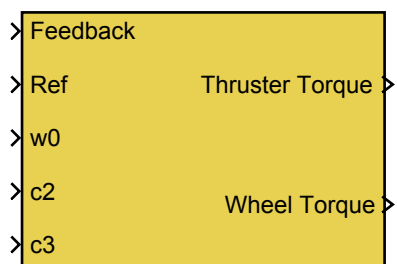
CONTROLLERS



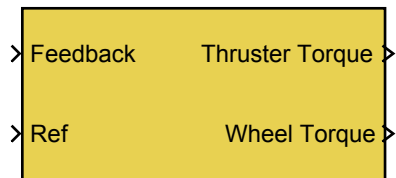
Sliding Mode Controller



Lyapunov Controller 3



Lyapunov Controller 1

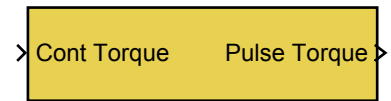


PD Controller

PULSE MODULATION



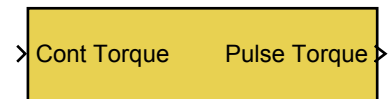
Bangbang control



Bangbang & deadzone



Schmitt trigger



PWPF modulator

Appendix D

Conference and Workshop Documents

This appendix contains a presentation of the SSETI ESMO ADCS team for the Space Technology Education Conference (STEC), a presentation of this team's work for the SSETI ESEO Workshop VII, and an article which summarizes this thesis. The article will be presented on the 55th International Astronautical Congress in Vancouver, which is held from the 4th to the 8th of October this year. STEC was held from the 14th to the 16th of April 2004. ESEO Workshop VII took place from the 10th to the 14th of May 2004.

NORWEGIAN UNIVERSITY OF SCIENCE AND TECHNOLOGY (NTNU) AND NARVIK UNIVERSITY COLLEGE (HIN)

Attitude Determination and Control System for the European Student Moon Orbiter

Abstract: This SSETI chapter is based in Trondheim and Narvik in Norway. It is responsible for the Attitude Determination and Control System (ADCS) for the European Student Moon Orbiter (ESMO). This work starts with a case study of the European Student Earth Orbiter (ESEO), in order to investigate to what extent the ADCS can be reused for the ESMO. Focus will also be on stability analysis of the ADCS.

Case study of ESEO

The ESMO ADCS team started their work in January 2004, as the first ESMO team. More ESMO teams will be recruited for fall 2004. This spring, the team is working on a case study of ESEO. The main objectives are mathematical modeling of the satellite and its actuators (thrusters and reaction wheel), stability analysis, orbital maneuvering and attitude control. The latter includes several control schemes, including linear and nonlinear control, as well as model predictive control (i.e. design of control laws to minimize power and fuel consumption). Finally, the closed-loop system will be extensively simulated in MATLAB and Simulink.

Some of this work has already been completed by the ESEO AOCS team. This way, the ESMO ADCS team can learn from them, and in return help them in areas where the ESEO AOCS team may have problems.

Future work

When the case study is finished, the ESMO ADCS team will start to work on the ADCS for ESMO.



The Moon

Contact: Morten Topland (NTNU)
(topland@stud.ntnu.no)
Joeran Antonsen (HiN)
(joraanto@student.hin.no)



NTNU Norwegian University of Science and Technology



- Located in Trondheim, 3rd largest town in Norway, 63° North
- 40 000 applicants each year - 5 500 are admitted
- 20 000 registered students
- 2 500 degrees awarded each year
- 200 PhD degrees awarded each year
- One person in six in Trondheim is a student



ESMO ADCS - Norway



ESEO mathematical model

Kinematics:
$$\begin{aligned} \dot{\eta} &= -\frac{1}{2}\epsilon^T \omega_{ob}^b \\ \dot{\epsilon} &= \frac{1}{2}[\eta\mathbf{1} + \epsilon^\times] \omega_{ob}^b \end{aligned} \left. \vphantom{\begin{aligned} \dot{\eta} \\ \dot{\epsilon} \end{aligned}} \right\} \text{Orientation (in quaternions)}$$

Dynamics:
$$\begin{aligned} \mathbf{h}^b &= \mathbf{I}\omega_{ib}^b + \mathbf{A}\mathbf{I}_s\omega_s \\ \dot{\mathbf{h}}_a^b &= \mathbf{I}_s\mathbf{A}^T\omega_{ib}^b + \mathbf{I}_s\omega_s \\ \dot{\mathbf{h}}^b &= (\mathbf{H}^b)^\times \omega_{ib}^b + \tau_e \\ \dot{\mathbf{h}}_a^b &= \tau_a \end{aligned} \left. \vphantom{\begin{aligned} \mathbf{h}^b \\ \dot{\mathbf{h}}_a^b \\ \dot{\mathbf{h}}^b \end{aligned}} \right\} \text{Angular momenta for satellite body and reaction wheel}$$

ESMO ADCS - Norway



Dynamics in angular velocity:

$\omega_{ib}^b \longleftarrow$ Angular velocity of ESEO in reference to Earth

$$\dot{\omega}_{ib}^b = \mathbf{J}^{-1} \left[-(\omega_{ib}^b)^\times (\mathbf{I}\omega_{ib}^b + \mathbf{A}\mathbf{I}_s\omega_s) + \tau_e \right] - \mathbf{J}^{-1}\mathbf{A}\tau_a$$

$$\begin{aligned} \dot{\omega}_s &= -\mathbf{A}^T\mathbf{J}^{-1} \left[-(\omega_{ib}^b)^\times (\mathbf{I}\omega_{ib}^b + \mathbf{A}\mathbf{I}_s\omega_s) + \tau_e \right] \\ &\quad + [\mathbf{A}^T\mathbf{J}^{-1}\mathbf{A} + \mathbf{I}_s^{-1}] \tau_a \end{aligned}$$

$$\mathbf{J} = \mathbf{I} - \mathbf{A}\mathbf{I}_s\mathbf{A}^T$$

$$\tau_e = \tau_c + \tau_g$$

↑ Thruster torque ↓ Gravity torque

ESMO ADCS - Norway



Attitude control

Control objective: $\tilde{\epsilon} \rightarrow 0 \longleftarrow$ Orientation (quaternion) error
 $\tilde{\omega} \rightarrow 0 \longleftarrow$ Angular velocity error

- Controllers:
- Linear Quadratic Control (LQR)
 - Explicit Model Predictive Control (eMPC)
 - Nonlinear Control
 - PD Control (no mathematical proof for nonlinear system model)

ESMO ADCS - Norway



Nonlinear controller

Applying Lyapunov stability analysis, the following controller has been found:

$$\tau_c = -k_1\tilde{\epsilon} - k_2\tilde{\omega}$$

$$\mathbf{A}\tau_a = k_3\tilde{\epsilon} + k_4\tilde{\omega} + \left((\mathbf{H}^b)^\times + \mathbf{J}\omega_0(c_2)^\times \right) \tilde{\omega} - (\mathbf{H}^b)^\times \omega_0 c_2$$

$$k_1 + k_3 > a$$

$$k_2 + k_4 > 0$$

Restriction:

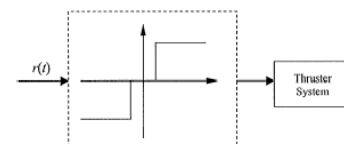
$$i_x, i_y > i_z$$

ESMO ADCS - Norway

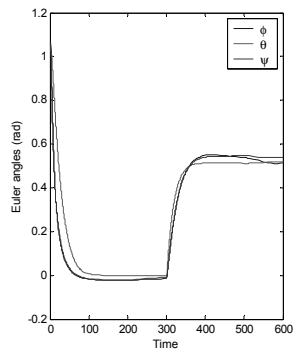
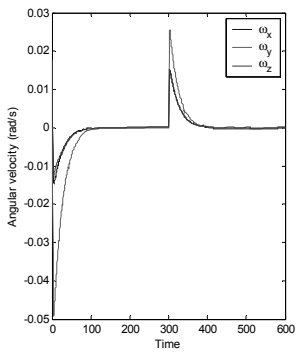


SIMULINK simulation

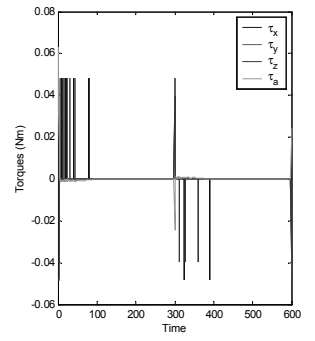
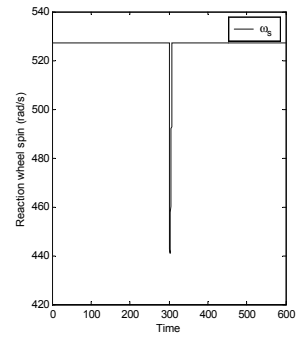
- Initial spin of 1 degree/sec about all axes
- Change of desired attitude after 300 sec
- A bangbang controller with deadzone generates thruster pulses:



ESMO ADCS - Norway



ESMO ADCS - Norway



ESMO ADCS - Norway



Recruitment

- Morten and Oeyvind finish their studies at NTNU in June.
- But next year 5 new students will join ESMO ADCS in Trondheim.
- And work on ESMO will finally begin!

IAC-04-A.P.12

NONLINEAR ATTITUDE CONTROL OF THE MICRO-SATELLITE ESEO

Morten Pedersen Topland and Jan Tommy Gravdahl

Department of Engineering Cybernetics and
Norwegian University of Science and Technology
N-7491 TRONDHEIM
NORWAY

July 1, 2004

Abstract

In this paper, attitude control of a spacecraft using thrusters and reaction wheels as actuators is studied. Linearization and Lyapunov theory is used to derive two linear and four nonlinear controllers. Three of the nonlinear controllers rely on cancellation of system nonlinearities, while the fourth is a sliding mode controller. By restricting the spacecraft inertia, simpler controllers can be found. Several controllers are compared in simulations. The simulations use data from the micro-satellite, European Student Earth orbiter (ESEO).

1 INTRODUCTION

1.1 Background

The micro-satellite ESEO is part of the Student Space Exploration and Technology Initiative (SSETI), which is a project supported by the Education Office of the European Space Agency (ESA). Students from ten different European countries participate in SSETI, and more information on SSETI can be found in [1]. SSETI is also planning a satellite which will orbit the moon, the European Student Moon Orbiter (ESMO). Work on this satellite is about to begin, and the first student team to be recruited was the ESMO Attitude Determination and Control System (ADCS) team. This Norwegian team is based at the Norwegian University of Science and Technology (NTNU) in Trondheim and Narvik University College (HiN) in Narvik. The first task of the ESMO ADCS team was to do a case study of ESEO. The work presented in this article is part of this study, and its contents is based on [2].

1.2 Previous work

A standard reference on spacecraft dynamics is [3]. Concerning attitude control of spacecraft, [4] describe nonlinear attitude control for a spacecraft with thrusters and an arbitrary number of reaction wheels, where the modified Rodrigues parameters are used to describe the attitude of the spacecraft. The use of Euler parameters or unit quaternions in attitude control problems, is studied by [5], but the results are applied to underwater vehicles. A nonlinear sliding mode controller is proposed by [6]. Vibration suppression during attitude control for flexible spacecraft is studied in [7], where various methods of transforming a continuous input torque to thruster torque pulses is presented.

At the Norwegian University of Science and Technology (NTNU), [8], [9] and others have studied attitude control of satellites with magnetic coils and reaction wheels as actuators. Their results are part of the foundation of the NCUBE projects, where pico-satellites are launched into Earth orbit. For more information on NCUBE, see [10] and [11].

2 MODELING

2.1 Reference frames

To analyze the motion of a satellite, it is necessary to define reference frames, which this motion is relative to. These frames are the same as those used by [12] and [9].

The Earth Centered Inertial (ECI) frame is denoted \mathcal{F}_i , and has its origin at the center of the earth. Its unit vectors are x_i, y_i, z_i , where z_i is directed along the Earth's rotation axis. This frame is non-accelerated, that is inertial, which means that the laws of Newton apply.

The Earth Centered Earth Fixed (ECEF) frame is denoted \mathcal{F}_e , and has the same origin as \mathcal{F}_i . However \mathcal{F}_e rotates relative to \mathcal{F}_i with a constant angular velocity

$\omega_e = 7.2921 \cdot 10^{-5}$ rad/s. This is the same as the angular velocity of the Earth about its rotation axis. The unit vectors of \mathcal{F}_e are x_e, y_e, z_e , where z_e is directed along the Earth's rotation axis.

The *Orbit (O) frame*, denoted \mathcal{F}_o , is located at the center of mass of the satellite, with the unit vectors x_o, y_o and z_o . z_o points towards the center of the Earth, while x_o points in the traveling direction of the satellite, tangent to the orbit. y_o is found using the right hand rule.

The *Body (B) frame*, denoted \mathcal{F}_b , has its origin at the center of mass of the satellite. This frame is fixed to the satellite body. Its unit vectors x_b, y_b and z_b are usually chosen to coincide with the spacecraft's principal axes of inertia. This simplifies the spacecraft's equations of motion. Rotations about x_b, y_b and z_b are called *roll, pitch* and *yaw* respectively.

2.2 Kinematics

Definition 1 A rotation matrix is a matrix $\mathbf{R} \in SO(3)$, defined by

$$SO(3) = \{ \mathbf{R} | \mathbf{R} \in \mathbb{R}^{3 \times 3}, \mathbf{R}^T \mathbf{R} = \mathbf{1}, \det \mathbf{R} = 1 \}, \quad (1)$$

where $\mathbf{1}$ is the identity matrix and $SO(3)$ is the special orthogonal group of order three. The rotation matrix transforms a coordinate vector from one reference frame to another, for instance the matrix \mathbf{R}_o^b transforms \mathbf{v}^o into \mathbf{v}^b : $\mathbf{v}^b = \mathbf{R}_o^b \mathbf{v}^o$.

The rotation matrix can be parameterized as

$$\mathbf{R}_{k,\theta} = \cos \theta \mathbf{1} + \mathbf{k}^\times \sin \theta + \mathbf{k} \mathbf{k}^T (1 - \cos \theta), \quad (2)$$

where \mathbf{k} is an arbitrary unit vector in an arbitrary reference frame, and the angle θ represents the rotation about \mathbf{k} . The parameters \mathbf{k} and θ are known as *angle-axis parameters*. Such a rotation is called a *simple rotation*. The elements of a rotation matrix \mathbf{R} are called directional cosines, and can be arranged into column vectors:

$$\mathbf{R} = [\mathbf{c}_1, \mathbf{c}_2, \mathbf{c}_3] \quad (3)$$

In fact, these vectors are unit vectors, hence $\mathbf{c}_i^T \mathbf{c}_i = 1$. A composite rotation is represented by the product of two rotation matrices. The rotation from \mathcal{F}_i to \mathcal{F}_b can be expressed as $\mathbf{R}_i^b = \mathbf{R}_o^b \mathbf{R}_i^o$.

Definition 2 The angular velocity vector of \mathcal{F}_o relative to \mathcal{F}_b , written in \mathcal{F}_b is defined by the corresponding rotation matrix, and its time derivative:

$$(\omega_{bo}^b)^\times = \dot{\mathbf{R}}_o^b (\mathbf{R}_o^b)^T \quad (4a)$$

$$\omega_{bo}^b = -\omega_{ob}^b \quad (4b)$$

The cross product operator is defined by:

$$\mathbf{v}^\times = \begin{bmatrix} 0 & -\omega_z & \omega_y \\ \omega_z & 0 & -\omega_x \\ -\omega_y & \omega_x & 0 \end{bmatrix}, \quad \omega = \begin{bmatrix} \omega_x \\ \omega_y \\ \omega_z \end{bmatrix} \quad (5)$$

It can be shown that a similar relation exists for the directional cosines:

$$\dot{\mathbf{c}}_i = (\mathbf{c}_i)^\times \omega_{ob}^b \quad (6)$$

The Euler parameters, also called unit quaternions, give a representation of the rotation matrix without singularities. These parameters will be used in this paper.

Definition 3 The Euler parameters are defined in terms of the angle-axis parameters, and are given by the scalar η and the vector ϵ . In coordinate form this is written

$$\eta = \cos \frac{\theta}{2} \quad (7)$$

$$\epsilon = [\epsilon_1, \epsilon_2, \epsilon_3]^T = \mathbf{k} \sin \frac{\theta}{2} \quad (8)$$

where \mathbf{k} is a unit vector. The Euler parameters satisfy the following property:

$$\eta^2 + \epsilon^T \epsilon = 1 \quad (9)$$

The rotation matrix $\mathbf{R}_{k,\theta}$ from (2) can now be expressed in Euler parameters as:

$$\mathbf{R}_{k,\theta} = \mathbf{R}_{\eta,\epsilon} = \mathbf{1} + 2\eta \epsilon^\times + 2(\epsilon^\times)^2 \quad (10)$$

As shown in [13], the kinematic differential equations in reference to \mathcal{F}_o and \mathcal{F}_b in Euler parameters are given as:

$$\dot{\eta} = -\frac{1}{2} \epsilon^T \omega_{ob}^b \quad (11a)$$

$$\dot{\epsilon} = \frac{1}{2} [\eta \mathbf{1} + \epsilon^\times] \omega_{ob}^b \quad (11b)$$

The actual attitude of a spacecraft is given by the rotation matrix $\mathbf{R} = \mathbf{R}_i^b$. Let \mathcal{F}_o be a desired orientation, represented by $\mathbf{R}_d = \mathbf{R}_i^o$. This means that we want \mathcal{F}_b to coincide with \mathcal{F}_o , that is $\mathbf{R} = \mathbf{R}_d$. In [5] the attitude error $\tilde{\mathbf{R}}$ is defined as

$$\tilde{\mathbf{R}} = \mathbf{R}_d^{-1} \mathbf{R} = \mathbf{R}_d^T \mathbf{R} \quad (12)$$

When the attitude error is zero, then $\tilde{\mathbf{R}} = \mathbf{1}$. When using unit quaternions, [5] has shown that the attitude error differential equations becomes

$$\dot{\tilde{\eta}} = -\frac{1}{2}\tilde{\epsilon}^T\tilde{\omega} \quad (13a)$$

$$\dot{\tilde{\epsilon}} = -\frac{1}{2}[\tilde{\eta}\mathbf{1} + \tilde{\epsilon}^\times]\tilde{\omega} \quad (13b)$$

where $\tilde{\omega}$ is the error in angular velocity. Note that (13) has the same form as (11). The error in angular velocity $\tilde{\omega}$ is given in reference to a desired reference frame \mathcal{F}_d . The error is zero when \mathcal{F}_b and \mathcal{F}_d have the same angular velocity. The angular velocity error is:

$$\tilde{\omega} = \omega_{db}^b = \omega_{ib}^b - \mathbf{R}_d^b \omega_{id}^d \quad (14)$$

This definition is used in [4] and [9].

2.3 Dynamical satellite model

In this paper we will use the model of a rigid satellite with N reaction wheels as found in [4]. The dynamics can be written as

$$\dot{\mathbf{h}}^b = (\mathbf{h}^b)^\times \mathbf{J}^{-1}(\mathbf{h}^b - \mathbf{A}\mathbf{h}_a^b) + \tau_e \quad (15a)$$

$$\dot{\mathbf{h}}_a^b = \tau_a \quad (15b)$$

where \mathbf{h}^b is the system angular momentum, which in \mathcal{F}_b is given by

$$\mathbf{h}^b = \mathbf{I}\omega_{ib}^b + \mathbf{A}\mathbf{I}_s\omega_s, \quad (16)$$

and \mathbf{h}_a^b is the N dimensional vector of axial angular momenta of the rotors:

$$\mathbf{h}_a^b = \mathbf{I}_s\mathbf{A}^T\omega_{ib}^b + \mathbf{I}_s\omega_s \quad (17)$$

The vector ω_s is N dimensional, representing the axial angular velocities of the rotors relative to the body, while τ_e is the 3 dimensional vector of external torques (e.g. thrusters and gravitation), τ_a is the N dimensional vector of internal axial torques applied by the rigid body to the rotors, \mathbf{A} is the $3 \times N$ matrix containing the axial vectors of the N rotors, and \mathbf{I} is the angular momentum, or inertia matrix, of the system, including the rotors. The matrix $\mathbf{I}_s = \text{diag}\{i_{s1}, \dots, i_{sN}\}$ is an $N \times N$ diagonal matrix containing the axial moments of inertia of the rotors. The matrix \mathbf{J} is an inertia-like matrix defined as

$$\mathbf{J} = \mathbf{I} - \mathbf{A}\mathbf{I}_s\mathbf{A}^T \quad (18)$$

and can be interpreted as the inertia matrix of an equivalent system where all the rotors have zero axial moment of inertia. The angular velocity ω_{ib}^b of the body frame in reference to an inertial frame, can be written as

$$\omega_{ib}^b = \mathbf{J}^{-1}(\mathbf{h}^b - \mathbf{A}\mathbf{h}_a^b) \quad (19)$$

In this paper we will assume that the origin of \mathcal{F}_b coincides with the origin of \mathcal{F}_o , and that \mathcal{F}_b is oriented along the principal axes of inertia of the rigid body, which implies that the inertia matrix is diagonal, that is $\mathbf{I} = \text{diag}\{i_x, i_y, i_z\}$.

2.4 Error dynamics

A mathematical model of the error dynamics as a function of the error in angular velocity can be derived from equations (14) to (19). This results in the following model where the control objective is to make \mathcal{F}_b coincide with \mathcal{F}_o :

$$\dot{\mathbf{h}}^b = \mathbf{I}(\tilde{\omega} + \mathbf{R}_o^b\omega_{io}^o) + \mathbf{A}\mathbf{I}_s\omega_s \quad (20a)$$

$$\dot{\mathbf{h}}_a^b = \mathbf{I}_s\mathbf{A}^T(\tilde{\omega} + \mathbf{R}_o^b\omega_{io}^o) + \mathbf{I}_s\omega_s \quad (20b)$$

$$\dot{\mathbf{h}}^b = (\mathbf{h}^b)^\times(\tilde{\omega} + \mathbf{R}_o^b\omega_{io}^o) + \tau_e \quad (20c)$$

$$\dot{\mathbf{h}}_a^b = \tau_a \quad (20d)$$

$$\mathbf{J} = \mathbf{I} - \mathbf{A}\mathbf{I}_s\mathbf{A}^T \quad (20e)$$

Since we are assuming a circular orbit, we will assume that the angular velocity $\omega_{io}^o = [0, -\omega_0, 0]$. It is shown in [2] that:

$$\begin{aligned} \mathbf{J}\dot{\tilde{\omega}} &= \omega_0\mathbf{J}(\mathbf{c}_2)^\times\tilde{\omega} - \tilde{\omega}^\times\mathbf{I}\tilde{\omega} + \omega_0\tilde{\omega}^\times\mathbf{I}\mathbf{c}_2 \\ &\quad - \tilde{\omega}^\times\mathbf{A}\mathbf{I}_s\omega_s + \omega_0(\mathbf{c}_2)^\times\tilde{\omega} - \omega_0^2(\mathbf{c}_2)^\times\mathbf{I}\mathbf{c}_2 \\ &\quad + \omega_0(\mathbf{c}_2)^\times\mathbf{A}\mathbf{I}_s\omega_s + \tau_e - \mathbf{A}\tau_a \end{aligned} \quad (21)$$

2.5 Disturbance torques

There are several external disturbance torques affecting a spacecraft. In [3] the gravitational torque, the aerodynamic torque, radiation torques and the magnetic torque are studied. The aerodynamic torque is only applicable at low altitudes. In this paper, we will suppose that all disturbance torques can be neglected, except for the gravitational torque. Assuming circular orbit, [3] has shown that the gravity gradient written in the body frame \mathcal{F}_b is

$$\tau_g = 3\omega_c^2\mathbf{c}_3 \times \mathbf{I}\mathbf{c}_3 = 3\omega_0^2(\mathbf{c}_3)^\times\mathbf{I}\mathbf{c}_3 \quad (22)$$

where \mathbf{c}_3 is defined in (3). It transforms the z_b axis to the z_o axis, and since $\tilde{z}_b = [0, 0, 1]^T$ in \mathcal{F}_b , the unit vector in \mathcal{F}_b corresponding to \tilde{z}_o is \mathbf{c}_3 . ω_0 is defined by $\omega_0^2 = \mu/r_c^3$ where r_c is the orbit radius, $\mu = Gm_p = 3.986 \cdot 10^{14} \text{ Nm}^2/\text{kg}$, G is the universal gravitational constant and m_p is the mass of the Earth.

2.6 Thruster modeling and control

ESEO will use a reaction wheel and thrusters for attitude control. The thrusters are on or off by nature. A reaction wheel on the other hand can give a continuous torque. This means that a continuous signal of commanded torques must be translated to pulses which decide

whether a thruster should be on or off. We will choose a bang-bang controller with dead-zone, presented in [7], where the thrusters are fired if the commanded torque is greater than a certain threshold value, as illustrated in figure 1. Tuning the size of the dead-zone, it is possible to emphasize fuel consumption by choosing it large, or place emphasis on accuracy by having a small dead-zone.

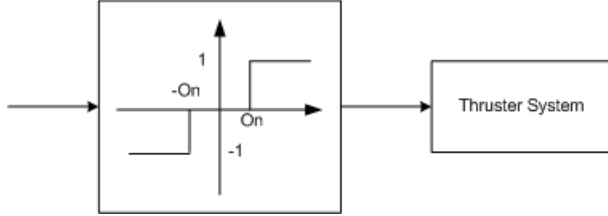


Figure 1: Bang-bang controller with dead-zone

3 CONTROLLER DESIGN

We will now derive controllers for ESEO, using Lyapunov's direct method and Krasovskii-LaSalle's theorem, which can be found in [14]. A linear controller based on a linearized system is presented first. We assume that the only external torques affecting the satellite are thruster torques τ_c and gravitational torques τ_g , thus $\tau_e = \tau_c + \tau_g$.

3.1 Local PD controller

The control law below is based on the linearized model of ESEO. The details of the derivation is found in [2].

$$\tau_c = -k_\epsilon \mathbf{I} \tilde{\epsilon} - k_\omega \tilde{\omega} \quad (23a)$$

$$\tau_a = 0 \quad (23b)$$

If the parameters k_ϵ and k_ω satisfy

$$k_\epsilon \gg i_s \quad (24a)$$

$$k_\omega > 0 \quad (24b)$$

$$k_\omega^2 > \omega_0^2 \left(i_z [2i_y - 2i_x - i_z] - [i_y - i_x]^2 \right) \quad (24c)$$

it follows that the system (20) is locally asymptotically stable.

3.2 Global linear controller

We will now analyze how a linear controller can stabilize ESEO globally. To do this, we will use Lyapunov analysis.

Proposition 4 *The linear controller*

$$\tau_c = -k_0 \tilde{\epsilon} - \mathbf{C} \tilde{\omega} \quad (25a)$$

$$\tau_a = -\mathbf{E} \omega_s \quad (25b)$$

makes the equilibrium of (20) globally asymptotically stable if $i_y > i_x > i_z$, where $\mathbf{C} > 0$ and $\mathbf{E} > 0$ are constant matrices. An obvious choice is $\mathbf{C} = k_\omega \mathbf{1} > 0$ and $\mathbf{E} = k_s \mathbf{1} > 0$ where k_ω and k_s are constants.

Proof. We choose the following Lyapunov function candidate (LFC) V :

$$V = \overbrace{\frac{1}{2} [\tilde{\omega}^T, \omega_s^T] \begin{bmatrix} \mathbf{I} & \mathbf{A} \mathbf{I}_s \\ \mathbf{I}_s \mathbf{A}^T & \mathbf{I}_s \end{bmatrix} \begin{bmatrix} \tilde{\omega} \\ \omega_s \end{bmatrix}}^{V_a} - \frac{1}{2} \omega_0^2 \mathbf{c}_2^T \mathbf{I} \mathbf{c}_2 + k_0 \left(\tilde{\epsilon}^T \tilde{\epsilon} + [\tilde{\eta} - 1]^2 \right) \quad (26)$$

$$+ \frac{3}{2} \omega_0^2 \mathbf{c}_3^T \mathbf{I} \mathbf{c}_3 + \frac{1}{2} \omega_0^2 (i_y - 3i_z) \\ V = \frac{1}{2} \tilde{\omega}^T \mathbf{I} \tilde{\omega} + \omega_s \mathbf{I}_s \mathbf{A}^T \tilde{\omega} + \frac{1}{2} \omega_s^T \mathbf{I}_s \omega_s \\ - \frac{1}{2} \omega_0^2 \mathbf{c}_2^T \mathbf{I} \mathbf{c}_2 + 2k_0 (1 - \tilde{\eta}) \quad (27) \\ + \frac{3}{2} \omega_0^2 \mathbf{c}_3^T \mathbf{I} \mathbf{c}_3 + \frac{1}{2} \omega_0^2 (i_y - 3i_z)$$

The state vector is

$$\mathbf{x} = [\tilde{\omega}^T, \omega_s, \tilde{\eta}, \tilde{\epsilon}^T, c_{12}, c_{32}, c_{13}, c_{23}]^T$$

where c_{12} , c_{32} , c_{13} and c_{23} are the respective components of the vectors \mathbf{c}_2 and \mathbf{c}_3 defined in (3). The desired state vector is

$$\mathbf{x}^* = [0^3, 0^N, 1, 0^3, 0, 0, 0, 0]^T.$$

The first three terms (V_a) and the fourth term in V represents the kinetic energy of the satellite, although it is not equal to its total kinetic energy. The fifth term comes from the attitude error where k_0 is a positive constant. The sixth term represents the potential energy of the satellite. The last term is constant in order to make V a true Lyapunov function, that is $V > 0$ and $V(\mathbf{x}^*) = 0$. In fact, V meets these requirements only when $i_y > i_x > i_z$, which is shown in [9]. It is shown in [2] that the time derivative of V_a is given by:

$$\dot{V}_a = \tilde{\omega}^T \tau_e + \omega_s^T \tau_a - \omega_0^2 \tilde{\omega}^T (\mathbf{c}_2)^\times \mathbf{I} \mathbf{c}_2 \quad (28)$$

The time derivative of V along the trajectories of (20) thus becomes:

$$\dot{V} = \dot{V}_a - \frac{1}{2} \omega_0^2 \mathbf{c}_2^T \mathbf{I} \dot{\mathbf{c}}_2 - 2k_0 \dot{\tilde{\eta}} + \frac{3}{2} \omega_0^2 \mathbf{c}_3^T \mathbf{I} \dot{\mathbf{c}}_3 \quad (29)$$

$$= \tilde{\omega}^T \tau_c + \omega_s^T \tau_a - \omega_0^2 \tilde{\omega}^T (\mathbf{c}_2)^\times \mathbf{I} \mathbf{c}_2 \\ + 3\omega_0^2 \tilde{\omega}^T (\mathbf{c}_3)^\times \mathbf{I} \mathbf{c}_3 - \omega_0^2 \mathbf{c}_2^T \mathbf{I} (\mathbf{c}_2)^\times \tilde{\omega} \quad (30) \\ + k_0 \tilde{\omega}^T \tilde{\epsilon} + 3\omega_0^2 \mathbf{c}_3^T \mathbf{I} (\mathbf{c}_3)^\times \tilde{\omega}$$

Since all the terms are scalars, they can be freely transposed. Exploiting the fact that $(\tilde{\omega}^\times)^T = -\tilde{\omega}^\times$ we obtain:

$$\dot{V} = \tilde{\omega}^T \tau_c + \omega_s^T \tau_a + k_0 \tilde{\omega}^T \tilde{\epsilon} \quad (31)$$

Combining (25) with (31), we get:

$$\dot{V} = -\tilde{\omega}^T \mathbf{C} \tilde{\omega} - \omega_s^T \mathbf{E} \omega_s \quad (32)$$

Since $\mathbf{C} > 0$ and $\mathbf{E} > 0$, $\dot{V} \leq 0$. Thus $\tilde{\omega} \rightarrow 0 \Rightarrow \dot{\tilde{\omega}} \rightarrow 0$ and $\omega_s \rightarrow 0 \Rightarrow \dot{\omega}_s \rightarrow 0$. Hence (21) becomes:

$$0 = -\omega_0^2 (\mathbf{c}_2)^\times \mathbf{I} \mathbf{c}_2 + 3\omega_0^2 (\mathbf{c}_3)^\times \mathbf{I} \mathbf{c}_3 - k_0 \tilde{\epsilon} \quad (33)$$

The terms to the right are bounded because \mathbf{c}_i is a unit vector and $\|\tilde{\epsilon}\| \leq 1$. Hence there should be a large enough choice of k_0 which makes $\tilde{\epsilon} = 0$ the only solution, as proposed by [8]. In [2] it is shown that choosing $k_0 > 5.5432 \omega_0^2 (i_y - i_z) \Rightarrow \tilde{\epsilon} \rightarrow 0$. Thus the equilibrium point will be globally asymptotically stable by Krasovskii-LaSalle's theorem. ■

3.3 Lyapunov controller 1

In section 3.2 there was a restriction on the inertia matrix of the satellite. In case such restrictions are not met by a satellite, we will derive a nonlinear controller which does not have these restrictions.

Proposition 5 *The nonlinear controller*

$$\tau_c = -k_1 \tilde{\epsilon} - \mathbf{C} \tilde{\omega} + \omega_0^2 (\mathbf{c}_2)^\times \mathbf{I} \mathbf{c}_2 - 3\omega_0^2 (\mathbf{c}_3)^\times \mathbf{I} \mathbf{c}_3 \quad (34a)$$

$$\tau_a = -\mathbf{E} \omega_s \quad (34b)$$

makes the equilibrium of (20) globally asymptotically stable, where $\mathbf{C} > 0$ and $\mathbf{E} > 0$ are constant matrices. A possible choice is $\mathbf{C} = k_\omega \mathbf{1} > 0$ and $\mathbf{E} = k_s \mathbf{1} > 0$ where k_ω and k_s are constants.

Proof. Consider the following LFC, which is almost the same LFC as (26):

$$V = V_a + 2k_1 (1 - \tilde{\eta}) \quad (35)$$

where k_1 is a positive constant. The time derivative of V along the trajectories of (20) is given by:

$$\dot{V} = \tilde{\omega}^T \tau_c + \omega_s^T \tau_a - \omega_0^2 \tilde{\omega}^T (\mathbf{c}_2)^\times \mathbf{I} \mathbf{c}_2 + 3\omega_0^2 \tilde{\omega}^T (\mathbf{c}_3)^\times \mathbf{I} \mathbf{c}_3 + k_1 \tilde{\omega}^T \tilde{\epsilon} \quad (36)$$

Inserting (34) into (36), we get:

$$\dot{V} = -\tilde{\omega}^T \mathbf{C} \tilde{\omega} - \omega_s^T \mathbf{E} \omega_s \quad (37)$$

Since $\mathbf{C} > 0$ and $\mathbf{E} > 0$, $\dot{V} \leq 0$. Thus $\tilde{\omega} \rightarrow 0 \Rightarrow \dot{\tilde{\omega}} \rightarrow 0$ and $\omega_s \rightarrow 0 \Rightarrow \dot{\omega}_s \rightarrow 0$. Hence (21) becomes $k_0 \tilde{\epsilon} = 0 \Rightarrow \tilde{\epsilon} \rightarrow 0$. Thus the system is globally asymptotically stable according to the theorem of Krasovskii-LaSalle. ■

3.4 Lyapunov controller 2

The preceding controllers do not use the reaction wheels directly as actuators for attitude control. It would be desirable to use the reaction wheels as actuators in the same way as the thrusters. This motivates an LFC where we omit ω_s from the state vector, and treat it as an external signal.

Proposition 6 *The nonlinear control laws*

$$\tau_c = -k_{\epsilon,1} \tilde{\epsilon} - \mathbf{C} \tilde{\omega} \quad (38a)$$

$$\mathbf{A} \tau_a = k_{\epsilon,2} \tilde{\epsilon} + \mathbf{D} \tilde{\omega} + \omega_0 (\mathbf{c}_2)^\times \mathbf{A} \mathbf{I}_s (\mathbf{A}^T \tilde{\omega} + \omega_s) \quad (38b)$$

makes the equilibrium of the system (20) globally asymptotically stable if $i_y > i_x > i_z$, where \mathbf{C} and \mathbf{D} are constant matrices satisfying $(\mathbf{C} + \mathbf{D}) > 0$, and $k_{\epsilon,1}$ and $k_{\epsilon,2}$ are constants satisfying $(k_{\epsilon,1} + k_{\epsilon,2}) > 0$. Obvious choices which ensure this are $\mathbf{C} = k_{\omega,1} \mathbf{1}$ and $\mathbf{D} = k_{\omega,2} \mathbf{1}$ where $k_{\omega,1}$ and $k_{\omega,2}$ are constants and $(k_{\omega,1} + k_{\omega,2}) > 0$.

Proof. Consider the LFC

$$V = \frac{1}{2} \tilde{\omega}^T \mathbf{J} \tilde{\omega} - \frac{1}{2} \omega_0^2 \mathbf{c}_2^T \mathbf{I} \mathbf{c}_2 + 2k_2 (1 - \tilde{\eta}) + \frac{3}{2} \omega_0^2 \mathbf{c}_3^T \mathbf{I} \mathbf{c}_3 + \frac{1}{2} \omega_0^2 (i_y - 3i_z) \quad (39)$$

where k_2 is a positive constant. The state vector is

$$\mathbf{x} = [\tilde{\omega}^T, \tilde{\eta}, \tilde{\epsilon}^T, c_{12}, c_{32}, c_{13}, c_{23}]^T,$$

and the desired state vector is

$$\mathbf{x}^* = [0^3, 1, 0^3, 0, 0, 0, 0]^T.$$

The first and second term in V represents the kinetic energy of the satellite, although it is not equal to its total kinetic energy. The other terms are the same as in the LFC (26). This means that V is a Lyapunov function if $i_y > i_x > i_z$. To calculate \dot{V} , we will use (21):

$$\dot{V} = \tilde{\omega}^T \mathbf{J} \dot{\tilde{\omega}} - \frac{1}{2} \omega_0^2 \mathbf{c}_2^T \mathbf{I} \dot{\mathbf{c}}_2 - 2k_2 \dot{\tilde{\eta}} + \frac{3}{2} \omega_0^2 \mathbf{c}_3^T \mathbf{I} \dot{\mathbf{c}}_3 \quad (40)$$

$$\begin{aligned} \dot{V} &= \omega_0 \tilde{\omega}^T \mathbf{J} (\mathbf{c}_2)^\times \tilde{\omega} + \omega_0 \tilde{\omega}^T (\mathbf{c}_2)^\times \mathbf{I} \tilde{\omega} \\ &\quad - \omega_0^2 \tilde{\omega}^T (\mathbf{c}_2)^\times \mathbf{I} \dot{\mathbf{c}}_2 + \omega_0 \tilde{\omega}^T (\mathbf{c}_2)^\times \mathbf{A} \mathbf{I}_s \omega_s \\ &\quad + \tilde{\omega}^T \tau_g + \tilde{\omega}^T \tau_c - \tilde{\omega}^T \mathbf{A} \tau_a \\ &\quad - \omega_0^2 \mathbf{c}_2^T \mathbf{I} (\dot{\mathbf{c}}_2)^\times \tilde{\omega} + k_2 \tilde{\omega}^T \tilde{\epsilon} + 3\omega_0^2 \mathbf{c}_3^T \mathbf{I} (\dot{\mathbf{c}}_3)^\times \tilde{\omega} \end{aligned} \quad (41)$$

Note that several terms have disappeared since $\tilde{\omega}^T \tilde{\omega}^\times = 0$. Transposing several terms we get:

$$\dot{V} = \omega_0 \tilde{\omega}^T (\mathbf{c}_2)^\times (\mathbf{I} \tilde{\omega} - \mathbf{J} \tilde{\omega} + \mathbf{A} \mathbf{I}_s \omega_s) + \tilde{\omega}^T \tau_c - \tilde{\omega}^T \mathbf{A} \tau_a + k_2 \tilde{\omega}^T \tilde{\epsilon} \quad (42)$$

$$\begin{aligned} &= \omega_0 \tilde{\omega}^T (\mathbf{c}_2)^\times \mathbf{A} \mathbf{I}_s (\mathbf{A}^T \tilde{\omega} + \omega_s) + \tilde{\omega}^T \tau_c \\ &\quad - \tilde{\omega}^T \mathbf{A} \tau_a + k_2 \tilde{\omega}^T \tilde{\epsilon} \end{aligned} \quad (43)$$

Inserting (38) into (43), we get:

$$\dot{V} = (k_2 - k_{\epsilon,1} - k_{\epsilon,2}) \tilde{\omega}^T \tilde{\epsilon} - \tilde{\omega}^T (\mathbf{C} + \mathbf{D}) \tilde{\omega} \quad (44)$$

Note that the control law for τ_a in (38) cancels the nonlinearities in \dot{V} . This is only possible if the reaction wheels are able to give torques about all three axes of rotation. If this is not the case, the thrusters should be used. We will get the same result for \dot{V} , if we choose to cancel them with τ_c instead. Choosing $k_2 = k_{\epsilon,1} + k_{\epsilon,2}$, we get:

$$\dot{V} = -\tilde{\omega}^T (\mathbf{C} + \mathbf{D}) \tilde{\omega} \quad (45)$$

Since $(\mathbf{C} + \mathbf{D}) > 0$, $\dot{V} \leq 0$. Thus, we have proved that $\tilde{\omega} \rightarrow 0 \Rightarrow \tilde{\omega} \rightarrow 0$. We will now apply Krasovskii-LaSalle's theorem. When $\dot{\tilde{\omega}} = \tilde{\omega} = 0$, (21) becomes:

$$0 = -\omega_0^2 (\mathbf{c}_2)^\times \mathbf{I} \mathbf{c}_2 + 3\omega_0^2 (\mathbf{c}_3)^\times \mathbf{I} \mathbf{c}_3 - k_2 \tilde{\epsilon} \quad (46)$$

The constant k_2 must be chosen large enough to make $\tilde{\epsilon} = 0$ the only possible solution to this equation. Since this is the same equation as (33) choosing $k_2 > 5.5432 \omega_0^2 (i_y - i_z)$ yields a globally asymptotically stable system according to Krasovskii-LaSalle's theorem. ■

3.5 Lyapunov controller 3

In section 3.4 there is a restriction on the inertia matrix of the satellite. The next controller will not have such restrictions.

Proposition 7 *The nonlinear control laws*

$$\tau_c = -k_{\epsilon,1} \tilde{\epsilon} - \mathbf{C} \tilde{\omega} \quad (47a)$$

$$\mathbf{A} \tau_a = k_{\epsilon,2} \tilde{\epsilon} + \mathbf{D} \tilde{\omega} + \omega_0 (\mathbf{c}_2)^\times \mathbf{A} \mathbf{I}_s (\mathbf{A}^T \tilde{\omega} + \omega_s) - \omega_0^2 (\mathbf{c}_2)^\times \mathbf{I} \mathbf{c}_2 + 3\omega_0^2 (\mathbf{c}_3)^\times \mathbf{I} \mathbf{c}_3 \quad (47b)$$

makes the equilibrium of the system (20) globally asymptotically stable, where \mathbf{C} and \mathbf{D} are constant matrices satisfying $(\mathbf{C} + \mathbf{D}) > 0$, and $k_{\epsilon,1}$ and $k_{\epsilon,2}$ are constants satisfying $(k_{\epsilon,1} + k_{\epsilon,2}) > 0$. Obvious choices which ensure this are $\mathbf{C} = k_{\omega,1} \mathbf{1}$ and $\mathbf{D} = k_{\omega,2} \mathbf{1}$ where $k_{\omega,1}$ and $k_{\omega,2}$ are constants and $(k_{\omega,1} + k_{\omega,2}) > 0$.

Proof. We will consider the following LFC V where k_3 is a positive constant:

$$V = \frac{1}{2} \tilde{\omega}^T \mathbf{J} \tilde{\omega} + 2k_3 (1 - \tilde{\eta}) \quad (48a)$$

This LFC is almost the same as (39), but two terms are removed. \dot{V} becomes:

$$\dot{V} = \tilde{\omega}^T \mathbf{J} \dot{\tilde{\omega}} - 2k_3 \dot{\tilde{\eta}} \quad (49)$$

$$\begin{aligned} \dot{V} = & \omega_0 \tilde{\omega}^T \mathbf{J} (\mathbf{c}_2)^\times \tilde{\omega} + \omega_0 \tilde{\omega}^T (\mathbf{c}_2)^\times \mathbf{I} \tilde{\omega} \\ & - \omega_0^2 \tilde{\omega}^T (\mathbf{c}_2)^\times \mathbf{I} \mathbf{c}_2 + \omega_0 \tilde{\omega}^T (\mathbf{c}_2)^\times \mathbf{A} \mathbf{I}_s \omega_s \\ & + 3\omega_0^2 \tilde{\omega}^T (\mathbf{c}_3)^\times \mathbf{I} \mathbf{c}_3 + \tilde{\omega}^T \tau_c \\ & - \tilde{\omega}^T \mathbf{A} \tau_a + k_3 \tilde{\omega}^T \tilde{\epsilon} \end{aligned} \quad (50)$$

Transposing the first term, and using the definition of \mathbf{J} in (20), we get:

$$\begin{aligned} \dot{V} = & \omega_0 \tilde{\omega}^T (\mathbf{c}_2)^\times \mathbf{A} \mathbf{I}_s (\mathbf{A}^T \tilde{\omega} + \omega_s) \\ & - \omega_0^2 \tilde{\omega}^T (\mathbf{c}_2)^\times \mathbf{I} \mathbf{c}_2 + 3\omega_0^2 \tilde{\omega}^T (\mathbf{c}_3)^\times \mathbf{I} \mathbf{c}_3 \\ & + \tilde{\omega}^T \tau_c - \tilde{\omega}^T \mathbf{A} \tau_a + k_3 \tilde{\omega}^T \tilde{\epsilon} \end{aligned} \quad (51)$$

Inserting (47) into (51), we get:

$$\dot{V} = (k_3 - k_{\epsilon,1} - k_{\epsilon,2}) \tilde{\omega}^T \tilde{\epsilon} - \tilde{\omega}^T (\mathbf{C} + \mathbf{D}) \tilde{\omega} \quad (52)$$

The control law for τ_a in (47) cancels the nonlinearities in \dot{V} . We choose $k_3 = k_{\epsilon,1} + k_{\epsilon,2}$, thus:

$$\dot{V} = -\tilde{\omega}^T (\mathbf{C} + \mathbf{D}) \tilde{\omega} \quad (53)$$

Since $(\mathbf{C} + \mathbf{D}) > 0$, $\dot{V} \leq 0$. Thus $\tilde{\omega} \rightarrow 0 \Rightarrow \tilde{\omega} \rightarrow 0$, and the system is globally asymptotically stable according to the theorem of Krasovskii-LaSalle. ■

3.6 Sliding mode controller

According to [14] sliding mode controllers are robust to system parameter uncertainties. Such uncertainties are often encountered in practice. A good example is change of a satellite's inertia when thruster fuel is consumed. We will define the error of a parameter α to be $\Delta \alpha = \alpha - \hat{\alpha}$ where the values denoted with a hat ($\hat{\cdot}$) are the best estimates, or nominal values, of the system parameters.

Proposition 8 *The sliding mode controller*

$$\tau_c = -\tau_{sgn} \quad (54a)$$

$$\begin{aligned} \mathbf{A} \tau_a = & (\hat{\mathbf{h}}^b)^\times [\tilde{\omega} + \hat{\omega}_0 \mathbf{c}_2] + \frac{3}{2} \hat{\omega}_0^2 \mathbf{c}_3^T \hat{\mathbf{I}} \mathbf{c}_3 \\ & + \hat{\omega}_0 \hat{\mathbf{J}} (\mathbf{c}_2)^\times \tilde{\omega} + \frac{1}{2} \hat{\mathbf{J}} \mathbf{P} [\hat{\eta} \mathbf{1} + (\tilde{\epsilon})^\times] \tilde{\omega} \\ & + \tau_{sgn,a} \end{aligned} \quad (54b)$$

$$\tau_{sgn} = \begin{bmatrix} \beta_x \text{sgn}(s_x) \\ \beta_y \text{sgn}(s_y) \\ \beta_z \text{sgn}(s_z) \end{bmatrix}, \quad \tau_{sgn,a} = \begin{bmatrix} \beta_{a,x} \text{sgn}(s_x) \\ \beta_{a,y} \text{sgn}(s_y) \\ \beta_{a,z} \text{sgn}(s_z) \end{bmatrix} \quad (54c)$$

makes the equilibrium of the system (20) globally asymptotically stable, where

$$\beta_i + \beta_{a,i} \geq \delta_i + \beta_{0,i},$$

$\beta_{0,i} > 0$ is a constant and the vector $\delta = [\delta_x, \delta_y, \delta_z]^T$ is given by:

$$\begin{aligned} \delta &= (\Delta \mathbf{h}^b)^\times \tilde{\omega} - (\Delta(\mathbf{h}^b \omega_0))^\times \mathbf{c}_2 \\ &+ \frac{3}{2} \mathbf{c}_3^T \Delta(\omega_0^2 \mathbf{I}) \mathbf{c}_3 + \Delta(\omega_0 \mathbf{J})(\mathbf{c}_2)^\times \tilde{\omega} \\ &+ \frac{1}{2} \Delta \mathbf{J} \mathbf{P} [\tilde{\eta} \mathbf{1} + (\tilde{\epsilon})^\times] \tilde{\omega} \end{aligned} \quad (55)$$

The sign function $\text{sgn}(\cdot)$ is defined by:

$$\text{sgn}(s_i) = \begin{cases} 1, & s_i > 0 \\ 0, & s_i = 0 \\ -1, & s_i < 0 \end{cases} \quad (56)$$

Proof. The first step in sliding mode control is to design a sliding manifold

$$\mathbf{s} = [s_x, s_y, s_z]^T,$$

and [15] suggest the following manifold where $\mathbf{s} = 0$ implies that $\tilde{\epsilon}$ and $\tilde{\omega}$ tend to zero. Define

$$\mathbf{s} = \tilde{\omega} + \mathbf{P} \tilde{\epsilon} \quad (57)$$

where $\mathbf{P} > 0$. We must now design a control law for the system states to reach the sliding manifold. Consider the LFC

$$\dot{V} = \mathbf{s}^T \mathbf{J} \mathbf{s} \quad (58)$$

Its time derivative along the trajectories of (20) is given as:

$$\dot{V} = \mathbf{s}^T (\mathbf{J} \dot{\tilde{\omega}} + \mathbf{J} \mathbf{P} \dot{\tilde{\epsilon}}) \quad (59)$$

$$\begin{aligned} \dot{V} &= \mathbf{s}^T \left((\mathbf{h}^b)^\times [\tilde{\omega} - \omega_0 \mathbf{c}_2] + \frac{3}{2} \omega_0^2 \mathbf{c}_3^T \mathbf{I} \mathbf{c}_3 \right. \\ &\quad \left. + \tau_c - \mathbf{A} \tau_a + \omega_0 \mathbf{J} (\mathbf{c}_2)^\times \tilde{\omega} \right. \\ &\quad \left. + \frac{1}{2} \mathbf{J} \mathbf{P} [\tilde{\eta} \mathbf{1} + (\tilde{\epsilon})^\times] \tilde{\omega} \right) \end{aligned} \quad (60)$$

Inserting (54) into (60), we get:

$$\begin{aligned} \dot{V} &= \mathbf{s}^T \left((\Delta \mathbf{h}^b)^\times \tilde{\omega} - (\Delta(\mathbf{h}^b \omega_0))^\times \mathbf{c}_2 \right. \\ &\quad \left. + \frac{3}{2} \mathbf{c}_3^T \Delta(\omega_0^2 \mathbf{I}) \mathbf{c}_3 + \Delta(\omega_0 \mathbf{J})(\mathbf{c}_2)^\times \tilde{\omega} \right. \\ &\quad \left. + \frac{1}{2} \Delta \mathbf{J} \mathbf{P} [\tilde{\eta} \mathbf{1} + (\tilde{\epsilon})^\times] \tilde{\omega} - \tau_{sgn} - \tau_{sgn,a} \right) \end{aligned} \quad (61)$$

$$= \mathbf{s}^T (\delta - \tau_{sgn} - \tau_{sgn,a}) \quad (62)$$

Since $\beta_i + \beta_{a,i} \geq \delta_i + \beta_{0,i}$, we have:

$$\dot{V} \leq -(\beta_{0,x} |s_x| + \beta_{0,y} |s_y| + \beta_{0,z} |s_z|) \quad (63)$$

For $\mathbf{s} \neq 0$, $\dot{V} < 0 \Rightarrow s \rightarrow 0$. Hence, we reach our manifold \mathbf{s} in finite time, and the system is globally asymptotically stable. ■

4 SIMULATION

4.1 Numerical values

The inertia matrix of ESEO is given by $\mathbf{I} = \text{diag}\{4.3500, 4.3370, 3.6640\}$. ESEO has one reaction wheel about its y axis, hence $\mathbf{A} = [0, 1, 0]^T$. The wheel inertia is given by $i_s = 4 \cdot 10^{-5} \text{ kgm}^2$, and the maximum angular velocity of the reaction wheel is given by $(\omega_s)_{max} = 5035 \text{ rpm}$. Table 1 shows the nominal torques of the thrusters. The altitude is 250 km, which corresponds to ESEO's planned elliptical orbit at perigee.

x axis	0.0484 Nm
y axis	0.0484 Nm
z axis	0.0398 Nm

Table 1: ACS nominal torques

4.2 Implementation of controllers

Since ESEO only has one reaction wheel, the cancellation of system nonlinearities cannot be done with the reaction wheel alone. Thus, the control laws are modified in order to let the thrusters cancel nonlinearities about the x and z -axes, while the reaction wheel takes care of the y -axis nonlinearities. Regarding the sliding mode controller, it is discussed in [14] that such controllers suffer from chattering. This problem can be solved by replacing the sign function with a saturation function, which leads to decreased accuracy:

$$\text{sat}(s_i, \gamma) = \begin{cases} 1, & s_i > \gamma \\ 0, & |s_i| < \gamma \\ -1, & s_i < -\gamma \end{cases} \quad (64)$$

In the implementation of the sliding mode controller, the saturation function is used instead of the sign function, and the gains β_i and $\beta_{a,i}$ are chosen constant, that is:

$$\beta_i + \beta_{a,i} = \beta_{0,i} > \delta_i$$

4.3 Simulations and results

A simple step simulation is performed, where the satellite has an initial spin. First with ideal conditions, that is no measurement noise and perfect estimates of system parameters (figure 2 to 5). Then with a 20 % uncertainty on the system inertial parameters, and finally with added white noise and perfect parameter estimates (figure 6 to 9). The second simulation results in approximately the same results as the first, so these plots are not included. The only difference is a slightly slower rate of convergence to the desired attitude. The attitude is presented in Euler angles where the three angles ϕ , θ and ψ give the rotation about the x , y and z -axes respectively. The desired accuracy is $\pm 1^\circ$. All Euler angles have the same desired value.

5 CONCLUSION

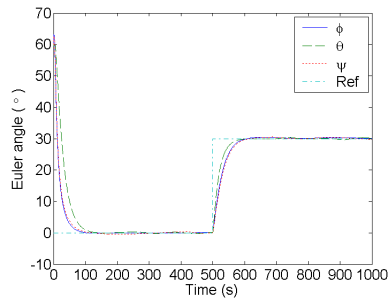
In this paper, a variety of nonlinear controllers are developed to control the attitude of a spacecraft using thrusters and reaction wheels as actuators. Note that simpler controllers are obtained if the diagonal inertia matrix of the spacecraft satisfies $i_y > i_x > i_z$. Simulations show that all controllers obtain a desired accuracy of $\pm 1^\circ$ in Euler angles. Some of the controllers do not use the reaction wheel actively to control the satellite's attitude, but they perform just as well as the others. Whether or not the reaction wheel is used actively, the Euler angle θ converges faster than the other Euler angles and it has a higher degree of accuracy. This is due to the presence of the reaction wheel, and it is suggested in [2] that it adds a damping effect to the system. Note that when using the reaction wheel actively to control the spacecraft's attitude, the reaction wheel reaches saturation quickly. It is observed that added noise to the measured states yields more thruster firings. This work will be part of a basis for the next SSETI project, ESMO.

6 ACKNOWLEDGMENTS

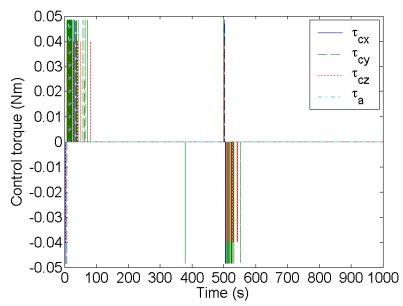
The first author gratefully acknowledges the financial support of the Department of Engineering Cybernetics and the Norwegian Space Centre. SSETI is also acknowledged for sponsoring the attendance to the 6th and 7th ESEO workshops.

References

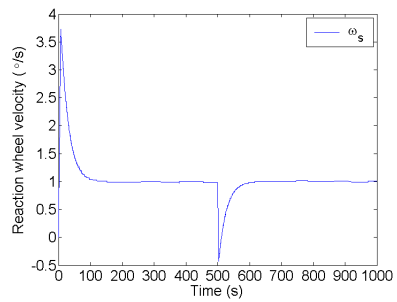
- [1] SSETI, P. R., "SSETI," [Online] Available from: URL <http://sseti.gte.tuwien.ac.at/WSW4/>, 2004, [Accessed 24 May 2004].
- [2] Topland, M. P., *Nonlinear Attitude Control of the Micro-Satellite ESEO*, Master's thesis, Department of Engineering Cybernetics, Norwegian University of Science and Technology, Trondheim, Norway, 2004.
- [3] Hughes, P. C., *Spacecraft Attitude Dynamics*, John Wiley & Sons, Inc., USA, 1986.
- [4] Hall, C. D. Tsiotras, P. and Shen, H., "Tracking Rigid Body Motion Using Thrusters and Momentum Wheels," *Journal of the Astronautical Sciences*, Vol. 50, No. 3, 2002, pp. 311–323.
- [5] Fjellstad, O. and Fossen, T. I., "Quaternion Feedback Regulation of Underwater Vehicles," *Proceedings of the Third IEEE Conference on Control Applications*, Glasgow, UK, 1994.
- [6] Lee, J. G. Park, C. G. and Park, H. W., "Sliding-Mode Controller Design for Spacecraft Attitude Tracking Maneuvers," *IEEE Transactions on aerospace and electronic systems*, Vol. 29, No. 4, 1993, pp. 1328–1333.
- [7] Song, G. and Agrawal, B. N., "Vibration suppression during attitude control," *Acta Astronautica*, Vol. 49, No. 2, 2001, pp. 73–83.
- [8] Soglo, P. K., *3-aksestyring av gravitasjonsstabilisert satellitt ved bruk av magnetpoler*, Master's thesis, Department of Engineering Cybernetics, Norwegian University of Science and Technology, Trondheim, Norway, 1994.
- [9] Kristiansen, R., *Attitude Control of a Microsatellite*, Master's thesis, Department of Engineering Cybernetics, Norwegian University of Science and Technology, Trondheim, Norway, 2000.
- [10] Gravdahl, J.T. Eide, E. et al., "Three Axis Attitude Determination and Control System for a Picosatellite: Design and Implementation," *Proceedings of the 54th International Astronautical Congress*, Bremen, Germany, 2003.
- [11] Riise, Å-R. Samuelsen, B. et al., "Ncube: The First Norwegian Student Satellite," *Proceedings of The 17th AIAA/USU Conference on Small Satellites*, Logan, Utah, USA, 2003.
- [12] Fossen, T. I., *Marine Control Systems*, Marine Cybernetics, Trondheim, Norway, 2002.
- [13] Egeland, O. and Gravdahl, J. T., *Modeling and Simulation for Automatic Control*, Marine Cybernetics, Trondheim, Norway, 2001.
- [14] Khalil, H. K., *Nonlinear Systems*, Pearson Education International Inc., Upper Saddle River, New Jersey, USA, 2000.
- [15] Fu, L-C. Tsai, C.-W. and Yeh, F.-K., "A Nonlinear Missile Guidance Controller with Pulse Type Input Devices," *Proceedings of the American Control Conference*, San Diego, California, USA, 1999.



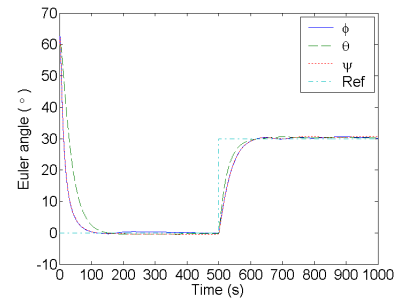
(a) Euler angles with reference



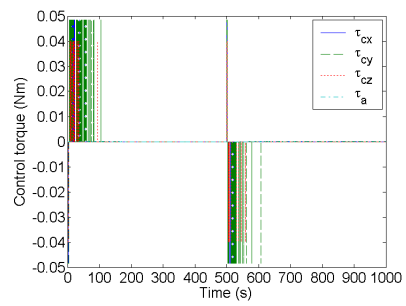
(b) Control torques



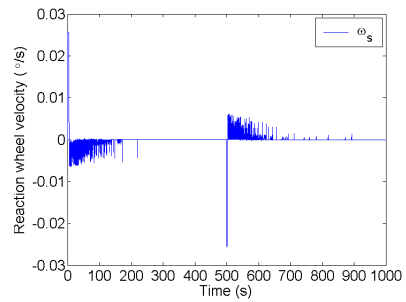
(c) Reaction wheel velocity



(a) Euler angles with reference



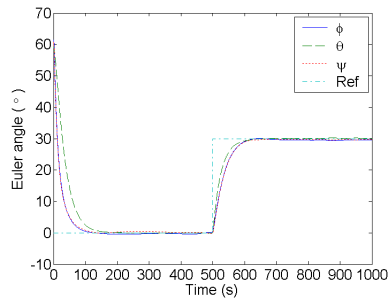
(b) Control torques



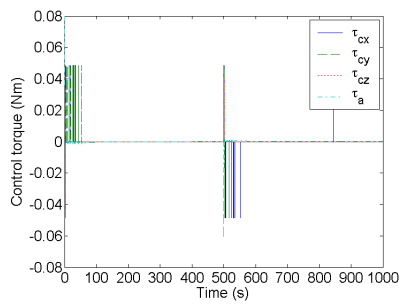
(c) Reaction wheel velocity

Figure 2: Simulation of local PD controller with ideal conditions

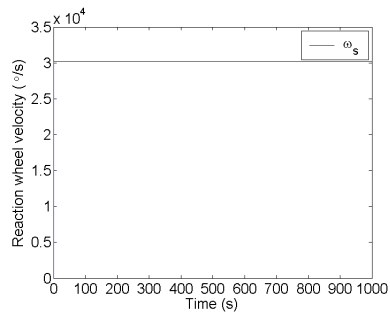
Figure 3: Simulation of Lyapunov controller 1 with ideal conditions



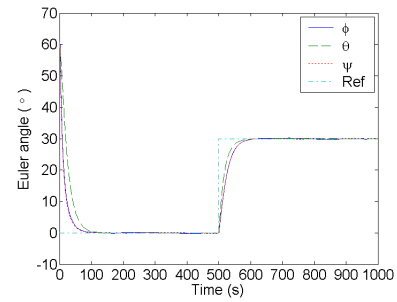
(a) Euler angles with reference



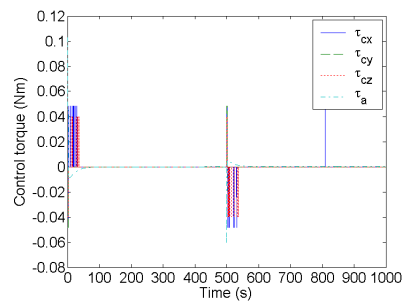
(b) Control torques



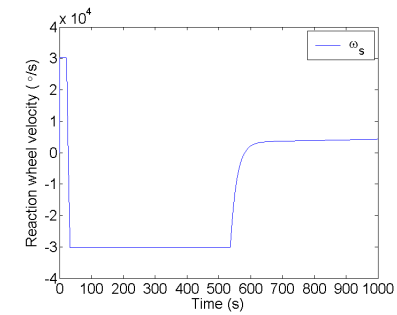
(c) Reaction wheel velocity



(a) Euler angles with reference



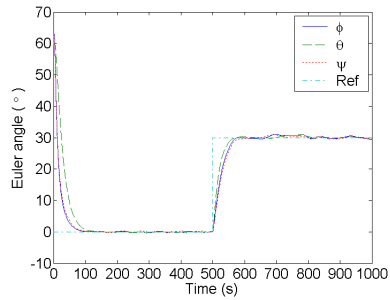
(b) Control torques



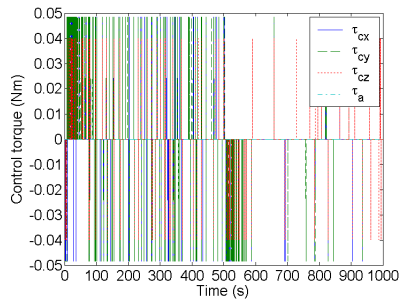
(c) Reaction wheel velocity

Figure 4: Simulation of Lyapunov controller 3 with ideal conditions

Figure 5: Simulation of sliding mode controller with ideal conditions

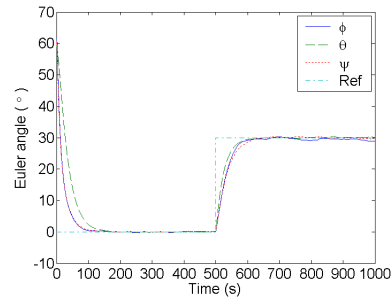


(a) Euler angles with reference

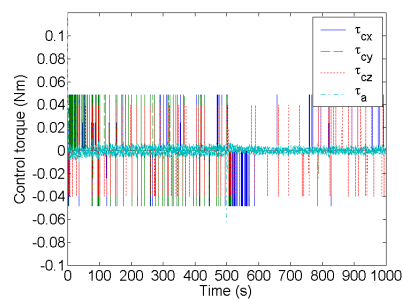


(b) Control torques

Figure 6: Simulation of local PD controller with added white noise

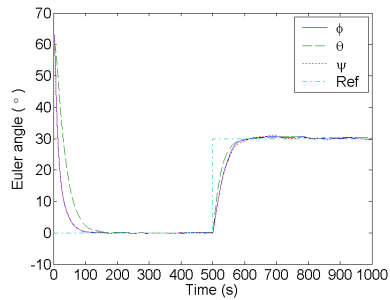


(a) Euler angles with reference

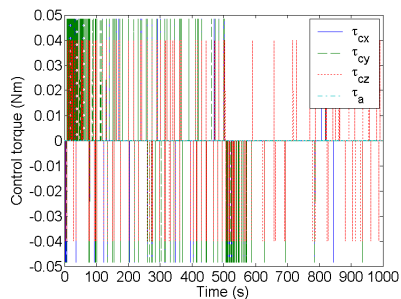


(b) Control torques

Figure 8: Simulation of Lyapunov controller 3 with added white noise

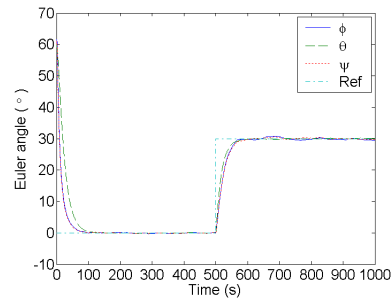


(a) Euler angles with reference

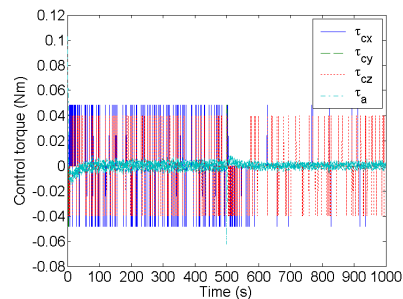


(b) Control torques

Figure 7: Simulation of Lyapunov controller 1 with added white noise



(a) Euler angles with reference



(b) Control torques

Figure 9: Simulation of sliding mode controller with added white noise

